NISTIR 4844

Ferroelectric Thin Films Prepared by Pulsed Laser Deposition Processing and Characterization

U.S. DEPARTMENT OF COMMERCE
Technology Administration
National Institute of Standards
and Technology
Materials Science and Engineering
Laboratory
Ceramics Division
Gaithersburg, MD 20899

NIST

NISTIR 4844

Ferroelectric Thin Films Prepared by Pulsed Laser Deposition Processing and Characterization

U.S. DEPARTMENT OF COMMERCE
Technology Administration
National Institute of Standards
and Technology
Materials Science and Engineering
Laboratory
Ceramics Division
Gaithersburg, MD 20899

May 1992

U.S. DEPARTMENT OF COMMERCE
Barbara Hackman Franklin, Secretary

TECHNOLOGY ADMINISTRATION
Robert M. White, Under Secretary for Technology

NATIONAL INSTITUTE OF STANDARDS
AND TECHNOLOGY
John W. Lyons, Director

PREFACE

This report describes the development of piezoelectric lead zirconate-titanate (PZT) and barium titanate (BT) thin films for application to non-volatile memories for electronic devices such as computers. The work was done in the period from January 1989 to December 1991 in the Ceramics and Metallurgy Divisions at NIST under partial support of the Department of the Army through Harry Diamond Laboratory.

Papers collected in this report (arranged in chronlogical order) have been presented at the following meetings:

Spring Meeting, Materials Research Society, April 1989.
Annual Meeting, American Ceramic Society, April 1989.
International Symposium on Applications of Ferroelectrics, June 1990.
Fall Meeting, Materials Research Society, November 1990.
Spring Meeting, Materials Research Society, April 1991.
SPIE Symposium, September 1991.
Fall Meeting, Materials Research Society, November 1991.

This interdisciplinary work includes many contributors from NIST and HDL.

Ceramics Division, NIST:
C. K. Chiang, L. P. Cook, H. M. Lee, W. Wong-Ng, M. D. Vaudin.

Metallurgy Division, NIST:
P. K. Schenck,

Harry Diamond Lab.:
P.S. Brody, K. W. Bennett, J. M. Benedetto, B. J. Rod.

We have enjoyed a close collaboration between the members of these groups. We would also like to thank T. J. Hsieh, A. Paul, and R. Gates for using their instruments and their consultation. Special thanks to Dr. David Bonnell for his constant interest and many valuable contributions during the course of the work.

L. P. Cook
P. K. Schenck
C. K. Chiang
M. D. Vaudin
W. Wong-Ng

TABLE OF CONTENTS

SUMMARY

Although pulsed laser deposition (PLD) is a relatively new method for preparing thin films, by comparison with somewhat more established technologies such as sol-gel, sputtering and CVD, progress has been rapid. PLD has now become widely accepted as a viable method for producing high-quality thin films for research.[1] This is also true for ferroelectric thin films, where commercial scale-up seems a possibility.

The evolution of PLD owes much to the impetus of high T_c research. From 1986 on, when the discovery of high T_c ceramic materials prompted the development of PLD as a rapid way of preparing stoichiometric or near-stoichiometric superconducting films for study, the number of research papers using PLD increased dramatically. Recently a similar growth has been observed in PLD papers on ferroelectric thin films. Our interest originated in 1989, when we demonstrated the remarkable versatility of PLD for preparing thin films of many oxide materials, including PZT (paper #1). A second discovery was the presence of a very finely particulate component in the films. Notwithstanding the abundance of a large particulate fraction characteristic of the early films deposited by Nd/YAG irradiation, the finely particulate fraction indicated promise for producing extremely fine-grained, high quality films. A third feature was the fact that as deposited, films are amorphous, and crystallize readily upon heating, paving the way for process-control of properties.

Our preliminary studies attracted the attention of HDL staff, who encouraged us to pursue the growth of PZT thin films by PLD. Sawyer-Tower measurements at HDL showed that despite the coarsely particulate (up to 1-2 um) microstructure, these films, after annealing above 500°C, were ferroelectric (paper #2). Thus the challenge was to improve the microstructure of the PZT, while retaining the ferroelectric properties. Experiments demonstrated that by using a line-of-sight shadowing technique, coarser particulate could be removed (paper #3); however, the rate of deposition was greatly reduced. Use of an excimer laser for target irradiation proved to eliminate most of the particulate problem (paper #4). However post annealing of film deposited on unheated substrates did not result in satisfactory microstructure. To circumvent this problem we developed a novel compact heater based on the electrical resistance heating effect in the silicon substrate. It was determined by DSC that the optimum deposition temperature must be above 300°C, where the as-deposited PZT films undergo a glass transition (paper #5). However at temperatures above ~700°C, the lead component did not deposit on the substrate in the required amounts. Because of the inability to precisely measure and control substrate temperatures during deposition, a post annealing step was still necessary to produce ferroelectric

---

[1]"Pulsed Laser Deposition" MRS Bull. v. 17, No. 2, February, 1992.

material. This post annealing had to be completed above 500°C to avoid the formation of a pyrochlore phase, which was difficult to convert to PZT, once formed.

A puzzling feature of the PZT films was the lack of tetragonal splitting in the x-ray patterns, in spite of ferroelectric behavior (paper #6). This same phenomenon was also observed in the $BaTiO_3$ grown by excimer PLD (paper #7). For the $BaTiO_3$, no post annealing was necessary and the films could be deposited at substrate temperatures of 700-800°C, as there were no volatility problems. We believe these ferroelectric $BaTiO_3$ thin films were among the first reported to have been produced by any method.

In order to better understand the deposition process, optical characterization of the laser plume was initiated (Paper #9). It was shown by spectral analysis that the species make-up of the plume varies markedly in time and space. This type of data is still being refined and developed for application to the deposition process. The problem of lack of tetragonal splitting was also investigated further, and it was determined that a combination of internal stress and preferred orientation of crystallites was the likely cause (papers #11 and 12). In the $BaTiO_3$ films the preferred orientation is pronounced, and was demonstrated to determine the presence or absence of ferroelectric behavior (paper #13).

Having improved the microstructure of the PLD thin films, properties measurements could be completed in more detail. Measurements demonstrated electrical properties similar to sol-gel films, including decay of switched polarization and apparent dielectric constant during extensive cycling (paper #8). Further characterization studies indicated that the laser-deposited PZT thin films had polarization/switching characteristics required for memory applications (paper #10). Measurements were extended to 2 MHz, and it was determined that films exhibited decreased remanent polarization and dielectric constant at higher frequencies. This was attributed to limitations imposed by the rate of domain wall migration. In a most recent series of measurements, ferroelectric PZT thin films were shown to have potentially important photovoltaic properties, as well (paper #16).

Our research to date has brought several important research issues on ferroelectric PLD thin films into clear focus:

1. The need for improved uniformity in thickness and composition
2. The close, though incompletely understood relationship between microstructure and ferroelectric properties (e.g. how to increase P_r of PZT films to the expected value of ~25)
3. The role of kinetic factors in influencing microstructure during alternative processing routes of PLD films (e.g. in-situ vs. post-processing)
4. The relation (if any) of fatigue to microstructure
5. New applications and new or modified materials

CERAMIC THIN FILMS BY LASER DEPOSITION

L. P. Cook, P. K. Schenck, Jianrong Zhao*
E. N. Farabaugh, C. K. Chiang and M. Vaudin
National Institute of Standards and Technology
Gaithersburg, MD 20899

ABSTRACT

The utility of the laser thin film deposition method is demonstrated for a variety of ceramic materials, including MgO, Al_2O_3, yttria/zirconia, mullite, and lead zirconate titanate, with emphasis on $Ba_2YCu_3O_x$. Our results confirm the existence of two well-defined particle size distributions in most film deposits: a coarser fraction in the 0.1 - 1.0 μm range, and a fine grained fraction with $<$ 10 nm dia. The coarse fraction probably originates from particulate ejecta, while the finer fraction may arise from vapor condensation. Not all target materials yield abundant ejecta, and there may exist a correlation with incongruent melting behavior. A mechanism for the formation of ejecta, based on the presence of phase microheterogeneities, is proposed.

Using a line-of-sight shadowing method, it is possible to eliminate ejected material, and form a relatively uniform deposit from the plume condensate. The bulk chemistry of this fine-grained fraction appears to be relatively independent of radial substrate-to-target distance within the vapor plume; however the optical emission from the plume varies both temporally and spatially. Study of the optical spectra will provide information useful in controlling precisely the film stoichiometry.

The as-deposited thin films are generally amorphous, but they crystallize and sinter readily at low to moderate temperatures. For certain films, annealing

---

* Guest Scientist, Chinese Academy of Science, Bejing, Peoples Republic of China

experiments have illustrated the importance of differential sintering of the fine-grained fraction in determining film microstructure.

INTRODUCTION

The vapor plumes produced by laser-induced vaporization have practical application as a material transport medium for the deposition of ceramic thin films. The literature on laser thin film deposition has been reviewed by Duly[1,2], who notes that the first thin films were deposited by laser as early as 1965[3], and also by Sankur and Hall[4], who emphasize the optical applications. Most notable, however, is the recent increase in usage of the technique, as indicated by the increase in technical publications as shown in Fig. 1. This phenomenon is due primarily to the utility of the method in preparing thin films of the various high T_c ceramic superconducting phases, the first of which was discovered in 1986[5]. Table 1 lists representative thin films of ceramic and related materials reported over the time period covered by Fig. 1. The majority of papers are concerned with deposition of $Ba_2YCu_3O_x$, Bi-Sr-Ca-Cu-O, and related materials.

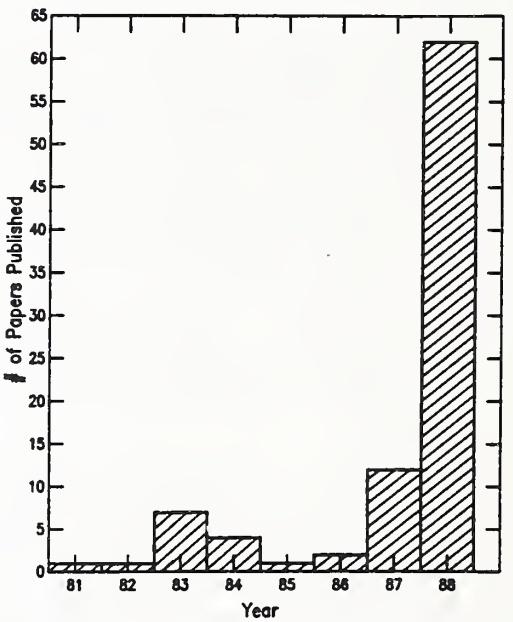

Figure 1. Results of literature survey on thin films by laser deposition.

Laser-based systems offer a number of advantages for film deposition. Small systems suitable for R & D use require less capital investment than, for example, comparable chemical vapor deposition (CVD) or molecular beam epitaxy (MBE) systems. Virtually any solid material can serve as a target, including those with complex multicomponent chemistries, so long as they are relatively homogeneous. Similarly, there are no inherent limitations on the substrate material, and films can be deposited under a variety of conditions, including the presence of active gases, or the use of heated substrates.

Table 1. Representative Thin Films Recently Grown By Laser Deposition (from data in Fig. 1)

$Ba_2YCu_3O_x$	$Bi_2Sr_2Cu_2O_x$
$Ba_2SmCu_3O_x$	$La_{1.85}Sr_{0.15}CuO_4$
PbTe	CdS_xSe_{1-x}
TiO_2	ZrO_2
SiO_2	SiC
Si_3N_4	Si
Ge	C
FeO_x	

The physical interactions occurring during laser-induced mass transport are numerous, and include, among others, melting, vaporization, particle ejection, ion etching, and plasma condensation. The absorption of the incident photons by a polycrystalline ceramic target is potentially inhomogeneous, due to the effect of grain boundaries and the optical anisotropies of the individual crystals. Ceramics vary greatly from material to material in their ability to absorb laser emission, including strong wavelength dependencies. In general, most have higher transmission than metals, leading to dissipation of the energy at a somewhat greater depth in the target. Most film deposition methods utilize pulsed, rather than continuous wave excitation, as this produces larger instantaneous power output without raising the temperature of the bulk target significantly. Time-dependent phenomena are important during laser irradiation. The material exiting the surface during initial plume generation may interact further with the tail of the incoming laser pulse. The laser-generated plume typically has a strong directional component, and the resulting optical spectra are very complex, with contributions from ions as well as neutrals which vary both temporally and spatially.

It is our intention to present new observations which provide additional support for the general utility of the laser method as a means for producing very fine-grained films of ceramic material, as well as films containing a mixture of particle sizes. Although the presence of both a relatively coarse and a relatively fine-grained component in laser-generated deposits has been noted in the literature[6], the fact that extremely fine-grained films of multicomponent bulk

compositions can be produced which are homogeneous both physically and chemically on a scale of a few nanometers may not be widely realized. These attributes appear to be related to the direct condensation of material from the vapor plume. We will demonstrate the use of optical diagnostics as a tool in studying the complex chemical interactions occurring in the vapor plume.

EXPERIMENTAL METHODS

Laser Deposition Facility

The laser deposition facility consists of a high power pulsed laser system, deposition chamber, and ancillary analysis equipment. The laser used in this work is a Nd/YAG 20 Hz pulsed laser with a typical pulse width of 10-15 ns.

Since the pulse duration of the laser is short compared to the pulse rate, the sample cools nearly to the ambient temperature between laser shots. Discrete wavelengths of 355, 532, and 1064 nm, with energies up to 200 mJ per pulse at 1064 nm, are available. For the present studies, the 532 nm wavelength has primarily been used, with energies of 10 - 40 mJ focused to a $\sim$250 μm beam spot diameter. A radiometer is used to directly measure the laser energy. These measurements are made periodically during experimental runs to confirm constant laser power conditions.

The cylindrical deposition chamber is constructed of stainless steel and has internal dimensions of $\sim$20 cm in diameter and $\sim$8 cm high. The chamber is equipped with multiple ports for: mounting targets and substrates, laser access to the targets, and optical spectroscopic observations of the laser generated plumes. The reaction chamber is continuously evacuated to 10 mPa by a roughing pump-backed diffusion pump. Sample targets are mounted on a continuously rotatable shaft to minimize cratering effects. The Nd/YAG laser is focused through an optical port onto the target using a 20 cm focal length lens. The laser fluence is varied by adjusting both the laser power and lens-to-target distance.

Substrates are mounted in the deposition chamber by several methods. A stationary substrate holder has been used to hold substrates at distances $>$ 2.0 cm from the target surface. Shorter deposition distances are obtained by mounting substrates directly over the target surface on a microscope slide with a hole to allow the focused laser beam to pass through to the target surface. Substrates can also be attached to wires and suspended into the luminous regions of the plume as

discussed below.

The background buffer/reaction gas pressure in the deposition chamber is introduced through a needle valve from a ballast tank whose pressure is servo controlled to obtain the desired background pressure.

Side ports on the chamber allow for several line-of-sight optical access paths perpendicular to the laser-plume axis. Other side ports on the chamber are available for future access, such as electrical probing of the plume ions (e.g. as in ref. 7) and optical probing of the plume particulates (e.g. as in ref. 8).

For typical laser heating experiments, a gas-dynamically stabilized vapor plume is generated by the pulsed Nd/YAG laser beam focused onto a target. The generated plume has instantaneous pressures ($\sim$0.1 MPa) much greater than those of classical free molecular flow techniques ($\sim$10 Pa) and a rapid isentropic expansion occurs to generate a non-perturbed mass transport situation. Ideally, the laser should serve as a heat source without perturbing the vaporization and plume formation processes. Establishment of these conditions may depend on such factors as; the optical and thermal properties of the target material; surface and system geometry; and laser energy, wavelength, and pulse width.

Optical Diagnostics

An optical multichannel analyzer (OMA), consisting of a 0.275 meter monochromator with a gateable intensified photodiode array, is used to record the emission spectra of the plume, synchronous with the laser. A fused silica 10 cm focal length lens is used at twice its focal length to obtain one-to-one imaging of the plume on the entrance slit of the OMA. By aperturing the entrance slits of the monochromator and moving the imaging lens, the emission spectra from the plume can be spatially resolved.

Two OMA detection time schemes are used. In the first approach, the detector gate is 100 ns long and fixed in time after the laser pulse to avoid saturating the detector array. In the second approach, the gate is 10 ns wide and is swept under computer control from before the laser onset to several hundred nanoseconds after the laser firing in order to time-resolve the plume emission spectra. The OMA controller averages the detector array output over 100 to 1000 laser pulses and subtracts a previously stored dark current signal from the emission spectrum prior to transfer to the laboratory computer.

Materials and Material Characterization

Sintered target materials for laser deposition experiments were either obtained from commercial sources, or fabricated in-house, as indicated in Table 2. In general, as-fired surfaces of the sintered ceramics were used as targets, and no special attempt was made to prepare highly polished surfaces, as these quickly become roughened by laser removal of material. Target materials were examined by x-ray diffraction to verify their phase chemistry, when necessary.

Grain sizes and porosities were estimated from examination of thermally etched surfaces with the scanning electron microscope (SEM). From the data in Table 2, it is clear that during typical experiments, the focused laser beam (~250 μm dia.) irradiated a large number of grains during any given pulse.

Table 2. Target Materials For Laser Deposition Experiments

Material	Source	Average Grain Size (μm)
Al_2O_3	commercial 99.8%	3
MgO	commercial 98%	3
$3Al_2O_3 \cdot SiO_2$ (mullite in glassy matrix)	commercial	2.5
PZT (lead zirconate titanate)	commercial	4
yttria-stabilized zirconia	sintered from sol-gel precipitated powders, 1600°C, 5 hr	0.5
$Ba_2YCu_3O_x$	sintered from commercial commercial powder, 6 hr, 940°C, 20 hr, 420°C	8

At the conclusion of laser deposition experiments, targets, as well as films, were examined by SEM and energy dispersive x-ray analysis (EDX). Selected thin films were deposited on electron-transparent carbon supports and examined by transmission electron microscopy (TEM) to determine grain size, crystallinity and microchemistry (the latter by EDX). Before and after annealing, thin films were subjected to x-ray analysis using a Read camera[9]. Selected $Ba_2YCu_3O_x$ films were characterized by electron spectroscopy (ESCA), and at very low temperatures, by four-probe d.c. resistivity and a.c. magnetic susceptibility measurements.

For most experiments, MgO substrates were used. It was found that MgO single crystals can be readily cleaved to yield relatively smooth, uncontaminated (100) surfaces. The chemical inertness of MgO, with regard to such oxides as CuO, BaO, and PbO, makes it an ideal substrate for post-deposition annealing of thin films of electronic ceramics. In situations where substrates of controlled area were desired, e.g. for ease of positioning in the Read camera, thin slices of polycrystalline MgO were cut and polished for this purpose.

RESULTS

$Ba_2YCu_3O_x$ Film Deposition

Laser/Target Interaction

The mechanisms of material transport from target to substrate could be expected to influence the structure of the resulting thin films. The effect of laser action on the surface of a $Ba_2YCu_3O_x$ ceramic target is shown in Fig. 2. The original as-fired surface in Fig. 2A is characterized by faceted grains with well-defined grain boundaries and obvious growth steps. After one laser pulse (10 ns, 532 μm), such features have been largely eliminated from a typical area of the surface, as shown in Fig. 2B, where the highest areas and sharpest edges have been removed. The rounded appearance of the surface suggests melting, but probably only in a very thin layer, as there appears to be no tendency for pooling of the liquid or filling of voids. Thus the liquid film is probably removed in this process by vaporization as rapidly as melting takes place.

During the deposition experiments reported here, the target material was rotated continuously at a speed such that each pulse irradiated an area different from the previous one. Gradually a circular trench was formed as material was removed

from the rotating target. Evidence for melting is clear from such features as congealed liquid streamers which appear to have flowed down the trench walls: these may represent molten or partially molten ejecta with inadequate escape velocities, or they may have originated from melting in the higher parts of the trench wall. The appearance of the trench bottom (Fig. 2C) strongly suggests melting of the surface, with formation of shrinkage cracks as the melt rapidly solidified after the termination of each laser pulse.

External to the trench and adjacent to it on the target surface, the effects of laser interaction are also evident; molten ejecta have congealed in the process of leaving the surface, with the effect resembling a liquid splash pattern. Such features occur in an area immediately adjacent to the trench, where laser intensity was nearly as great as that in the trench, but apparently insufficient to cause extensive vaporization. Further away from the trench, an oriented pattern of grain boundaries occurs, suggesting textured solid state growth on the surface. Closer examination of these areas indicates that a combination of growth, leading to straight, smooth inclined surfaces, and etching, indicated by pitted, recessed areas, is responsible for the textured effect. The degree of alignment of the growth surfaces is somewhat unexpected. Presumably the growth/removal mechanisms are related to the vapor/solid, plasma/surface

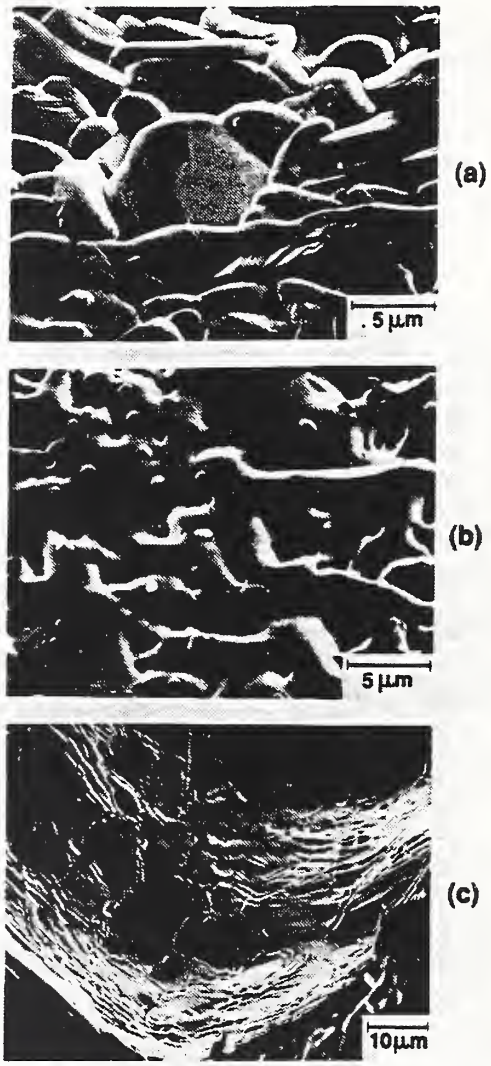

Figure 2. Effect of laser irradiation on $Ba_2YCu_3O_x$ target surface. A) As-sintered original surface. B) Typical area after single laser pulse. C) Bottom of laser-produced pit in target after numerous pulses.

interaction, as there is no evidence for melting in these areas. If the growth surfaces are crystallographically aligned, this implies the possibility of plasma phase epitaxy, which we have not further explored at this time.

By far the dominant mass transfer occurs from mechanisms operative in the removal trench, directly under the area of maximum irradiation. A typical rate of material removal for $Ba_2YCu_3O_x$ would be ~ 10 mg/hr under the experimental conditions outlined above. To reiterate, a combination of melting and instantaneous vaporization is envisioned as responsible. However, the details of the target melting/cooling process may be significant, as will be discussed further in the final section of this paper.

Spectral Analysis of the Plume

Time and spatially resolved emission spectra can be obtained by using a 10 ns gate on the OMA and aperturing the entrance slit of the OMA's monchomator as described above.

Fig. 3 shows two representative OMA emission spectra obtained from the $Ba_2YCu_3O_x$ target plume. In Fig. 3 the sample position was static, and the spectrum in Fig. 3A was obtained with a fresh target, while Fig. 3B shows the spectrum after cratering of the surface had occurred from repeated laser impact. Note the dependence of relative intensities on the number of accumulated laser shots. The more volatile Y and Ba species have been depleted, relative to Cu, after 5000 laser shots in the emission spectra of the plume. This result is consistent with the observation[10] that films deposited with higher energy are deficient in Cu and rich in Ba and Y.

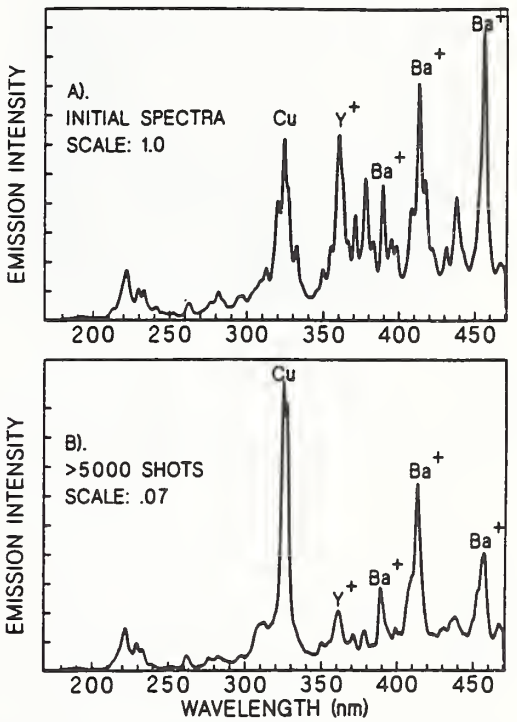

Figure 3. Optical emission spectra from laser-generated plume from a $Ba_2YCu_3O_x$ target. A) shows the average spectra from the first 1000 shots, and B) shows the averaged spectra of 1000 shots averaged after 5000 shots impacted the target.

Mass spectrometric studies of the laser-induced plumes were carried out by other workers in our laboratory[11]. The major plume species observed from the high temperature superconductor target, $Ba_2YCu_3O_x$, were Y, Ba, Cu, Cu^+, CuO^+, O_2, and O. In addition to these species, mass spectrometric signals identified as H_2O, CO_2, BaO, YO, Na^+, K^+ and bimetallics (CuBa, YCu) were also observed in the plume. Species assignments were confirmed by isotopic ratio measurements. Oxygen atoms and ions, which are known to be present from the optical emission spectra, were not detectable in the mass spectrometer.

Geometrical Effects on Film Deposition

In order to observe variation in film deposition as a function of angular position relative to the $Ba_2YCu_3O_x$ target, substrates were positioned as shown in Fig. 4. Small TEM grids were placed at regular intervals along the glass slide near the substrates, to provide a mask which could then be lifted off after deposition to create a well-defined edge along which film thickness could be measured. Some results of this experiment are shown in Fig. 5. The film deposited at 10° off the plume axis obviously has much more material than the one deposited at 40° off axis. The particulate nature of the film is evident in both Fig. 5A and Fig. 5B; the visible structure of the films is dominated by particles in the 0.1 to 1.0 μm size range, believed to have been ejected from the target surface during laser irradiation. Venekatesan et al.[6], have noted a cosine dependence of the fine grained component of film thickness for geometries of the type in Fig. 4, and interpret this as due to thermal evaporation. With extended material removal from the target, the cone of particle ejection eventually becomes somewhat narrowed due to the collimating effect of the crater walls, leading to an increased concentration of coarse material near the plume axis.

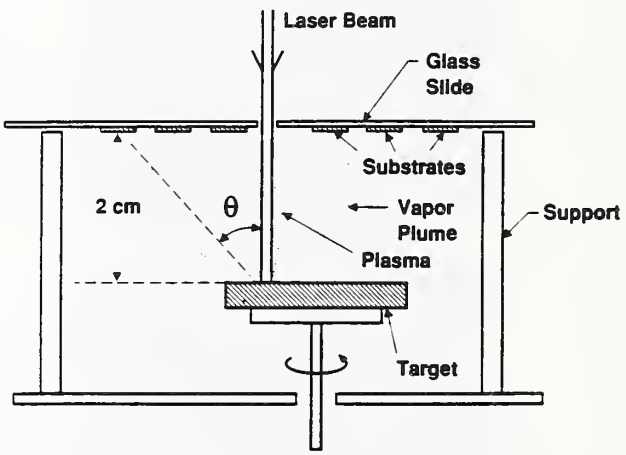

Figure 4. Experimental set-up for studying film deposition as a function of substrate position.

Based on data of the type in Fig. 5, the maximum $Ba_2YCu_3O_x$ film deposition rate, which occurs at the substrate position nearest the beam and plume axes in Fig. 4 is ~1.0 - 2.0 μm/hr. Deposition rates further off-axis are difficult to measure because of the discontinuous nature of the particulate coverage. The comments thus far have applied chiefly to the particulate deposits; as noted below, there is evidence for a smaller sized fraction, as well.

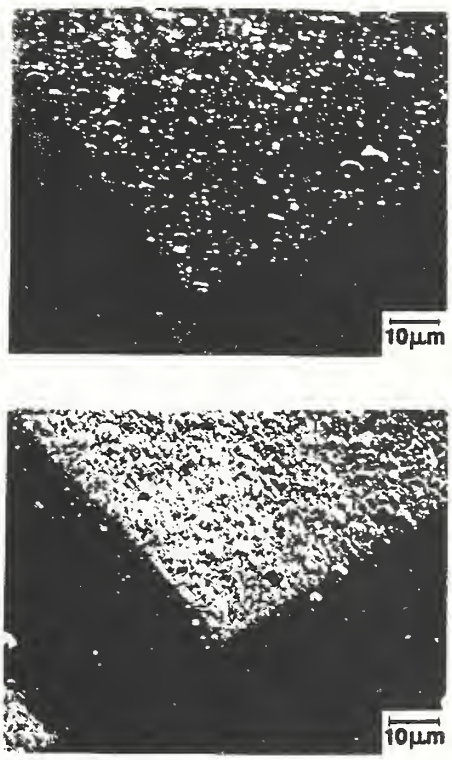

Figure 5. Results of 2 hr $Ba_2YCu_3O_x$ laser deposition experiment, after removal of masking grids. A) $\theta = 40°$, B) $\theta = 10°$.

Evidence for Two Depositional Modes

In certain areas, when TEM grids used for the masking experiments in Fig. 5 were removed, a very thin, coherent layer was observed at the point of detachment (Fig. 6). This film was analyzed by EDX with difficulty, due to its thinness, but was observed to have a composition indistinguishable from the rest of the deposit. The particle sizes in this material are below the limit of resolution in the SEM (~6 nm). Upon further observation, it was noted that the fine grained material had penetrated under the TEM grids in areas where they were not firmly bonded to the substrate surface by carbon cement. This implied that it should be possible to prepare a thin film free of the coarser ejecta and composed entirely of fine particles, simply by utilizing line-of-sight screening of the coarser material. This was in fact confirmed by experiments in which carbon planchets were suspended in the plasma and carbon-film covered TEM grids were placed on the shielded back side of the planchets to collect material from the plume. Fig. 6C shows a TEM micrograph of condensate collected in such an experiment within a 10 min. period. No evidence of the coarser particles was noted. The film is estimated to be ~50 nm thick, and the implied deposition rate is ~300 nm/hr. The fine particles are notably uniform in size (avg. dia. ~5 nm). As deposited they are amorphous; however they become

crystalline under electron beam irradiation. EDX spectra are qualitatively indistinguishable from bulk $Ba_2YCu_3O_x$. In another experiment, a series of planchets was strung along a wire and suspended so as to sample the vapor plume radially over a distance of 2.5 cm. EDX spectra taken from the fine grained material on the shielded side of the planchets were indistinguishable from each other the entire 2.5 cm length. Although the chemistry of the fine grained deposits may not vary dramatically, thickness is usually sharply gradational, and such gradations are usually symmetrical relative to the vapor plume and any obstructions, such as support assemblies, it has flowed around. Quite probably, it is variations in thickness of the fine-grained component of the laser-deposited films which are responsible for the interference fringes commonly observed.

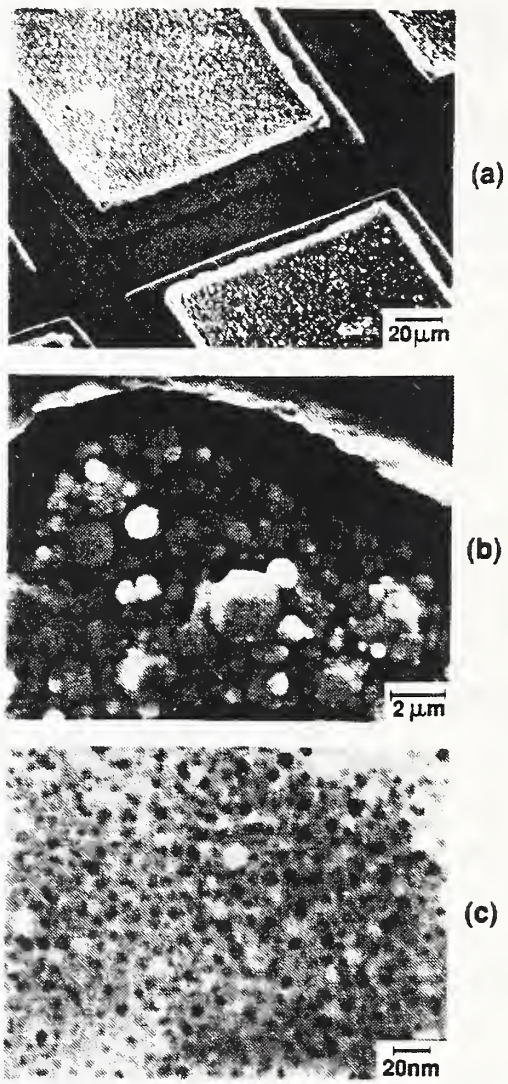

Figure 6. Microstructure of fine-grained component of masked $Ba_2YCu_3O_x$ film. A) Pattern after grid removal. Note upturned film edges. B) Edge of masked area at higher magnification. C) TEM micrograph of film shielded from coarser ejecta.

Effect of Annealing

Read camera x-ray diffraction analysis of as-deposited $Ba_2YCu_3O_x$ films showed a general lack of crystallinity; these films also showed a very high room temperature resistivity. Annealing for 10 min. at 910°C in air yielded material with ESCA and x-ray diffraction patterns similar to those of bulk $Ba_2YCu_3O_x$, with a room temperature resistivity which was essentially metallic. The film resistivity could not be made superconducting at any temperature down to 20K, however, despite

extended annealing in oxygen at 500-600°C. Comparative microstructures of as-deposited and annealed films are shown in Fig. 7. As Fig. 7 shows, the sintering process of these films is associated with development of a honeycombed structure, presumably as the fine grained component shrinks differentially around the larger particles during sintering. There are several possibilities for the lack of superconductivity. If the fine grained component were slightly off stoichiometry, then the film would contain isolated islands of superconducting phase (coarser ejecta) surrounded by a web of the nonsuperconducting fine component. Also it could be that a small amount of Ba/CO_2 reaction prior to the annealing step could prevent the superconducting stoichiometry from being completely maintained during annealing. Finally, if the entire film were superconducting, it is possible that the interconnecting bridges of fine material are so narrow the critical current density is exceeded, with resultant quenching of the superconductivity. Independent measurements of the superconducting properties of the films were carried out using the a.c. magnetic susceptibility method, and the results indicate that the percentage of the superconducting phase is very small, thus, eliminating the first and last possibilities, and emphasizing the need for careful control of post-depositional processing. It is significant in this respect that, to date, most successful experiments with $Ba_2YCu_3O_x$ have involved heated substrates [12-15].

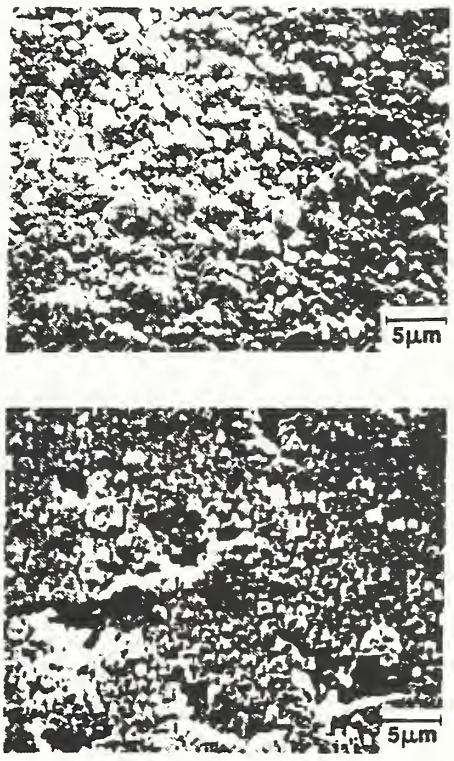

Figure 7. Effect of annealing on $BaYCu_3O_x$ film. A) As-deposited. B) After 910°C, 10 min. anneal.

Laser Deposition of Other Ceramics

As indicated in Table 1, although the major part of the study has centered on $Ba_2YCu_3O_x$, other targets were also used for laser deposition experiments. Thin

films of yttria/zirconia and Al_2O_3 on MgO, and MgO, on sapphire, were prepared. In the SEM, apart from scattered particles (presumably ejecta) of 0.05 to 0.25 μm size, these films were virtually featureless and their presence could be established mainly by the appropriate lines in the EDX spectrum. The lack of coarser particles was most notably true of the yttria/zirconia films. Films were colorless and it is assumed that the elements were present as oxides. The films which were examined by x-ray diffraction showed no crystalline pattern other than the substrate. These films appear to be composed dominantly of the finer-grained type of deposit noted above.

By contrast, the lead zirconate titanate (PZT) and mullite films show considerable SEM-resolvable microstructure (see Fig. 8). The microstructure of the as-deposited PZT film in Fig. 8A resembles that of the as-deposited $Ba_2YCu_3O_x$ film in Fig. 7A, in that both are characterized by a large number of particles in the 0.1 - 1.0 μm size range, although the PZT particles are strongly grouped near the lower end of this range. As deposited, the PZT film is amorphous; however, a 10 min. anneal at 900°C produces a material with an x-ray diffraction pattern nearly identical to that of the target. The shrinkage on sintering observed for $Ba_2YCu_3O_x$ does not appear to be nearly as great for PZT, however. The mullite target produces a film characterized by much less abundant ejecta (Fig. 8B), presumably indicating a higher percentage of the finer-grained film component. Melting of the mullite ejecta is clearly indicated by their shape; these may have originated in part from glassy matrix material in the target (see Table 2).

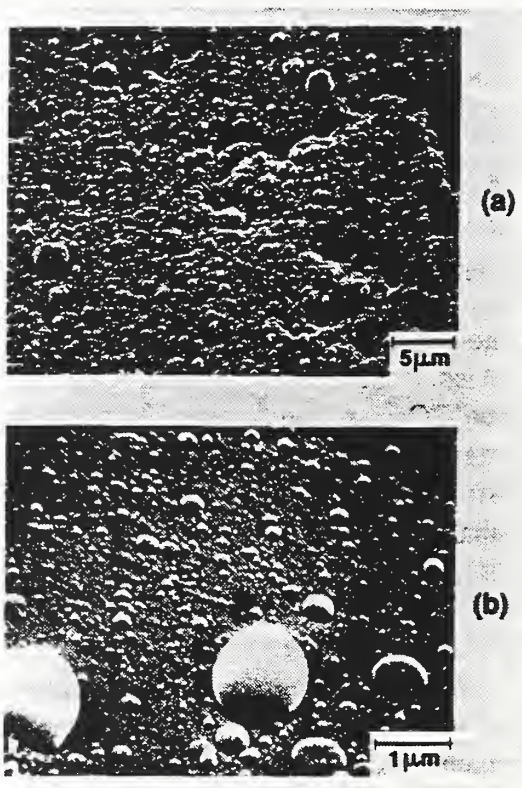

Figure 8. Microstructure of other ceramic films. A) PZT as deposited. B) Mullite as deposited.

Fig. 9 shows the spatially and time-resolved emission spectra from the plume

above a PZT target irradiated by the focused 1.06 μm laser beam. A horizontal 0.5 mm slit was used in front of the OMA's vertical entrance slit to obtain the spatial resolution. The imaging lens was translated vertically to image the plume 10.0 mm above the target surface on the horizontal slit. Spectral features attributed to doubly ionized Ti and Zr appear at the early times after the laser (nominally at 200 ns). The dominant spectral features which appear in Fig. 9 at later times are due to slower-moving, singly-ionized Zr and Ti. Identification of spatially and time-resolved spectral features is aided by analysis of plume emission from Ti, Zr, and Pb pure targets.

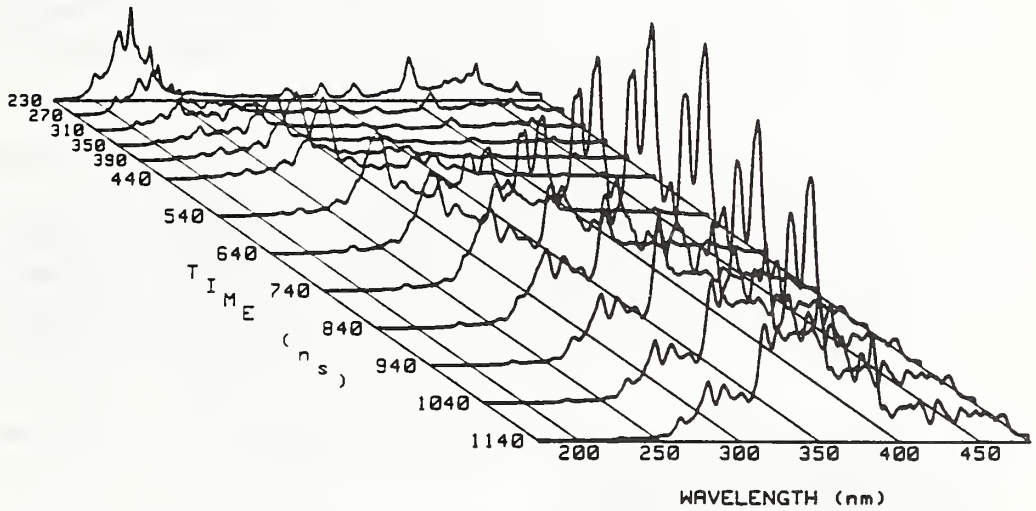

Figure 9. Time-resolved optical emission spectra of the laser generated plume from a PZT target from 10-10.5 mm above the surface. The laser is on at 200 ns.

DISCUSSION

The present results indicate that the vaporization and ejection of vapor species by laser heating and excitation can produce both equilibrium and non-equilibrium effects. Vapor plume formation is non-homogeneous, both in space and time. Fast, very hot, non-equilibrated ions result from ions produced, preferentially, on-axis early in the laser-surface interaction phase. These ions are accelerated by the laser driven plasma formed just above the surface. On-axis hot neutrals are also formed prior to the full development of an expansion-cooled plume jet. At later sampling times, and with off-axis sampling, only cool neutrals are observed.

Our experiments have confirmed that the films formed by the laser deposition process consist of two components, a relatively coarse fraction in the range 0.1 - 1.0 μm, believed to have been physically ejected from the target, and a much finer-grained fraction ($<$ 10 nm), which may represent plasma condensation. The thickness of the former is largely determined by geometrical factors having to do with the ability of projectiles to escape from the target surface. Hence the coarse material can be effectively eliminated by line-of-sight shadowing, if desired. The thickness of the fine-grained component may vary according to a number of factors as the vapor plume penetrates the space above the substrate; these factors include the presence of an electrical field, and the substrate temperature. From results to date, the bulk chemistry of the finer-grained deposits does not appear to vary substantially with radial distance in the plume; however, additional observations are needed to bear this out fully.

It is perhaps significant that some materials yield a much higher percentage of the coarser fraction than others. While the melting temperatures of Al_2O_3, MgO, and yttria stabilized zirconia are all high relative to the materials which form abundant ejecta, this alone doesn't appear to be the causative factor, as separate experiments with gold targets (to be reported elsewhere) show that despite extensive target melting (Au melts at 1063°C), no discernible ejecta are deposited on the substrate surface. However it should be noted that $Ba_2YCu_3O_x$, PZT, and possibly, mullite, are all incongruently melting compounds, and so there is a possibility that this aspect of the melting behavior could be a factor.

A mechanism for formation of the ejecta can be proposed as follows. With reference to the idealized time-temperature plot in Fig. 10, it is assumed that post-pulse cooling of the target is slow relative to heating. Thus, referring to incongruently-melting target compound AB in the schematic phase diagram, if surface temperature were to remain in the AB + liquid field of Fig. 10 sufficiently long during post-pulse cooling for the higher-melting compound A to form, this phase could be metastably retained on the target surface as a microheterogeneity when the residual melt crystallizes. This is thought to be a plausible interpretation of the type of feature in Fig. 11, which according to this hypothesis, might be a region composed of BaY_2CuO_5 (bright round area at top of multiphase region) and quenched melt (dark area at base of region), a combination resulting from the incongruent melting behavior of $Ba_2YCu_3O_x$[16].

Upon the next pass of the laser over this area it is likely that the feature could result in an ejectum, as the lower melting material at the base becomes vaporized,

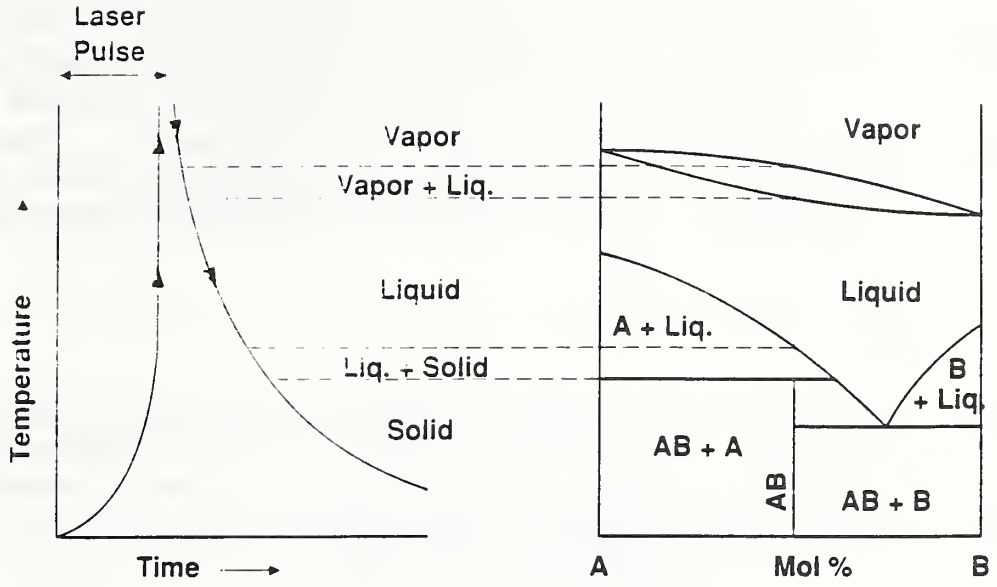

Figure 10. Proposed Mechanism for origin of ejecta in incongruently melting systems. As surface of compound "AB" cools, local phase separation occurs, which persists, leaving micro-inhomogenieties which influence subsequent laser/target interaction.

propelling the more refractory part of the globule away from the surface. Since target features of the type seen in Fig. 11 are close in size to ejecta deposited on the substrate, it is possible that the coarser fraction of the film deposits may have originated in part in this fashion. Further examination of incongruently vs. congruently melting target materials will evaluate this possibility. It is also possible that laser action on multicomponent targets has a tendency to produce microheterogeneities, regardless of melting behavior, due to the inevitable differential volatility of the components involved.

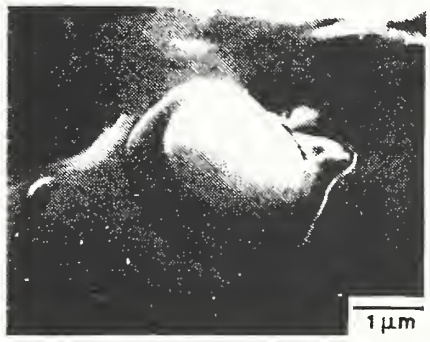

Figure 11. SEM micrograph of possible ejectum precursor on laser-irradiated $Ba_2YCu_3O_x$ target surface.

Future studies are planned to determine more precisely the relation between target properties and film microstructures. Also, the effect of post depositional annealing, perhaps in conjunction with heated substrate experiments, is a necessary area of investigation. Since the electronic properties of thin films depend in a crucial way upon microstructure and microchemistry, efforts aimed at understanding how these features are related to the basic physics and chemistry of the vapor plume will be pursued, including the use of time and spatially resolved optical spectral analysis.

ACKNOWLEDGEMENTS

The authors wish to thank Dr J. Kelly for providing EDX analyses. Dr. C. Ostertag has given useful comments on the sintering and microstructure. Dr. John Blendell provided the yttria-stabilized zirconia target used in the experiments, and Mr. M. Hill fabricated the $Ba_2YCu_3O_x$ target. Dr. L. Bennett provided the a.c. magnetic susceptibility measurements.

REFERENCES

1. W.W. Duley, "CO_2 Lasers: Effects and Applications", Academic Press, New York, 1976.

2. W.W. Duley, "Laser Processing and Analysis of Materials", p. 171-172, Plenum Press, New York, 1983.

3. H.M. Smith and A.F. Turner, "Vacuum Deposited Thin Films using a Ruby Laser", Appl. Opt., 4 [1], 147-148 (1965).

4. H. Sankur and R. Hall, "Thin-Film Deposition by Laser-Assisted Evaporation", Appl. Opt. 24 [20], 3343-3347 (1985).

5. J.G. Bednorz and K.A. Muller, "Possible High T_c Superconductivity in the Ba-La-Cu-O System", Z. Phys. B, 64, 189-193 (1986).

6. T. Venkatesan, X.D. Wu, A. Inam and J.B. Wachtman, "Observation of Two Distinct Components During Pulsed Laser Deposition of High T_c Superconducting Films", Appl. Phys. Lett., 52 [14], 1193-1195 (1988).

7. P. Krehl, F. Schwirke and A.W. Cooper, "Correlation of Stress-Wave Profiles and the Dynamics of the Plasma Produced by Laser Irradiation of Plane Solid Targets", J. Appl. Phys., 46 [10], 4400-4406 (1975).

8. G. Shen and E.S. Yeung, "A Spatial and Temporal Probe for Laser-Generated Plumes Based on Density Gradients", Anal. Chem., 60 [9], 864-868 (1988).

9. M.H. Read , 27th Annual Pittsburgh Diff. Conf., November, 1964.

10. U. Sudarsam, N.W. Cody, M.J. Bozach and R. Solanki, "Excimer-Laser-Induced Sputtering of $YBa_2Cu_3O_{7-x}$", J. Mater., Res., 3 [5], 825-831 (1988).

11. P.K. Schenck, D.W. Bonnell, and J.W. Hastie, "In situ Analysis of Laser-Induced Vapor Plumes", Am. Vac. Soc., Proc. Joint Int. Laser Science and Am. Vac. Soc. Conf., Atlanta, October, 1988 (in Press).

12. J. Narayan, N. Biunno, R. Singh, O.W. Holland, and O. Auciello, "Formation of Thin Superconducting Films by the Laser Processing Method", Appl. Phys. Lett., 51 [22], 1845-1847 (1987).

13. L. Lynds, B.R. Weinberger, G.G. Peterson, and H.A. Krasinski, "Superconducting Thin Films of Y-Ba-Cu-O Produced by Neodynium: Yttrium Aluminum Garnet Laser Ablation", Appl. Phys. Lett. 52 [4], 320-322 (1988).

14. H.S. Kwok, P. Mattocks, L. Shi, X.W. Wang, S. Witanachchi, Q.Y. Ying, J.P. Zheng, and D.T. Shaw, "Laser Evaporation Deposition of Superconducting and Dielectric Thin Films", Appl. Phys. Lett., 52 [21], 1825-1827, (1988).

15. A. Inam, M.S. Hegde, X.D. Wu, T. Venkatesan, P. England, P.F. Miceli, E.W. Chase, C.C. Chang, J.M. Tarascon, and J.B. Wachtman, "As-Deposited High-T_c and T_c Superconducting Thin Films Made at Low Temperatures", Appl. Phys. Lett., 53 [10], 908-910 (1988).

16. R.S. Roth, C.J. Rawn, F. Beech, J.D. Whitler and J.O. Anderson, "Phase Equilibria in the System Ba-Y-Cu-O-CO_2 in Air", p. 12-26 in "Ceramic Superconductors II", M.F. Yan, ed., Amer. Ceram. Soc., Westerville, OH 1988.

LEAD ZIRCONATE-TITANATE THIN FILMS PREPARED BY THE LASER ABLATION TECHNIQUE

C. K. CHIANG*, L. P. COOK*, P. K. SCHENCK*, P. S. BRODY** AND J. M. BENEDETTO**
*National Institute of Standards and Technology
Gaithersburg, MD 20899
**Harry Diamond Laboratories
Adelphi, MD 20783

ABSTRACT

Lead zirconate-titanate (PZT) thin films were prepared by the laser ablation technique. The PZT (Zr/Ti=53/47) target was irradiated using a focused q-switched Nd:YAG laser (15 ns, 100 mJ at 1.064 μm). The as-deposited films were amorphous as indicated by X-ray powder patterns, but crystallized readily with brief annealing above 650°C. The dielectric constant and the resistivity of the crystallized films were studied using a parallel-plate type capacitor structure.

INTRODUCTION

Recently, there has been a renewed interest in the growth of ferroelectric thin films for potential use in non-volatile memories and other devices. The laser ablation technique, in which a plume of ionized and ejected material is produced by high intensity laser irradiation of a solid target,[1,2] offers several advantages for film deposition, e.g., no inherent limitations on substrate materials and deposition conditions.[3] It is also a technique that can be easily integrated into semiconductor processing. We have applied the laser ablation technique to produce various thin films including barium titanate and lead zirconate-titanate (PZT) thin films.[3,4] In this paper we report the x-ray, microstructural and electrical characterization of PZT thin films from a PZT (53/47) ceramic target.

EXPERIMENTAL

Thin Film Preparation

To prepare lead zirconate-titanate thin films by the laser ablation technique, a PZT (Zr/Ti=53/47) target was irradiated using a focused q-switched Nd:YAG 20 Hz pulsed laser with a typical pulse width of 15 ns. For the present studies, the 1064 nm wavelength was used, with energies of ~100 mJ focused to a ~250 μm diameter. The reaction chamber was continuously evacuated to < 1 mTorr by oil free pumps. During deposition, oxygen was bled into the chamber to produce a background pressure of 100 mTorr. Sample targets were mounted on a continuously rotating shaft to minimize cratering effects. A stationary substrate holder was used to hold substrates (Pt or Pt-coated Si, typically 7 mm by 15 mm) directly over the target surface at distances > 2.0 cm from the target surface. The growth rate of the film was typically 1-2 microns per hour. The average thickness of the films was about 1-2 μm, as measured by profilometry.

Mat. Res. Soc. Symp. Proc. Vol. 200. ©1990 Materials Research Society

Film Characterization

X-ray diffraction patterns were measured for the as-deposited PZT films as well as for the films after heat treatment. Conventional scanning electron microscopy was used to examine the microstructure of the films. More detailed analysis of these films will be reported elsewhere.

Electrical Measurements

The resistivity and the dielectric constant of the bulk PZT thin films were calculated from the impedances using the Cole-Cole relation.[5] The impedances were measured using an automated Hewlett Packard 3570A network analyzer[6] for the frequency range from 100 Hz to 13 MHz. The hysteresis loop was measured using a balanced Sawyer-Tower circuit operated at 10 kHz. The electrodes were sputtered platinum. The electrode sizes for the impedance measurements and the hysteresis loop measurements were 0.16 cm^2 and 5.0 x 10^{-4} cm^2, respectively.

RESULTS AND DISCUSSION

A micrograph of a PZT thin film prepared by the laser ablation technique is shown in Figure 1. The surface structure is dominated by particles with diameters between 0.1 μm and 1.0 μm. These particles originated as melted or partially melted material which was physically ejected from the target.[3]

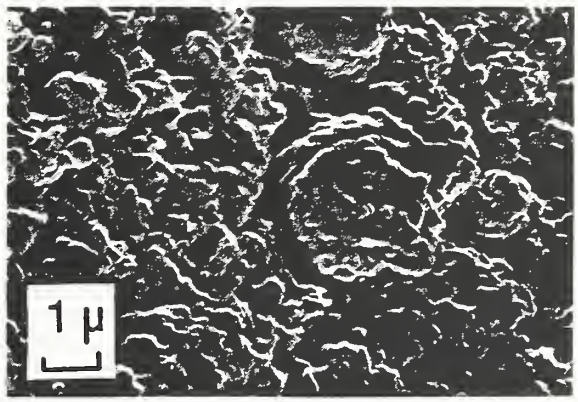

Fig. 1 The PZT ceramic film by the laser ablation technique.

The as-deposited films were amorphous but crystallized readily with heat treatment above 650°C. An x-ray diffraction pattern for a film subject to post-depositional annealing at 800°C is shown in Figure 2. This pattern suggests cubic PZT has formed rather than the tetragonal PZT expected from the phase diagram, although, as will be described below, the presence of ferroelectric properties indicates that at least a fraction of the material must be non-cubic. Possibly, line-broadening due to small crystallite size obscures the tetragonal splitting in these materials. The films were analyzed microchemically by EDX

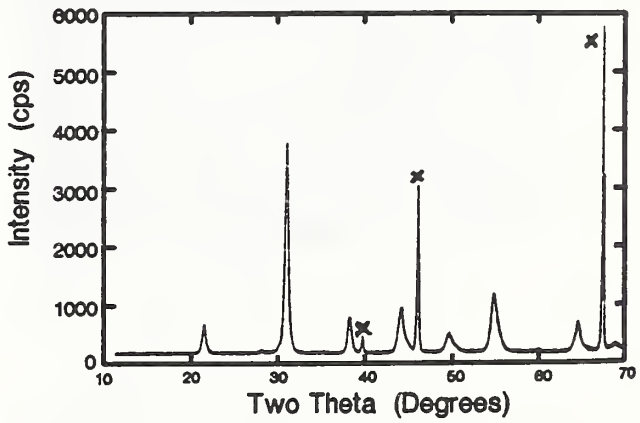

Fig. 2 X-ray diffraction pattern of PZT ceramic film. "x" refers to the lines from the platinum substrate.

and were found not to vary appreciably in their chemistry across their central 2 cm portion. The composition of the film was the same as or very close to that of the original target. Based on this analysis, we believe that the cubic x-ray pattern may result from the stress and restriction of the small particles in the very thin film.[7]

Figure 3 shows the Cole-Cole plot of the ac impedance of a PZT film after one hour annealing at 850°C in air. In this type of plot, the extent to which the arc falls short of being a complete half circle is an indication of the presence of inhomogeneities. The depressed impedance arc indicates that the film indeed does have regions of inhomogeneity.[8] The

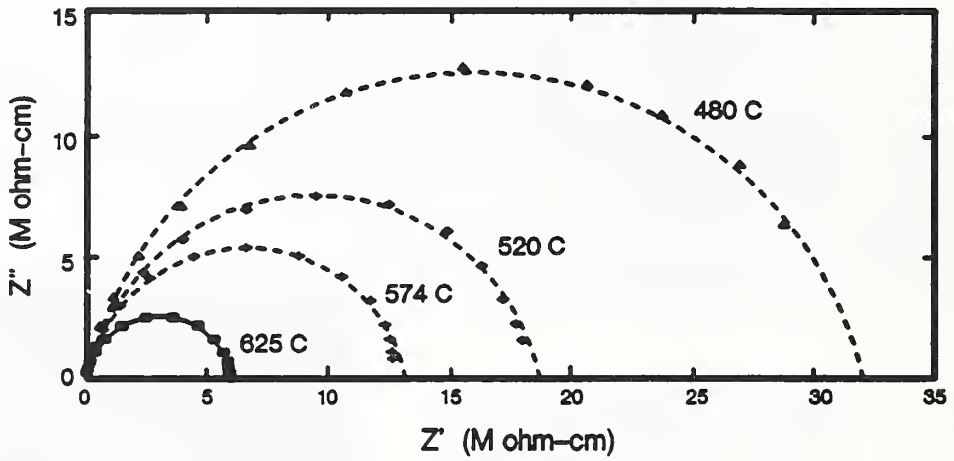

Fig. 3 AC impedance of the PZT film; the dashed lines are the results of a Cole-Cole fit.

depression angles found in the temperature range that a complete arc were measured varied from 19° at 480°C to 15° at 625°C. These relatively large depression angles are usually interpreted as due to the different relaxation effects caused by the inhomogeneities in the sample.[8] One of the sources of the inhomogeneities is the extensive porosity seen in the Figure 1.

The dc resistivity of the PZT film was calculated from impedance data shown in Figure 3. The temperature dependence of the resistivity is shown in Figure 4. The change of temperature dependance near 480°C is usually attributed to the cross over from grain boundary dominated resistivity to the grain dominated resistivity.[8] By extrapolating the fitted line (Fig. 3) to room temperature we obtained a

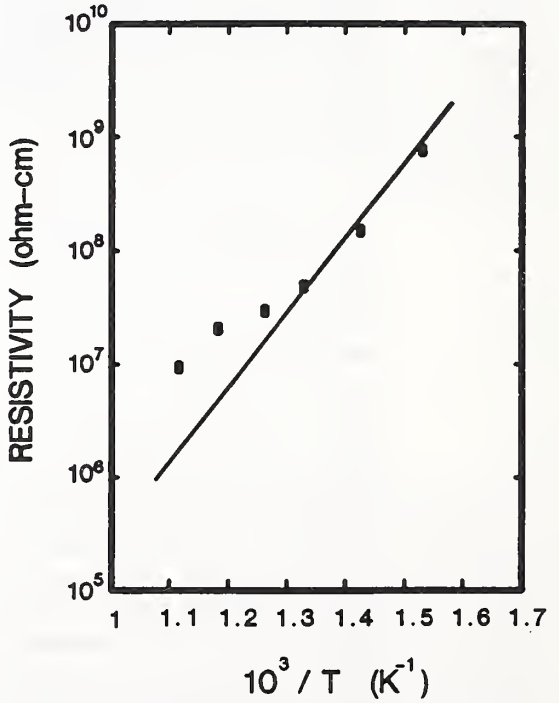

Fig. 4 DC resistivity of PZT ceramic film as a function of inverse temperature.

resistivity of 8 x 10^{20} ohm-cm. Using 1 x 10^{18} ohm-cm for bulk resistivity of PZT at room temperature, we estimated the effective geometric correction factor (defined as the ratio of observed resistivity to that of the bulk for the same material) to be 800.

The dielectric constant was calculated by fitting the complex impedance spectra to a Cole-Cole arc.[5] From 480°C to 625°C we obtain a dielectric constant of 2.5 to 3.5 for the PZT film. The dielectric constants can also be calculated using a simple RC parallel equivalent circuit to examine the frequency dependence. The frequency dependence of the dielectric constant at 209°C, 329°C, 425°C, 625°C and 672°C is shown in Figure 5. The dielectric constant observed at low frequency and low temperature is 2. Since these apparent dielectric constants are deduced from the same impedance data as the resistivities, we can use the same geometric factor obtained from resistivity discussed above. Thus, we obtain a dielectric constant of 1600 to 2800 for the PZT film after geometric correction.

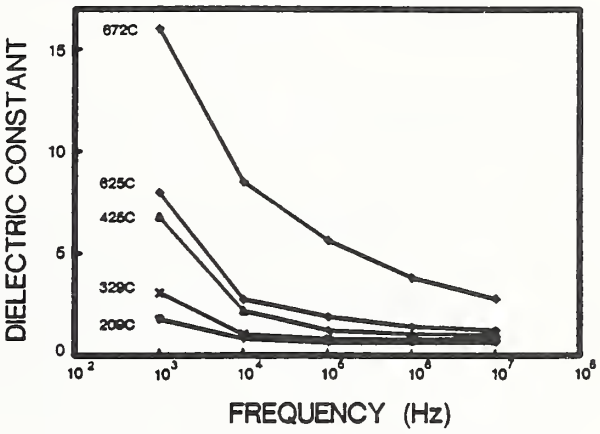

Fig. 5 Frequency dependence of the dielectric constants of PZT film.

For practical applications the most important feature of these laser ablated PZT films is the presence of ferroelectric hysteresis, as demonstrated in Figure 6. Hysteresis measurements were done with electrodes of 0.25 mm diameter. The dielectric constant calculated from these measurements is about 600. The remanent polarization is 0.036 C/m^2. These values are approaching those of the bulk material. The difficulty in interpreting the impedance data is thus attributed largely to microstructural discontinuities and variations in thickness. Both factors could distort the impedance data. On other hand, the impedance data serves as a diagnostic tool for investigating the relationships between the properties of the film and its crystallinity, microstructure, and preparation conditions. For the present PZT films, further improvement of the microstructure is desirable, which can be achieved by varying the deposition conditions.

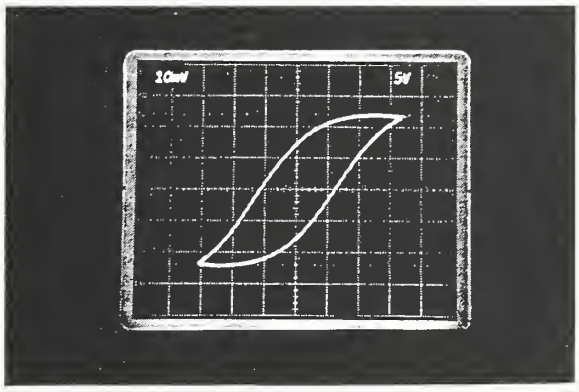

Fig. 6 Compensated hysteresis loop of a PZT thin film.

In summary we have produced lead zirconate-titanate ceramic thin films by the laser ablation technique. The X-ray diffraction patterns, electrical resistivity, dielectric constant and ferroelectric hysteresis were studied. Experimental evidence shows that the laser ablated lead zirconate-titanate ceramic thin films can have ferroelectric properties approaching those of the bulk material.

ACKNOWLEDGEMENTS

The authors would like to acknowledge helpful discussions with R. S. Roth, W. Wong-Ng, J. Zhao and D. W. Bonnell, and technical support from Marvin Wilke and Arthur Sessoms.

REFERENCES

1. P. Krehl, F. Schwirke and A.W. Cooper, J. Appl. Phys., 46 [10], 4400-4406 (1975).

2. P.K. Schenck, D.W. Bonnell, and J.W. Hastie, J. Am. Vac. Soc., Proc. Joint Int. Laser Science and Am. Vac. Soc. Conf., Atlanta, October, 1988 (in Press).

3. L. P. Cook, P. K. Schenck, J. Zhao, E. N. Farabaugh, and C. K. Chiang, Proc. Symp. on Ceramic Thin and Thick Films, Am. Ceram. Soc., (Apr. 1989)

4. P. K. Schenck, L. P. Cook, J. Zhao, E. N. Farabaugh, and C. K. Chiang, Proc. Symposium on Beam Solid Interaction: Physical Phenomena, Mat. Res. Soc., 157A, (1990)

5. K. S. Cole and R. H. Cole, J. Chem. Phys. 9, 341, (1941).

6. Certain commercial materials and equipment are identified in this article to specify the experimental procedure. In no instance does such identification imply recommendation or endorsement by the National Institute of Standards and Technology or imply that the material and equipment identified are necessarily the best available for the purpose.

7. P. Wurfel and I. P. Betra, Ferroelectrics, 12, 55, (1976)

8. C. K. Chiang, J. R. Bethin, A. L. Dragoo, A. D. Franklin and K. F. Young, J. Electrochem. Soc., 129, 2113, (1982).

LASER VAPORIZATION AND DEPOSITION OF LEAD ZIRCONATE TITANATE.

PETER K. SCHENCK*, LAWRENCE P. COOK*, JIANRONG ZHAO**, JOHN W. HASTIE*, EDWARD N. FARABAUGH*, CHWAN-KANG CHIANG*, MARK D. VAUDIN* AND PHILIP S. BRODY***
*National Institute of Standards and Technology, Gaithersburg, MD 20899
**Guest Scientist, Chinese Academy of Science, Beijing, Peoples Republic of China
***Harry Diamond Laboratories, Adelphi, MD.

ABSTRACT

Laser-induced vaporization of ceramics shows promise as a technique for the deposition of thin films of these materials. Critical to the utility of this technique is an understanding of the laser material interaction, plume formation and dynamics, material transport and how variations in the vaporization conditions effect the deposited film. Lead zirconate titanate (PZT, Zr/Ti~47/53) targets were irradiated using a q-switched NdYAG laser (15 ns, 100 mJ at 1.064 μm). The deposition chamber was maintained at a pressure of 100 mTorr oxygen. Material from the plume was collected on silicon wafer substrates, suspended 1.0 - 3.0 cm above the target. The films were characterized by SEM/EDX, TEM, x-ray diffraction and electrical measurements before and after annealing. Very thin films were deposited on carbon coated metal grids for observation in the TEM using a hot stage to study crystallization.

Temporally and spatially resolved spectra of the light emitted by the laser-generated plume were obtained with an optical multichannel analyzer (OMA) to yield information on the plume generation and chemistry of the deposition process. These spectra indicate that under these conditions a plasma is created above the target surface which persists for ~100 ns after the laser pulse.

EXPERIMENTAL

Deposition Apparatus

The Laser Deposition Facility consists of a high power pulsed laser system, deposition chamber, and ancillary analysis equipment. The laser used in this work is a NdYAG 20 Hz pulsed laser with a typical pulse width of 15 ns. Discrete wavelengths of 355, 532, and 1064 nm, with energies up to 200 mJ per pulse at 1064 nm, are available. For the present studies, the 1064 nm wavelength has primarily been used, with energies of ~100 mJ focused to a ~250 μm beam spot diameter.

The cylindrical deposition chamber is constructed of stainless steel and has internal dimensions of ~20 cm in diameter and ~8 cm high. The chamber is equipped with multiple ports for: mounting targets and substrates, laser access to the targets, and optical spectroscopic observations of the laser generated plumes. The reaction chamber is continuously evacuated to <1 mTorr by oil free pumps. Sample targets are mounted on a continuously rotating shaft to minimize cratering effects. The NdYAG laser is focused through an optical port onto the target using a 20 cm focal length lens.

Substrates are mounted in the deposition chamber by several methods. A stationary substrate holder has been used to hold substrates at distances > 2.0 cm from the target surface. Shorter deposition distances are obtained by mounting substrates directly over the target surface for line-of-sight deposition on a microscope slide with a hole to allow the focused laser beam to pass through to the target surface as shown in Fig 1. Substrates can also be attached to wires and suspended into the luminous regions of the plume for shadowed deposition as shown in Fig. 2. The shadowed deposition technique was generally used to prepare films for TEM observation. A heated substrate holder has been constructed, with geometry similar to that in Fig. 1. At present the maximum temperature attainable with this apparatus is ~450°C.

The background buffer/reaction gas pressure in the deposition chamber is

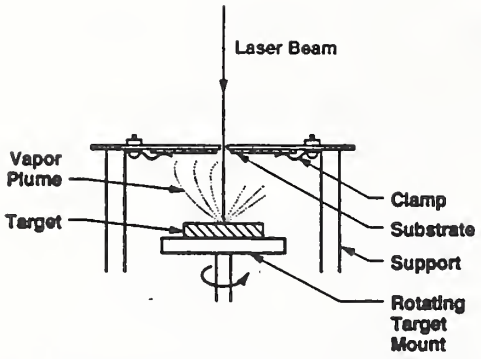

Figure 1 Line-of-sight deposition geometry for laser deposited thin films.

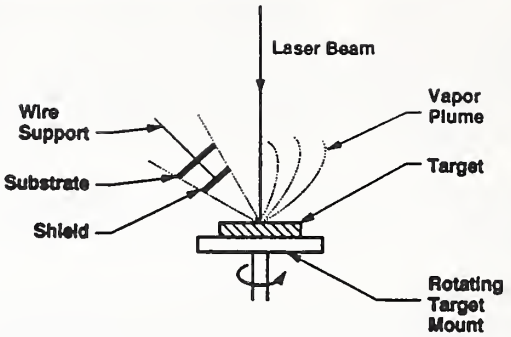

Figure 2 Shadowed deposition geometry for laser deposited thin films.

introduced through a needle valve from a ballast tank whose pressure is servo controlled to obtain the desired background pressure.

Side ports on the chamber allow for several line-of-sight optical access paths perpendicular to the laser-plume axis. Other side ports on the chamber are available for future access, such as electrical probing of the plume ions (e.g. as in [1]), optical probing of the plume particulates (e.g. as in [2]) and mass spectrometric analysis of the plume (e.g. as in [3]).

The laser target for the experiments reported here was a dense PZT of nominal Zr/Ti ratio 47/53 as supplied by a commercial source. The x-ray pattern of this material indicated only the presence of the well-crystallized tetragonal form.

Optical Spectroscopy

As shown in Fig 3., an optical multichannel analyzer (OMA) consisting of a multiple grating 0.275 meter monochromator with a gateable intensified photodiode array, is used to record the emission spectra of the plume, synchronous with the laser. A fused silica 10 cm focal length lens is used at twice its focal length to obtain one-to-one imaging of the plume on the entrance slit of the OMA. By aperturing the entrance slits of the monochromator with a 0.5 mm horizontal slit and moving the imaging lens (L2 in Fig. 3), the emission spectra from the plume can be spatially resolved.

The intensifier gate is set at 10 ns wide and is swept under computer control from before the laser onset to several hundred nanoseconds after the laser firing in order to time-resolve the plume emission spectra. The OMA controller averages the detector array output over 100 laser pulses and subtracts a previously stored dark current/background signal from the emission spectrum prior to transfer to the laboratory computer.

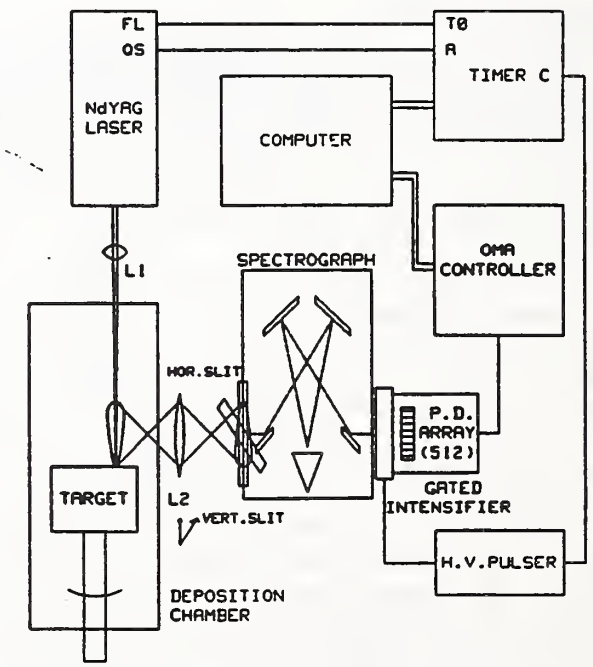

Figure 3 Schematic of apparatus for temporally and spatially resolved optical emission spectra of the laser induced plume.

Hot-Stage TEM Studies

To make specimens suitable for hot-stage transmission electron microscopy (TEM), 3 mm nickel grids coated with a carbon film were placed on the back side of a planchet in the plume for between 3 and 10 minutes; the planchet shielded the grids from the direct line-of-sight ejecta. The specimens were heated in the TEM hot-stage to temperatures in excess of 900°C. Conventional and diffuse-dark-field microscopy and electron diffraction were used to study the films during the heating experiments. Before and after the heating experiments the films were characterized by TEM and energy-dispersive x-ray analysis (EDX) using a beryllium specimen holder; the hot-stage was not suitable for the collection of x-ray spectra.

Electrical Measurements

The dielectric constant of the thin film was measured at 1 MHz. To determine the dielectric constant of the as-deposited films, we sputtered on a gold electrode. For the annealing runs interdigitized silver electrodes were painted on the as-deposited film. After the capacitance of the film was measured at room temperature, the whole film assembly was annealed at a higher temperature for 10 minutes. The film was removed from the furnace and air cooled to room temperature while the capacitance was measured. This procedure was repeated for the next annealing temperature.

RESULTS AND DISCUSSION

SEM and X-ray Characterization

A typical as-deposited film by the line-of-sight method is shown in Fig. 4 before annealing and in Fig. 5 after annealing. The films are about 1 μm thick. These films were analyzed microchemically by EDX and were found not

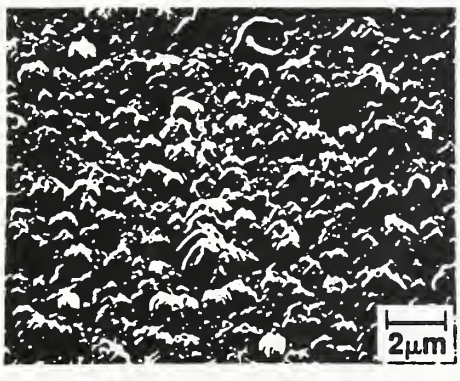

Figure 4 SEM micrograph of as-deposited line-of-sight film.

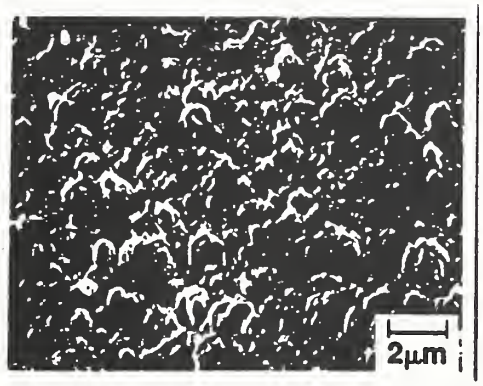

Figure 5 SEM micrograph of line-of-sight film after annealing.

to vary appreciably in their chemistry across their central 2 cm portion. These films are amorphous to x-rays in the as-deposited form , but they crystallize readily with a brief annealing at 750°C in air, giving an x-ray pattern having the proper two thetas for most of the reported PZT lines. However, it does not show the splitting required for tetragonal symmetry, and thus is probably cubic.

The microstructural changes accompanying the annealing are shown in Figure 5, where it can be seen that relative to the as-deposited film, some densification of the finer-grained fraction has occurred. While the as-deposited films are generally dark gray, with annealing, they take on lighter gray color which is similar to that of the target. The morphology of films deposited on a heated substrate (~450°C) differs subtly from that of the unheated substrate film in that the mass of material between the large particles is somewhat more dense. However, x-ray analysis shows no indication of PZT crystallization, and the as-deposited film is largely amorphous. Future experiments will utilize a new apparatus capable of moderately higher substrate temperatures.

According to the PZT phase diagram 47/53 composition thin films should become ferroelectric below 250-300°C. Thus we attempted to cause the material to transform from cubic to tetragonal by slow cooling, However efforts in this area were not successful. Future research will be focused to deal with this problem.

Optical Spectroscopy

Fig. 6 and Fig 7 show representative emission spectra from the laser-induced plume at 2.0-2.5 mm and 7.0-7.5 mm above the PZT target with a background pressure of 100 mTorr O_2. These spectra are part of a series of spectra taken with 0.5 mm spatial resolution in two dimensions relative to the laser impact point. The spectra were taken at each location at 10 ns intervals (near the time of the laser pulse) and 20 ns intervals (100 ns after the laser pulse). In Fig. 6 and Fig. 7 only every other spectra is plotted for clarity.

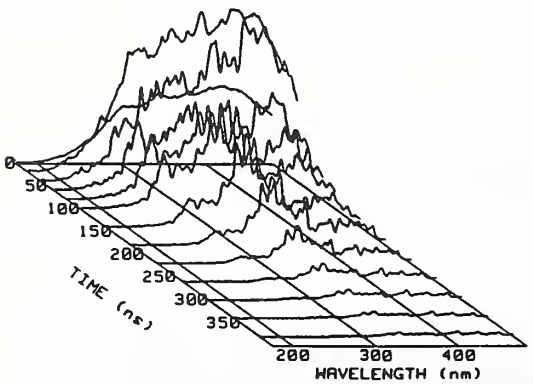

Figure 6 Time-resolved emission spectra from the laser-induced plume 2.0-2.5 mm above the PZT target (Scale:256048).

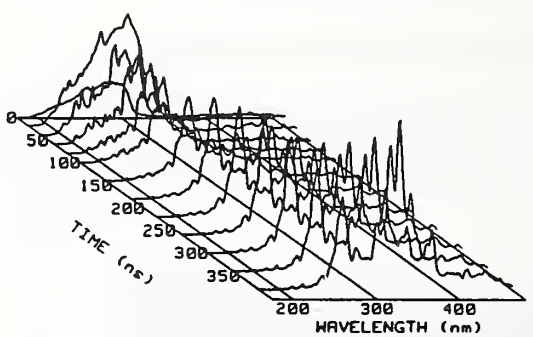

Figure 7 Time-resolved emission spectra from the laser-induced plume 7.0-7.5 mm above the PZT target (Scale:18186).

The PZT plume emission spectra were compared with emission spectra from laser-induced plumes above pure Ti, Zr, and Pb targets to aid in their analysis. The emission from the PZT targets is at early times (<100 ns) by emission from singly, doubly and triply ionized Ti and Zr, and with singly ionized Pb emission to a lesser extent. At longer times the spectra are due to singly ionized and neutral species. This is particularly true 7mm above the target surface, as in Fig. 7, compared to nearer the target surface. The strong ionic emission is consistent with the formation of a plasma extending from the laser impact point to about 12 mm above the target in the center of the laser-induced plume. The velocities of the various ionic and neutral species can be estimated from the most probable arrival times at various heights above the PZT target. The higher the state of ionization the faster the velocity of the species. Ti^{+++} and Zr^{+++} have velocities in excess of 10^7 cm/s. These velocities and those of the other ionic species present correspond to kinetic energies of from 50 to >100 ev. The role of these highly energetic species in the deposition process is unclear and

is under study by adjusting the laser fluence which in turn alters the ratio of higher ionized species to singly ionized/neutral species.

Hot-Stage TEM Studies

The as-deposited films consisted of ≈ 5 nm particles clustered in ≈ 50 nm aggregates (Fig. 8). Electron diffraction patterns show diffuse rings typical of amorphous or nanocrystalline material, with the strongest ring corresponding to a distance of 2.85 Å - 3.05 Å and weaker rings corresponding to 1.82 Å and 1.52 Å. Diffuse dark-field microscopy has not as yet been able to determine whether the films are truly amorphous, or nanocrystalline, or a mixture of amorphous and nanocrystalline phases. EDX spectra indicate the presence of Pb, Zr and Ti. Qualitatively the ratios of Pb:Zr:Ti appear to be close to 2:1:1, but accurate quantitative measurements remain to be done.

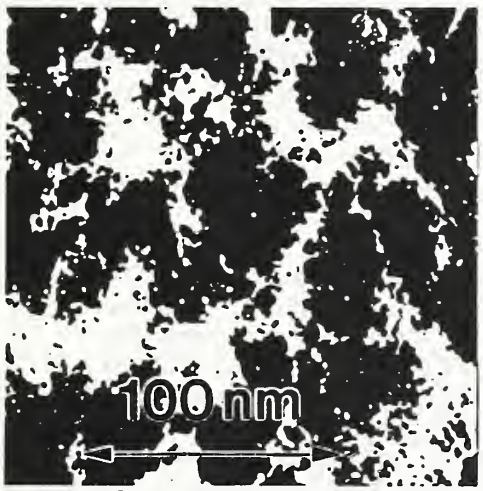

Figure 8 TEM micrograph of the as-deposited 5 minute film.

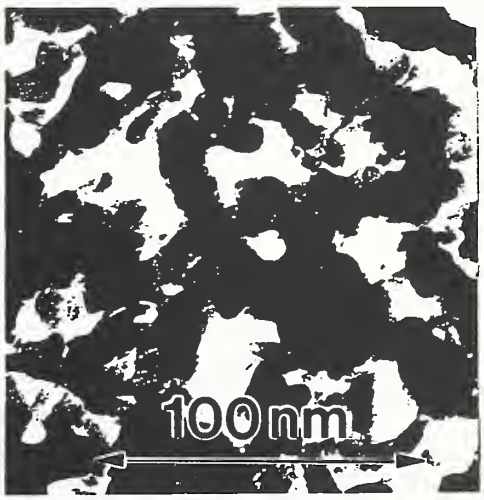

Figure 9 TEM micrograph of the 3 minute film heated above 775°C for 30 minutes.

On heating in the TEM to 775 ± 10°C, rings of sharp spots developed in the diffraction pattern. The more intense sharp rings were found to superimpose on the diffuse rings from the as-deposited film. The d-spacings calculated from the sharp spots matched tetragonal ZrO_2 (a_o = 3.64 Å, c_o = 5.27 Å). EDX spectra from before and after heating show that the lead content of the films has been reduced to a very low level by heating above 950°C, presumably by volatilization of the PbO in the vacuum of the TEM. The Zr to Ti ratio appears to have been very little affected by the heating. There were no significant differences between the 3 and 5 minute films except thickness.

Fig. 9 shows the microstructure of a 5 minute deposition film after heating to 800°C in the TEM; the film was above the crystallization temperature of 775°C for over 30 minutes. A continuous but open structure has been formed by the sintering together of rounded particles between 6 and 18 nm in diameter. The distinction between the crystalline ZrO_2 and the presumably amorphous TiO_2 particles is difficult because of the fine scale of this structure.

The as-deposited PZT film has been characterized in the TEM. One of the most important questions that remains to be answered is whether the as-deposited film is nanocrystalline. The volatility of lead precludes hot-stage TEM as a technique for observing the crystallization of these PZT films. However, the results of parallel studies show that the crystallization of less volatile films such as $BaTiO_3$ can probably be studied in-situ in the TEM. There is also potential for determining the sintering behavior of these fine particle films.

The resistivity of the as-deposited film was 2.5 x 10^6 ohm-cm. The low resistivity value suggests that the as-deposited film was not in its original PZT form. Fig. 10 shows the capacitance of the as deposited thin film being annealed. As the annealing temperature increases, the capacitance shows a minimum near 500°C. The capacitance increases when further increasing the annealing temperature. The capacitance transition may reflect the crystallization of the amorphous thin film.

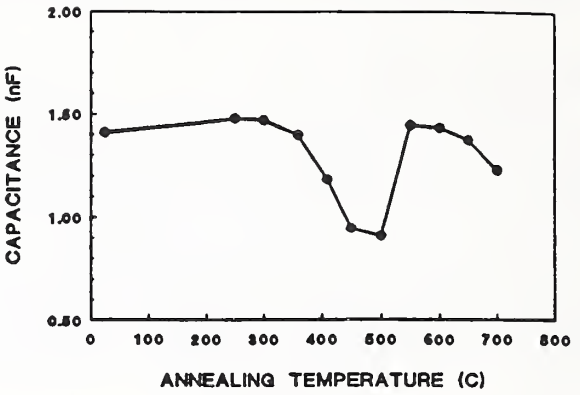

Figure 10 Capacitance of as-deposited PZT thin film during annealing.

CONCLUSIONS

As noted in an earlier study [4], there are two discrete particle size groupings in many laser deposited films: a coarser fraction in which particles range between ~0.1 and 1.0 μm and a finer fraction of <10 nm. The coarser fraction apparently originates as melted or partially melted material which has been physically ejected from the target; the finer fraction is believed to represent vapor condensate. The ejecta follow essentially a line-of-sight trajectory and can be prevented from reaching the substrate by use of a suitable barrier, whereas the vapor condensate forms on all surfaces in the vicinity of the target, regardless of whether they are facing the target. Thus there exists the possibility for controlling the particulate morphology over a wide range. As would be expected, the fine-grained fraction totally sinters readily, as confirmed by our TEM observations on PZT shadowed films. There would seem to be large potential for such fine-grained deposits in microelectronic processing, provided crystalline films can be with the correct stoichiometry.

ACKNOWLEDGEMENTS

The authors would like to acknowledge helpful discussions with David W. Bonnell and technical support from Marvin Wilke and Arthur Sessoms.

REFERENCES

1. P. Krehl, F. Schwirke and A.W. Cooper, "Correlation of Stress-Wave Profiles and the Dynamics of the Plasma Produced by Laser Irradiation of Plane Solid Targets", J. Appl. Phys., 46 [10], 4400-4406 (1975).
2. G. Shen and E.S. Yeung, "A Spatial and Temporal Probe for Laser-Generated Plumes Based on Density Gradients", Anal. Chem., 60 [9], 864-868 (1988).
3. P.K. Schenck, D.W. Bonnell, and J.W. Hastie, "Insitu Analysis of Laser-Induced Vapor Plumes", Am. Vac. Soc., Proc. Joint Int. Laser Science and Am. Vac. Soc. Conf., Atlanta, October, 1988 (in Press).
4. L. P. Cook, P. K. Schenck, J. Zhao, E. N. Farabaugh, and C. K. Chiang, "Ceramic Thin Films by Laser Deposition", to be published in Proc. Symp. on Ceramic Thin and Thick Films, April, 1989, ACerS.

MICROSTRUCTURAL CHANGES DURING PROCESSING OF LASER-DEPOSITED $BaTiO_3$ AND PZT THIN FILMS

L.P. COOK*, M. D. VAUDIN*, P. K. SCHENCK*, W. WONG-NG*, C. K. CHIANG*, and P. S. BRODY**
*National Institute of Standards and Technology, Gaithersburg, MD 20899
**Harry Diamond Laboratories, Adelphi, MD 20783

ABSTRACT

Thin films of $BaTiO_3$ and PZT (lead zirconate titanate, 47%$PbTiO_3$, 53%$PbZrO_3$) have been produced by laser irradiation of the appropriate ceramic targets and deposition of the ejected and vaporized material on planar substrates. The microstructural changes during thermal processing of these films have been studied by scanning electron microscopy/energy dispersive x-ray spectrometry (SEM/EDX), transmission electron microscopy (TEM), differential scanning calorimetry (DSC), x-ray diffraction (XRD), and by measurement of electrical properties. Films have been deposited using both Nd/YAG and excimer lasers and on unheated as well as heated substrates. Excimer films are considerably smoother than the Nd/YAG films, and the uniformity of the as-deposited microstructures is promoted by substrate heating. However, ferroelectric hysteresis loops were only observed for the considerably less smooth Nd/YAG PZT films; thermal treatment did little to improve the smoothness of these films. An excimer $BaTiO_3$ film deposited on a heated substrate showed crystallographic alignment and had a dielectric constant of ~100. Efforts are underway to combine the best features of films produced by both methods.

INTRODUCTION

The utility of laser deposition for preparation of ceramic thin films has become increasingly appreciated in the last few years [1], first with application to high T_c materials, and more recently for ferroelectric thin films [2,3,4]. The advantages of laser deposition have included: wide variety of possible solid targets, close compositional similarity of deposited films to targets, large selection of substrates and substrate deposition conditions, and high degree of flexibility in laser operating parameters, including wavelength, fluence, and both temporal and spatial variation in energy density. A major requirement is understanding of the materials science issues such as nucleation and crystallization, phase equilibria, sintering and grain growth in these films.

EXPERIMENTAL METHODS

Films were deposited using both Nd/YAG and excimer lasers. For the Nd/YAG films, typical laser operating conditions were: 20 Hz pulse rate, 15 ns pulse width, 100 mJ/pulse at 1064 nm, and fluence of ~300 J/cm^2. For the excimer films, operating conditions were: 10 Hz pulse rate, 23 ns pulse width, 200 mJ/pulse at 193 nm, and fluence of ~30 J/cm^2. The deposition chamber was maintained at a pressure of 100 mTorr (13 Pa) oxygen. Most films were deposited on substrates positioned 1.5-3 cm above the target. Substrates were generally either Pt-coated Si or pure Pt to facilitate electrical measurements. Targets were commercially prepared calcium-doped $BaTiO_3$, and PZT formulation "5A", consisting of 47%$PbTiO_3$, 53%$PbZrO_3$. During film depositions, the targets were rotated with the laser pulses to expose fresh material. Deposition times ranged from 5 min. (TEM specimens) to 1 hr. During the 1 hr runs as much as 5 μm of material was deposited on the substrate area closest to the source.

A few $BaTiO_3$ films were deposited on substrates heated resistively to dull red heat, estimated by optical pyrometry to be 700-800°C. Because of Pb volatility PZT films were annealed after deposition in a PZT cell. Films were examined by SEM/EDX and XRD using conventional methods. For the EDX analyses, standardless data analysis [5] allowed the estimation of relative elemental ratios as a function of position on the films. Real time backscattered electron diffraction patterns were obtained in the SEM from submicron areas of the surface of selected PZT films according to the methods described in [6]. DSC measurements were made on PZT thin films deposited on Pt; weight of the deposited film was ~0.5 mg. Dielectric and ferroelectric properties were measured using parallel plate capacitors formed between sputtered electrodes on the film surfaces and the underlying platinum-coated wafer [4]. Specimens for TEM examination, principally of excimer films, were prepared in two different ways. (1) Thin films were deposited directly on carbon films supported by copper grids; for some depositions the grids were attached with carbon or silver paint to a Pt/Si substrate which was held at dull red heat.

(2) Thin films were deposited directly on a heated Pt/Si substrate and 3 mm disks were cut from the substrate and thinned to electron transparency from the back side.

RESULTS

SEM/EDX

A marked difference was observed between the Nd/YAG and excimer films at magnifications obtainable in the SEM. Whereas the excimer films are virtually featureless at all magnifications, except for scattered ejecta, the Nd/YAG films have a much rougher surface dominated by ejecta in the range from 0.1 μm to a few μm in diameter. A less obvious component of the Nd/YAG films is a finely particulate (5-10 nm) fraction, observable principally by TEM [1,2], which appears to represent condensate from the vapor plume. This overall microstructure (Fig. 1a) is typical of both $BaTiO_3$ and PZT films deposited by Nd/YAG. EDX analysis of chemical variations in the Nd/YAG PZT films showed, within the limits of the method ($\pm$ 10% relative), no significant variation in the films with respect to Pb, Zr, Ti along a radial distance of 1 cm from the center (nearest the plume).

An attempt was made to improve the microstructure of the Nd/YAG PZT films by thermal annealing. Typical results are shown in Fig. 1-b. As is evident, the heat treatment results simply in coarsening of the microstructure as the amorphous as-deposited material crystallizes. This coarsening is manifested by an increase in pore size, which has accompanied sintering and growth of grains to a few tenths of a micron in diameter. Thus although a successful attempt was made to preserve Pb stoichiometry at annealing temperatures as high as 1100°C by controlling the Pb pressures as outlined above, no improvement in the density and smoothness of the film was achieved.

A relatively thick excimer PZT film annealed in air at 650°C was examined initially by reflected light microscopy. The film nearest the target was observed to consist of tightly-packed, equiaxed particles 5 to 10 μm in size; further from the target, the particles are 1 to 5 μm in size, round and dispersed in a homogeneous medium. Electron backscattered diffraction patterns were obtained in the SEM from these areas, and it was determined that each particle is a single crystal, and that the medium surrounding the dispersed particles is either amorphous or microcrystalline. EDX analysis of the crystals gave (normalized metal at.%): Pb-49, Zr-33, Ti-18. EDX of the surrounding medium showed Pb-37, Zr-41, Ti-22.

Powder x-ray diffraction analysis

As deposited, all Nd/YAG and PZT thin films prepared on unheated substrates were amorphous to x-rays. These films crystallized readily upon annealing at 500°C or less to yield x-ray patterns similar to those published (patterns 5-0626 and 33-784, ref. [7]). One important difference suggesting cubic symmetry is the lack of splitting of pseudocubic {00l} and {0kl} lines. In fact a 750°C anneal of Nd/YAG PZT could be indexed with a cubic cell of a_0 = 4.07 Å. A pattern for a similar material is shown in Fig. 2.

A series of Nd/YAG PZT films, part of which are indicated in Fig. 1, were heated at various temperatures in a cell designed to control Pb loss. Samples retained XRD patterns without peak splitting until >800°C. Above this temperature, peak splitting occurs giving patterns suggesting tetragonal symmetry, but which vary in detail from the published tetragonal PZT pattern for this composition (a complete investigation will be published elsewhere [8]). Curiously, these films exhibit ferroelectric hysteresis at temperatures below the observation of peak splitting, indicating the symmetry - while apparently cubic in terms of lack of observed peak splitting - cannot be strictly cubic in a crystallographic sense.

Thin films of $BaTiO_3$ deposited on a heated substrate at dull red heat give x-ray patterns without obvious evidence of splitting. Upon more detailed examination, they do show slight evidence of non-cubicity, as in the example of Fig. 3, which leads to a tetragonal cell of a = 3.993(1) and c = 4.013(3) Å. However these films are not ferroelectric.

Transmission electron microscopy

The PZT films deposited by excimer laser at room temperature on a carbon film were amorphous, very uniform and practically featureless, apart from some larger particles or ejecta 50 to 1000 nm in size, as shown in Fig. 4. Most of the ejecta appeared to have landing tracks that lead up to their ultimate resting place and are aligned in the same direction. The excimer $BaTiO_3$ films deposited at room temperature on carbon films (Fig. 5) were also amorphous; the microstructure was fissured and

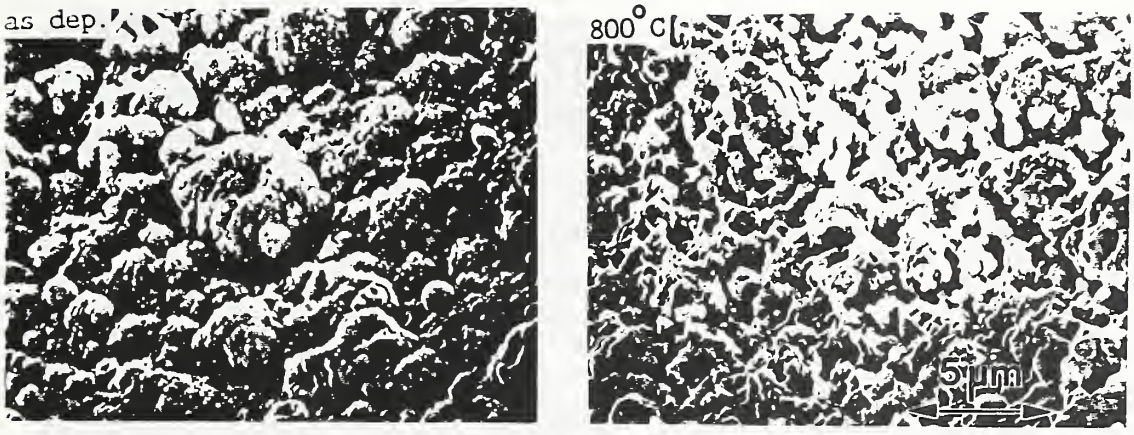

Fig. 1. SEM micrographs indicating effect of 800°C anneal on as-deposited Nd/YAG PZT films.

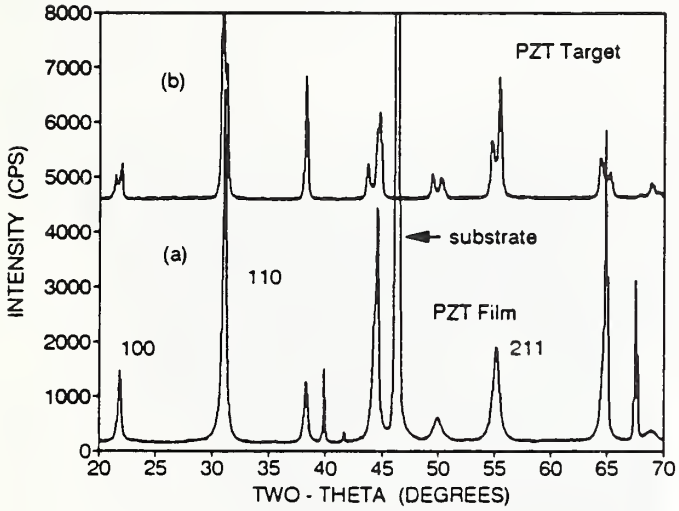

Fig. 2.a. XRD pattern of Nd/YAG PZT film annealed at 750°C (no peak splitting). b. Pattern of tetragonal target material for comparison.

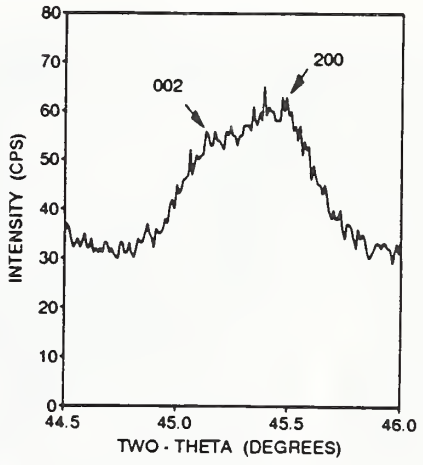

Fig. 3. XRD pattern of excimer $BaTiO_3$ film on heated substrate (Fig. 8) showing incipient peak splitting.

contained some larger ejecta 50 to 500 nm in size. A higher magnification micrograph (Fig. 6) of the same film shows that it has an open structure of low density and is composed of equiaxed particles 10 to 30 nm in diameter. The arrowed region of the $BaTiO_3$ film in Fig. 5 was heated with the electron beam and as can be seen it became smoother and denser but no crystallization was detected. Deposition of $BaTiO_3$ on a carbon film attached with carbon paint to a substrate at dull red heat produced a film that was uniformly dense (Fig. 7) and resembled the PZT films deposited on a room temperature carbon substrate. The carbon paint did not provide good thermal contact between the substrate and the film, which was therefore at a temperature intermediate between red heat and room temperature.

Beam heating of large ejecta in $BaTiO_3$ films deposited on both room and intermediate temperature carbon films caused both the ejecta and a region about 0.5 μm in diameter around them to crystallize to tetragonal $BaTiO_3$ of particle size 15-50 nm. Electron beam heating of the PZT film caused crystallization to a fcc fluorite structure with a_o = 5.05 Å as determined by electron diffraction; note that a_o for cubic ZrO_2 is 5.09 Å. EDX spectra showed that the Pb content of the film was reduced by beam heating. The crystallite size was in the range 10 - 100 nm. The $BaTiO_3$ deposited on a heated Pt/Si substrate was in the form of rod-shaped crystals with their long axes approximately normal to the plane of the film. The rods are 25 to 50 nm in diameter, but their length cannot be accurately determined as the specimen preparation may have reduced the thickness of the film; however, they are

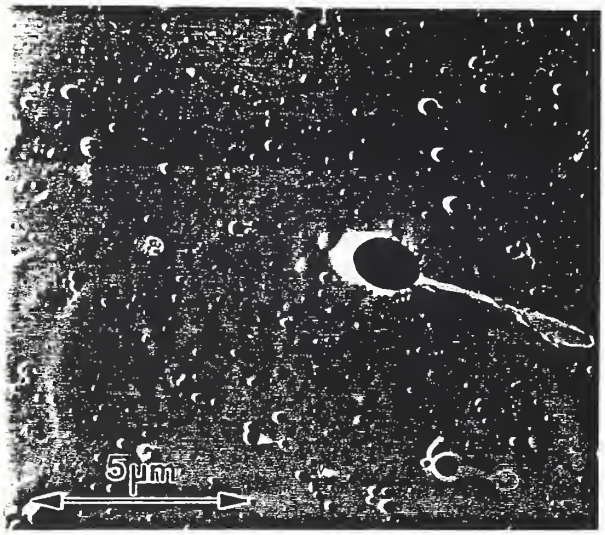

Fig. 4. TEM micrograph of excimer PZT on room temperature carbon film.

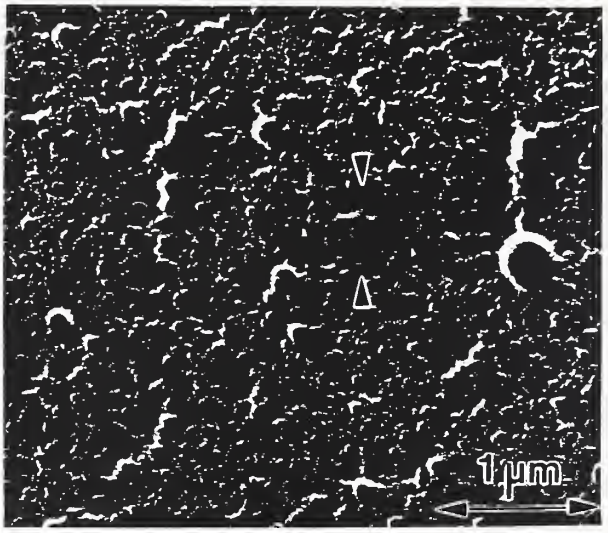

Fig. 5. TEM micrograph of excimer $BaTiO_3$ on room temperature carbon film.

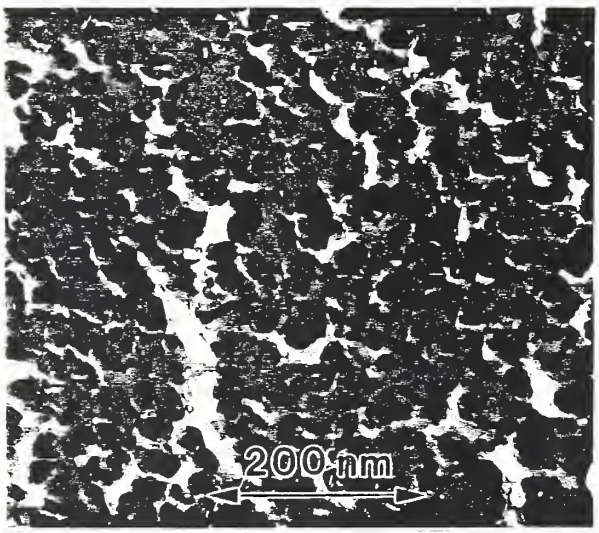

Fig. 6. High magnif. TEM micrograph of excimer $BaTiO_3$ on room temperature carbon film.

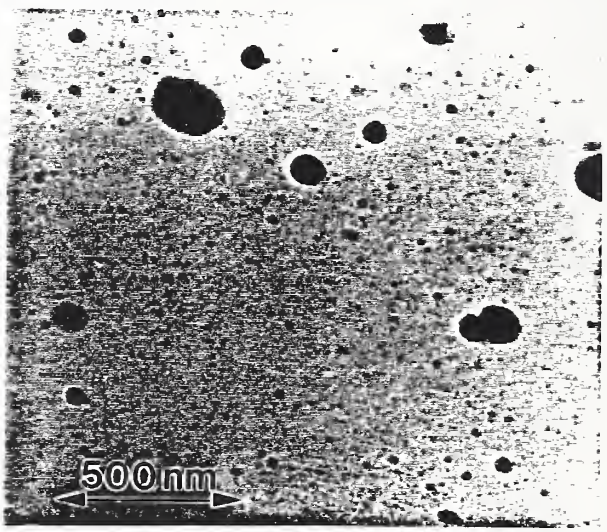

Fig. 7. TEM micrograph of excimer $BaTiO_3$ on "warm" carbon film.

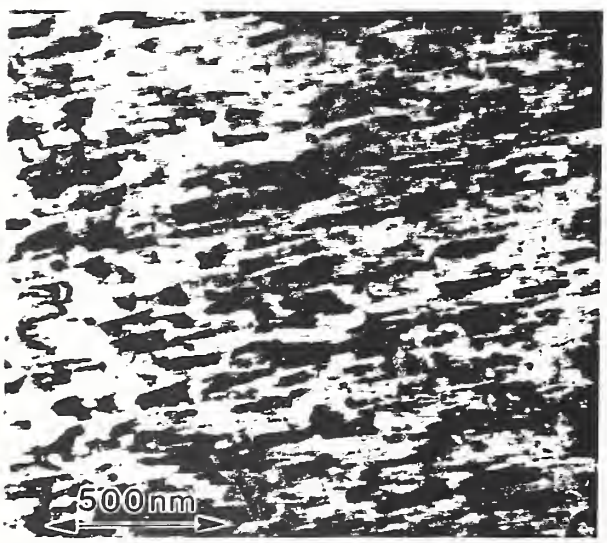

Fig. 8(a). TEM micrograph of excimer $BaTiO_3$ on heated Pt/Si substrate.

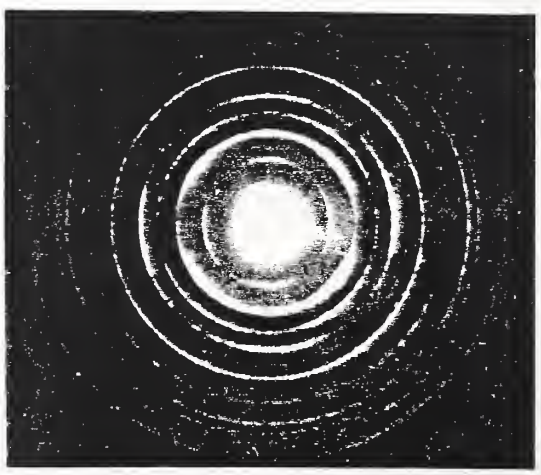

Fig. 8(b). Selected area electron diffraction from area in Fig. 8(a).

at least 250 nm long. Fig. 8(a) is a TEM image of the $BaTiO_3$ taken when the film was tilted 60° from normal to the electron beam so that the rods are nearly side-on; Fig. 8(b) is the corresponding selected area electron diffraction pattern correctly oriented with respect to the image. The arcs of greater and lesser intensity in a number of the diffraction rings indicate crystalline texture in the film. In particular, the first ring, 100/001, and the fourth ring, 200/002, have sharp, relatively intense arcs centered on a line parallel to the direction of the rods in the image showing that during deposition the rods grow with their axes aligned with one of the cube axes of the cubic perovskite structure. The electron diffraction patterns were better fitted to the tetragonal $BaTiO_3$ structure with a = 3.994 and c = 4.038 Å than to a cubic structure; however only one of the expected peak splittings, 200/002 (also observed by XRD, as noted above), was visible and this result is not seen as confirming that tetragonal $BaTiO_3$ was produced. After tilting the film to an orientation where the image showed no texture, the rings in the diffraction pattern showed no variation in intensity.

Differential scanning calorimetry and electrical measurements

Only the excimer PZT films on Pt substrates were analyzed by DSC. Two events were observed on heating up from room temperature to 730°C, in flowing air at a heating rate of 20°C/min. Fig. 9 shows behavior indicating a glass transition in the vicinity of 300°C; this is consistent with the as-deposited film being amorphous. At higher temperatures (not shown) the crystallization behavior of the PZT thin film is evidenced by a broad exotherm centered near 500°C, suggesting that the nucleation and growth proceed gradually, with completion near 700°C.

As indicated above, ferroelectricity has only been observed in the Nd/YAG PZT thin films; a typical hysteresis loop for this material is shown in Fig. 10. The electrical properties of other films similar to those in Fig. 1 are reported in more detail elsewhere [4]. The excimer $BaTiO_3$ thin film, while having excellent structural properties, is not ferroelectric. It does have an excellent dielectric constant of about 100, however. The excimer PZT films have not to date proved electrically measurable, due to shorting of sputtered electrodes. Further work is in progress on these and other films.

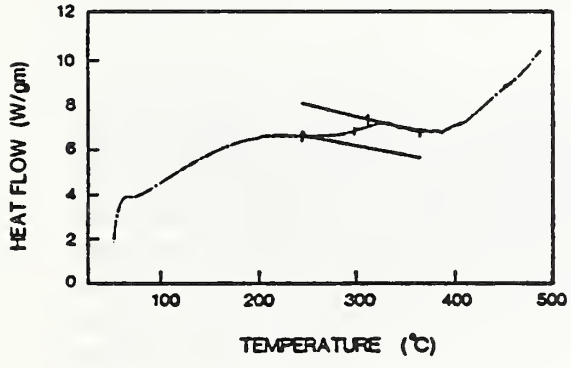

Fig. 9. DSC of excimer PZT film on unheated substrate, showing glass transition region.

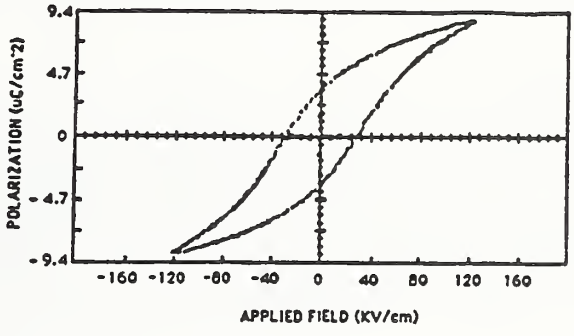

Fig. 10. Applied field vs. polarization hysteresis loop for Nd/YAG PZT film (700°C).

DISCUSSION

For the Nd/YAG films to be of device quality, a way must be found to improve the smoothness and density; our experiments suggest that post-depositional annealing is not the answer; shadowed deposition [2] offers possibilities which we are exploring further. However, although the films are not smooth, the ferroelectric properties offer encouragement.

The excimer films, on the other hand, approach device quality in terms of smoothness, density, and crystallinity. Furthermore, they can be readily processed. Excimer $BaTiO_3$ films deposited on a carbon film of intermediate temperature as well as excimer PZT films deposited on a room temperature carbon film were uniform and dense except for the relatively few large ejecta on the surface. The $BaTiO_3$ film on a room temperature carbon film (Fig. 6) is composed of small particles 15-40 nm in size but can be made more uniform by beam heating the film. By contrast, the Nd/YAG films had a very open, low

density structure composed of very fine particles (≈5 nm for PZT and 10-15 nm for $BaTiO_3$) in larger aggregates [2]. Thus for $BaTiO_3$, the more abundant or larger excimer-produced particles depositing on a heated substrate favor the production of a dense, uniform film. The DSC results suggest that the PZT films go through a glass transition at about 300°C, and above this temperature the ability of the particles to flow together and form a dense layer would be enhanced. The density and level of uniformity are relevant to processing these films since volume changes that occur in post deposition heat treatments have been observed (in our unpublished work) to cause undesirable delamination and cracking of the film. The observations of landing tracks for the large ejecta (up to a micron in size) show that the ejecta constitute a small fraction of the plume produced by the laser; attempts to eliminate them will center on modifying the plume production conditions.

The similarity in size between the excimer $BaTiO_3$ particles deposited on the carbon film at room temperature and the diameter of the rods in the $BaTiO_3$ film deposited on the Pt/Si film at 700°C suggests that each particle that lands on the film in the initial layer crystallizes immediately and is a seed for subsequent crystal growth. The development of rods aligned with a perovskite cube axis suggest that the cube directions may be the fastest to grow and as the film thickens grains that are close to cube aligned grow at the expense of any others. On cooling from the deposition temperature of ~700°C the $BaTiO_3$ should go through a cubic to tetragonal phase transformation at the Curie temperature (~100°C). At this point the film is under tension in the plane of the substrate because the coefficient of thermal expansion for Pt is $4x10^{-6}$ less than for $BaTiO_3$. Since c/a for tetragonal $BaTiO_3$ is ~1.01, alignment of the tetragonal a-axis normal to the substrate will reduce the tensile stress. The electron diffraction results described above for the $BaTiO_3$ deposited on heated Pt/Si indicate the film may be at least partially tetragonal, and the splitting is such that the c axis may be aligned in the plane of the film. Electrical measurements indicate that the film is not ferroelectric. Efforts are under way to determine the relation between particle size, stress, orientation and electrical properties in these films.

Annealing amorphous excimer PZT films in air causes crystallization to the PZT perovskite structure in which the Pb ion occupies a site that has 12-fold oxygen coordination. However, annealing PZT films at a low pressure using beam heating for about a minute in the TEM causes some volatilization of the lead, and produces a fcc fluorite structure with each cation having 8-fold oxygen. Thus, while a post annealing step is essential for production of PZT films, care must be taken to avoid Pb loss. The EDX analyses described above for the partially crystallized, two-phase excimer PZT film suggest that as-deposited chemistry is not as close to the target as for Nd/YAG films.

SUMMARY

All the laser-produced films examined are amorphous as deposited on unheated substrates, but crystallize readily to the perovskite structure upon heating to 500°C or less; these temperatures are compatible with most device processing. Heated substrates improve film density and result in crystallographic alignment, in situations where volatility is not a problem. Nd/YAG and excimer films differ considerably in their microstructure. Ideally laser processing will ultimately produce films with both the desirable ferroelectric and stoichiometric properties of the Nd/YAG films, and the microstructural attributes of the excimer-deposited films.

REFERENCES

1. L. P. Cook, P. K. Schenck, J. Zhao, E. N. Farabaugh, C. K. Chiang, and M. Vaudin, Ceramic Thin and Thick Films, Ceramic Trans. V. 11, Amer. Ceram. Soc., Westerville, OH, pp. 99-117 (1990).
2. P. K. Schenck, L. P. Cook, J. Zhao, J. W. Hastie, E. N. Farabaugh, C. K. Chiang, M. D. Vaudin, and P. S. Brody, Beam-Solid Interactions, Mat. Res. Soc. Symp. Proc. v. 157, pp. 587-592 (1990).
3. C. K. Chiang, L. P. Cook, P. S. Brody, J. M. Benedetto, Ferroelectric Thin Films, Mater. Res. Soc. Symp. Proc. v. 200, pp. 133-138 (1990).
4. P. S. Brody, J. M. Benedetto, B. S. Rod, K. W. Bennett, L. P. Cook, P. K. Schenck, C. K. Chiang, and W. Wong-Ng, Proc. Seventh Int'l. Symp. on Applic. of Ferroelectrics, June 6-8, 1990, Univ. Illinois, Urbana-Champaign.
5. Scanning Electron Microscopy, 1982, III, pp. 981-993.
6. D. J. Dingley, Scanning Electron Microscopy (USA), Part 2, pp. 569-575 (1984).
7. JCPDS-International Centre for Diffraction Data, Swarthmore, PA.
8. W. Wong-Ng, in preparation.

CHARACTERIZATION OF LEAD ZIRCONATE-TITANATE THIN FILMS PREPARED BY PULSED LASER DEPOSITION

C.K. CHIANG, W. WONG-NG, P.K. SCHENCK, L.P. COOK, M.D. VAUDIN

National Institute of Standards and Technology
Gaithersburg, MD 20899

P.S. BRODY, B.J. ROD, and K.W. Bennett

Harry Diamond Laboratories
Adelphi, MD 20783

ABSTRACT

Dense smooth lead zirconate-titanate thin films have been prepared by excimer laser deposition. The as-deposited films are amorphous as indicated by x-ray powder patterns. Differential scanning calorimetry studies show that the film has a glass transition at 301°C, and the amorphous to crystalline transformation takes place above 350°C to 650°C. Phase formation as a result of post-deposition heat treatment is described.

INTRODUCTION

For electrical and electronic applications of ceramic materials, we have applied pulsed laser deposition to produce various thin films, including barium titanate and lead zirconate-titanate (PZT).[1-3] The PZT films produced in our laboratory using a Nd/YAG laser showed ferroelectric hysteresis, indicating potential for application as non-volatile memories and related devices. However, these films had unsuitable microstructure, including large ejected particles and rough surfaces.[2] One cause of this morphology may be the thermal energy produced by the Nd/YAG laser during the sputtering. To improve these films we have since used an excimer laser, and in this paper we report the effect of post-depositional annealing on PZT films deposited by pulsed eximer laser deposition.

EXPERIMENTAL

The thin film deposition system was the same as reported earlier[1], except that we used an ArF excimer laser (193 nm). The deposition was done at a repetition rate of 10 Hz and nominal pulse width of 23 ns. The laser beam was focused to produce a fluence of typically 10-30 J/cm^2. A commercial PZT target (PZT 5A, 47% $PbTiO_3$ and 53% $PbZrO_3$) was used. During the deposition, the target was rotated and the laser beam was rastered across the target to maintain uniform material removal. A rotating substrate holder was used to hold substrates directly over the target surface at distances 3.0 cm from the target surface. The reaction chamber was continuously evacuated to <1 mTorr by oil free pumps. During deposition, oxygen was metered into the chamber to produce a background pressure of 100 mTorr. The growth rate of PZT film was about 50 nm/min. Typical thickness of the thin film was from 150 nm to 500 nm.

For electronic studies we used silicon <100> single crystal wafers as substrates which were coated with 500 nm platinum. For the materials processing studies, we used platinum substrates. After deposition, the films were annealed in air at various temperatures and times.

To determine the crystallization temperatures of the as-deposited PZT films differential scanning calorimetry (DSC) measurements were made. A platinum substrate similar to that upon which the film was deposited was used as the reference. DSC curves were measured at 20°C/min in flowing air. Each sample was measured for two cycles from 50°C to approximately 720°C. In one measurement, about 0.6 mg of as-deposited material was removed from the substrate mechanically and run in the DSC using an aluminum pan as the sample holder. The use of low mass aluminum pans for the sample holder and reference increased sensitivity and allowed us to detect the exact location of the glass transition temperature.

For an amorphous material, crystallization will not occur if it is annealed at a temperature less than its glass transition temperature. The DSC data provided us the guide for selecting the annealing temperature for the PZT film. We have annealed a series of the as-deposited amorphous PZT films in air for one hour at 350°C, 400°C, 450°, 500°, 550°C and 600°C.

The annealed films were studied by x-ray powder diffraction. The x-ray diffraction patterns were measured directly with the film in place on the platinum or silicon substrates, using Cu $K\alpha_1$ radiation. Because the x-ray measurements were done under the same conditions, the peak-heights could be used for a semi-quantitative analysis of the relative amounts of phases. We measured the peak-heights of selected major peaks to indicate variations in the ratio of the phases present as a function of annealing conditions. The different peak-heights were re-scaled relative to the intensity of the (101,110) peak for comparison.

Optical microscopy was used for examining the gross features of the films and scanning electron microscopy was used to examine the microstructure of the films. The hysteresis loop was measured using a balanced Sawyer-Tower circuit operated at 10 kHz. The electrode size for the hysteresis loop measurement was 5.0×10^{-4} cm^2. Extensive characterization on these films has been done, with details of the electrical characterization reported elsewhere.[3-4]

RESULTS

The as-deposited films were amorphous, as determined by their x-ray diffraction pattern which showed an amorphous hump with no sharp crystalline peaks. The films are of uniform thickness of approximately 400 nm over a region of 1 cm and have clear interference patterns indicating that they are transparent at this thickness. Optical microscopy of the films showed a smooth surface.

The DSC signal from the sample is very small due to the small amount of available material from the thin film samples. Since the amorphous to crystalline transition is a non-reversible transformation, only the initial heating trace contains the phase transformation information. The signals from the subsequent cooling trace or the second heating trace, or any other runs after that, showed only a smooth variation with temperature. The second heating trace of the same film reflects only the heat capacity of the film and the substrate. Hence, the second heating trace could be used as the background for analysis of the transition of the film. The background subtracted DSC traces of the as-deposited PZT film are shown in figures 1 and 2.

Figure 1 shows the initial heating trace of the PZT film on platinum. On heating at 20°C/min from room temperature to 720°C, the thin film on the platinum substrate showed a broad exothermal peak. This peak is due to re-crystallization, which transforms the amorphous film to crystalline form. The broadness of the peak is partially due to the heating rate which is high compared with the rate of crystallization. Nevertheless, the thermal process is completed at approximately 670°C. Examining figure 1 closely, one could identify T_g in figure 1, although it is not very clear.

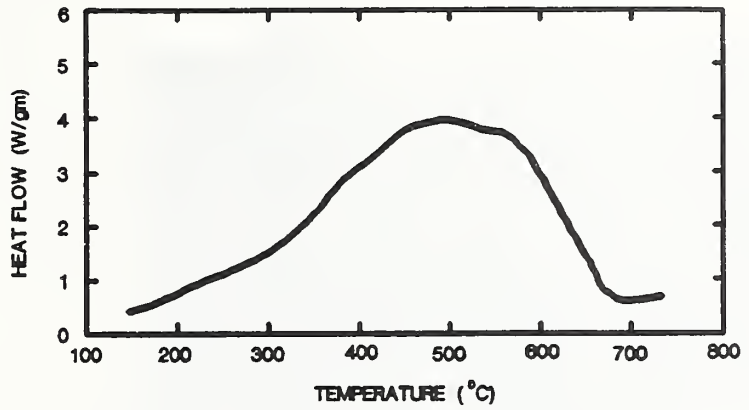

Figure 1 DSC trace of an as-deposited PZT film on a Pt substrate.

Figure 2 shows the trace obtained from the PZT film removed from the platinum substrate. The glass transition of the amorphous film is clearly shown as a step in the curve. It is identified with two parallel lines in the figure 2. From this data we determine the mid-point of the glass transition temperature of the film is 301°C.

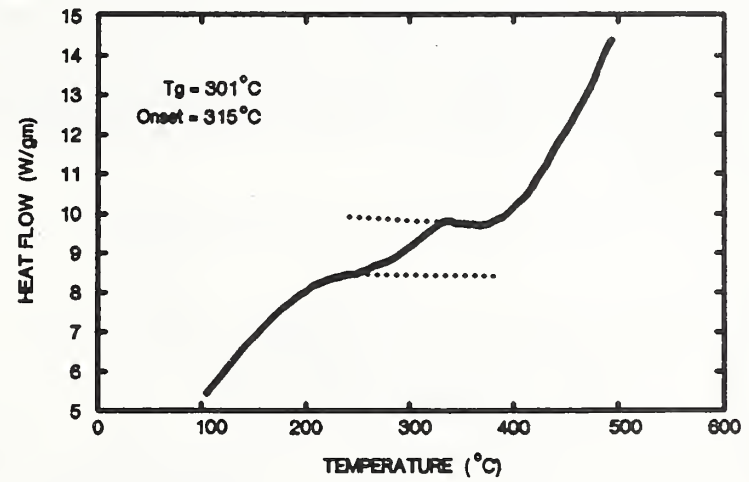

Figure 2 DSC traces of PZT material removed from an as deposited film. The parallel lines indicate the location of T_g.

The x-ray patterns of the PZT films after annealing at various temperatures are shown in figure 3. The 357°C pattern shows only an amorphous hump and the peaks from the platinum substrate. The patterns of 398°C, 450°C and 500°C shows that the crystalline peaks increase with increasing annealing temperature. The amorphous hump decreases at the same time.

These peaks are identified as the pyrochore phase of PZT. The volume fraction of the pyrochore phase reached a maximum at 500°C. At 550° and 602°C the x-ray patterns show nearly the same strength of the crystalline peaks. These patterns were identified as the perovskite phase of PZT[5]. At 500°C there is small amount of perovskite phase, but the pyrochore phase is not seen in the 550°C pattern.

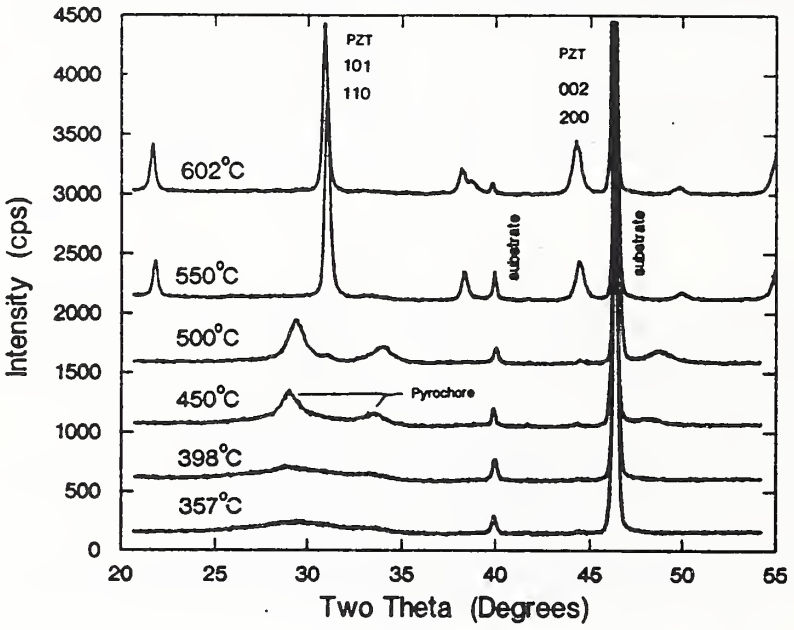

Figure 3 The x-ray diffraction patterns of the PZT films heat-treated at different temperatures.

Figure 4 shows the formation of the pyrochore and perovskite phases as a function of the annealing temperature. In the figure the formation of the pyrochore phase is plotted using the intensity of the strongest peak ($2\theta=29°$). The formation of perovskite phase is plotted using the intensity of both the (110,101) and (200,002) peaks (figure 3). This result indicates that there are two types of crystals formed in two temperature regions. The two regions separated by a relatively short temperature region of less than 50°. The two crystalline regions were not revealed in the DSC studies.

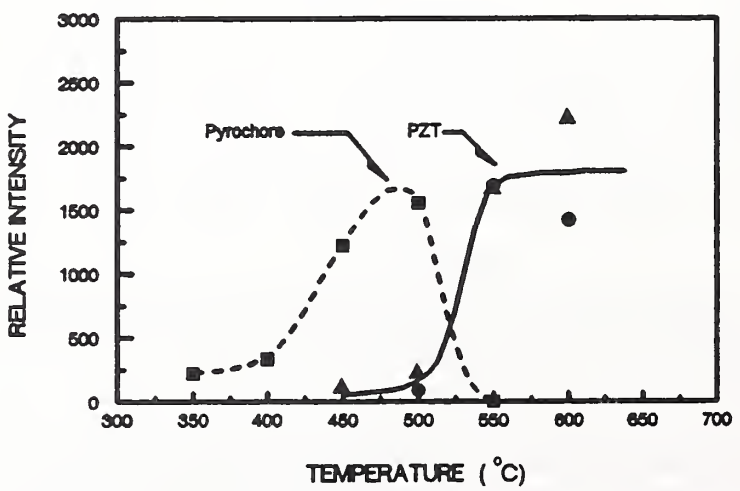

Figure 4 The formation of crystalline phases of PZT film as a function of isothermal heat-treatment.

These heat treated films have essentially no change in surface morphology examined with optical and electronic scanning microscopies. Figure 5 is a typical micrograph of the PZT film on platinum substrate. It can be seen that the smooth surface is decorated by many particles with diameters less then 1 μm.

Figure 6 shows a typical ferroelectric hysteresis loop obtained from an PZT thin film produced by excimer laser deposition. This film was about 180 nm in thickness. The maximum applied voltage was about 12 volts. The coercive field is approximately 80 kV/cm and the remanent polarization is approximately 14 $\mu C/cm^2$.

Figure 5 A SEM micrograph of a PZT film heat-treated at 550°C.

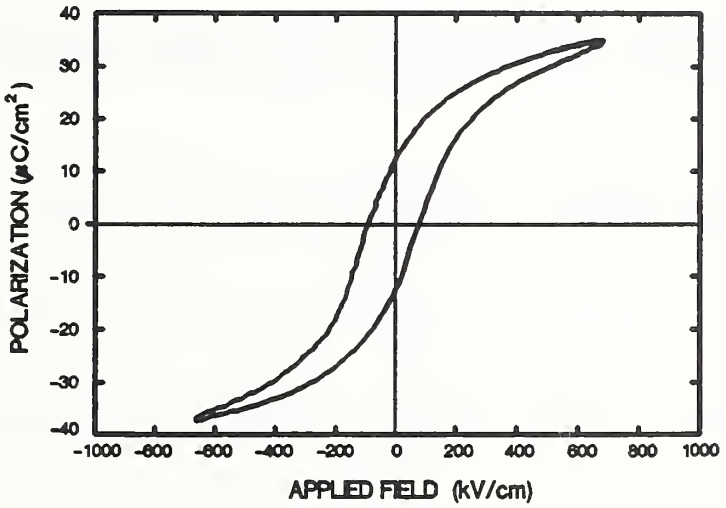

Figure 6 A typical hysteresis loop of a PZT film after post-depositional heat-treatment.

DISCUSSION AND CONCLUSION

The surface morphology of the excimer laser deposited films are significantly better than those of Nd/YAG laser[1,2]. Ejected particles are seen in both cases, but the number of particles seen in the excimer laser film is much less[4,6]. The ferroelectric properties of the

eximer deposited film are also improved, the remanent polarization is almost a factor of two higher than in the Nd/YAG deposited film[2].

Using pulsed laser deposition to produce a PZT thin film, the as-deposited film is in an amorphous state if the substrate temperature is at ambient temperature. DSC data suggests that the film should remain in an amorphous state as long as the heat treatment temperature is less than its T_g or 301°C. The control of nucleation should be at a temperature slightly above T_g. Crystallization should occur if heat treated at a temperature higher than 400°C. However, the PZT processing should be designed to avoid the pyrochore phase which crystallized at temperature range between 400°C and 500°C. Also, the lead oxide in lead zirconate and its solid-solution is known to be volatile[5]. Care must be taken to avoid lead loss at temperatures higher than those reported here, especially at long annealing times. Because lower temperatures will be compatible with the processing of silicon substrates, it is concluded that the optimum processing temperature is in the vicinity of 550°C.

REFERENCES

1. P.K. Schenck, L.P. Cook, J. Zhao, E.N. Farabaugh, and C.K. Chiang, Proc. Symposium on Beam Solid Interaction: Physical Phenomena, ed. E.R. Myers and A.I. Kingon, Mat. Res. Soc., 157A, 587, (1990)

2. C.K. Chiang, L.P. Cook, P.K. Schenck, P.S. Brody, and J.M. Benedetto, "Ferroelectric Thin Films", Mat. Res. Soc., Vol. 200, 133, (1990).

3. P.S. Brody, B.S. Rod, J.M. Benedetto, K.W. Bennett, L.P. Cook, P.K. Schenck, C.K. Chiang and W. Wong-Ng, Proc. Seventh Intl Symp. on Applic. of Ferroelectrics, Univ. Ill, Urbana-Champaign, IL., (1990).

4. L.P. Cook, M.D. Vaudin, P.K. Schenck, W. Wong-Ng, C.K. Chiang, and P.S. Brody, p. 241-246 in C.V. Thompson, J.Y. Tsao, and D.J. Srolovitz, eds., Evolution of Thin-Film and Surface Microstructure, Mat. Res. Soc. Symp. Proc., vol. 202, (1991).

5. B. Jaffe, R.S. Roth, and S. Marzullo, J. Res. National Bur. Stds., 55, 239, (1955).

6. L.P. Cook, P.K. Schenck, J. Zhao, E.N. Farabaugh, C.K. Chiang and M.V. Vaudin, Ceramic Transactions: Ceramic Thin and Thick Films, ed. B.V. Hiremath, page 99, (1990).

PZT FILMS PREPARED BY THE PULSED LASER DEPOSITION TECHNIQUE

W. Wong-Ng, T. C. Huang*, L.P. Cook, P.K. Schenck, M.D. Vaudin, C.K. Chiang, and P.S. Brody**, National Institute of Standards and Technology (NIST), Gaithersburg, MD, USA.

*IBM Almaden Research Center, San Jose, CA, USA
**Harry Diamond Laboratory (HDL), Adelphi, MD, USA.

INTRODUCTION

In recent years, ferroelectric $Pb(Zr_{.53}Ti_{.47})O_3$ (PZT) films on silicon wafers for silicon-integrated nonvolatile memories have become increasingly important, particularly in the semiconductor industry. Although $PbZrO_3$ is anti-ferroelectric, its solid solutions with more than about 10 mole percent $PbTiO_3$ are ferroelectric [1]. These solid solutions show rhombohedral and tetragonal distortion from the ideal cubic perovskite structure. A morphotropic phase boundary occurs near 55 mole % $PbZrO_3$. Solid solutions richer in $PbZrO_3$ are rhombohedral, while those richer in $PbTiO_3$ are tetragonal.

Pulsed laser deposition is a technique in which a plume of vaporized and ionized material is produced by the irradiation of a target material by using a high intensity laser. In this investigation, two different types of pulsed lasers, Nd/YAG and excimer, were used to produce films on Pt-coated Si wafers and Pt substrates using a lead zirconate-titanate (PZT[Zr/Ti=53/47]) target.

This paper is part of a continuous joint effort to investigate the processing and characterization of ferroelectric thin films [2-4]. The goals of this study are to investigate the optimum conditions for preparing PZT films; to understand the phase formation at various heat treatment conditions; to characterize the properties of these films by using a variety of techniques such as X-ray diffraction, scanning and transmission electron microscopy, energy dispersive X-ray, and electrical measurements, etc.; to compare properties of films prepared with the Nd/YAG and the excimer lasers; and to understand the crystallography of the thin film materials.

EXPERIMENTAL

The fully dense target PZT ceramic disk was obtained commercially. The films were produced with the use of both a focused Q-switched Nd/YAG pulsed laser and a focused ArF excimer laser. The schematic of the Nd/YAG laser deposition apparatus is shown in Figure 1. A laser beam was passed through a hole in the substrate holder and was focused onto a rotating target in a vacuum chamber to produce a laser-induced plume. The pulse width was 15 ns and the 1064 nm fundamental wave length was used. During deposition, oxygen was metered into the chamber to produce a background pressure of 13.33 Pa (100 mTorr). The growth rate of the film was about 1-2 μm per hour, and the distance between the target and the substrate was about two centimeters. Although the excimer laser deposition apparatus was similar to the Nd/YAG schematic (see Fig. 1), the 192 nm laser beam did not pass through a hole in the substrate. Instead, it impinged the target surface with an inclination angle of approximately 35° from the horizontal direction. Available analytical diagnostics for both the plume and the deposition process in both laser systems were mass spectroscopy, optical spectroscopy, electrical probes and optical scattering.

All films reported here were deposited onto room temperature substrates and post-annealed at various temperatures up to 1200°C in order to understand the phase formation. In the case of the Nd/YAG system, heat-treatments were performed at 500, 600, 650, 700 and 750°C in air, and also at higher

temperatures of 800, 900, 1000, 1100 and 1200°C by using a lead-buffered cell. Two substrates, Pt metal foil and Pt coated silicon wafers, were used. The average thickness of the films was estimated by profilometry.

RESULTS AND DISCUSSION

Both the Nd/YAG and the excimer laser produced amorphous films (X-ray diffraction patterns showed the presence of a broad amorphous hump at around 25 to 35° 2θ) and under appropriate heat-treatment the ferroelectric perovskite PZT phase was formed. The average thickness of the films was about 2 μm. The energy dispersive x-ray spectra of these films show compositions similar to the target.

In general, the excimer laser appears to produce films with finer microstructure and better electrical properties. The SEM micrographs of the films annealed at around 600°C are shown in Figure 2a for the Nd/YAG and in Figure 2b for the excimer laser. The Nd/YAG film shows the presence of large particles. This coarseness seems to be absent in the excimer-produced films.

The ferroelectric nature of these films was demonstrated by the hysteretic behavior relating the remanent polarization and the applied field. Figures 3a and 3b illustrate such loops for the films deposited by the Nd/YAG laser and annealed at 700°C, and deposited by the excimer laser and annealed at 600°C. While both lasers produce ferroelectric films, the excimer films show relatively higher remanent polarization.

X-ray diffraction patterns of the thin-films of $Pb(Zr_{.53}Ti_{.47})O_3$ annealed at various temperatures between 15 minutes (1200°C) and 6 hours (500°C) as prepared with the Nd/YAG laser are illustrated in Figures 4a and 4b. The perovskite PZT phase appears to form as a result of the reaction between the Pb, Zr and Ti oxides at a temperature as low as 500°C (the stick pattern of PZT from the JCPDS Powder Diffraction File is shown for comparison). These diffraction peaks, however, are characteristic of cubic symmetry. After annealing at temperatures between 500 to 750°C, the pseudocubic symmetry was still observed (the film annealed at 750°C can be indexed by a unit cell of $\approx$ a=4.067(2)Å). The hkl indices are illustrated for the tetragonal case.

At higher anneal temperatures (800-1200°C), splitting of the cubic peaks was observed. This splitting could either be due to the appearance of tetragonal symmetry or the presence of a second phase. At 1100°C, a tetragonal cell of $\approx$ a=3.937(4) and c=4.068(5)Å can be used to index these lines. In these high-temperature films, small amounts of other phases such as ZrO_2 appear to be present. At 1200°C, the pattern was drastically different; the peaks corresponding to PZT diminished and the presence of a much larger amount of ZrO_2 was identified. The possible presence of $ZrTiO_4$, PbO and the pyrochlore phase, $Pb_2Ti_2O_6$, were also observed. Some unknown peaks still remain to be identified.

X-ray results from a set of films produced by the excimer laser show the formation of the pyrochore phase at low annealing temperatures and the formation of a pseudocubic pervoskite PZT phase between 500 and 550°C.

Since the ferroelectric nature of these films rules out the possibility of cubic symmetry, the apparent conflict between the observed cubic symmetry and the lower symmetry required for ferroelectric behavior is possibly due to the presence of surface stress (strain) as a result of thermal mismatch between PZT and the substrate, and/or the small crystallite size of the material. At higher temperatures, the annealing effect could release the strain and allow the tetragonal splitting to appear.

Current efforts continue in the X-ray profile analysis of these films.

SUMMARY

Thin films of $Pb(Zr_{.53}Ti_{.47})O_3$ (PZT) deposited on Pt and Pt-coated silicon substrates using laser deposition techniques (Nd/YAG and excimer) produced amorphous films at room temperatures. Upon annealing, these films crystallized and gave rise to well-defined X-ray powder patterns with pseudocubic symmetry. Higher annealing temperature appeared to relieve the strain and allowed the tetragonal symmetry to appear. In general the excimer laser produced films with better surface morphology and possibly better electrical properties as well.

ACKNOWLEDGEMENT

Dr. R. Gates is thanked for his measurement of the thickness of the film.

REFERENCES

1. B. Jaffe, R.S. Roth and S. Marzullo, J. Res. Nat'l Bur. Stds, 55, 1955.
2. P.K. Schenck, L.P. Cook, J.W. Hastie, E. Farabaugh, C.K. Chiang, M.D. Vaudin and P.S. Brody, Proc. Symp. Beam Solid Interaction; Mat. Res. Soc., vol. 157A, 1990.
3. P.S. Brody, J.M. Benedetto, B.S. Rod, K.W. Bennett, L.P. Cook, P.K. Schenck, C.K. Chiang, and W. Wong-Ng, Proc. Seventh Int'l Symp. on Applic. of Ferroelectrics, 1990, Univ. Illinois, Urbana-Champaign.
4. L.P. Cook, M.D. Vaudin, P.K. Schenck, W. Wong-Ng, C.K. Chiang and P.S. Brody, Proceeding of Symposium on Evolution of Thin film and Surface Microstructure, Mat. Res. Soc. Fall Meeting, Boston, November, 1990, in press.

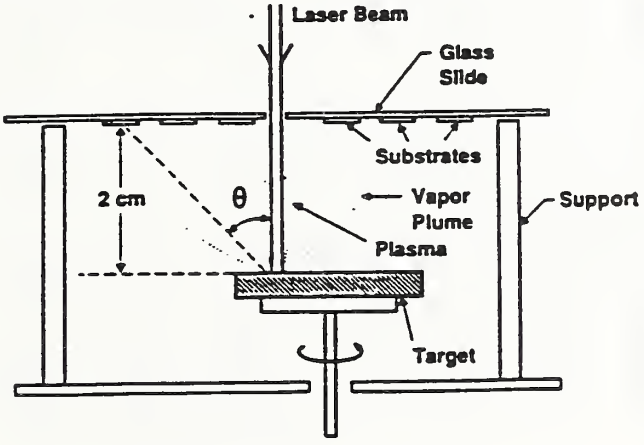

Figure 1. Schematic of the Nd/YAG laser ablation apparatus

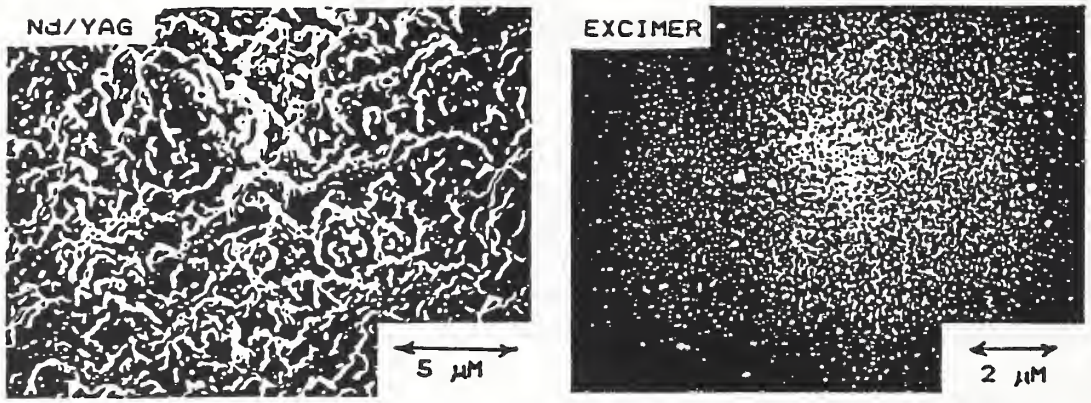

(a) (b)

Figure 2. SEM micrograph of PZT films (a) ND/YAG, annealed at 700°C and (b) excimer, annealed at 600°C

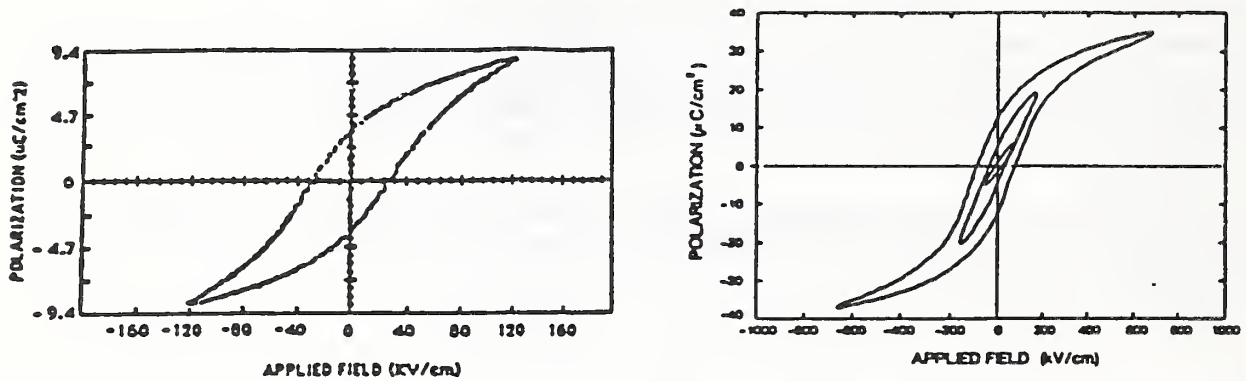

Figure 3. Applied field vs. polarization (a) Nd/YAG annealed at 700°C and (b) excimer, annealed at 600°C

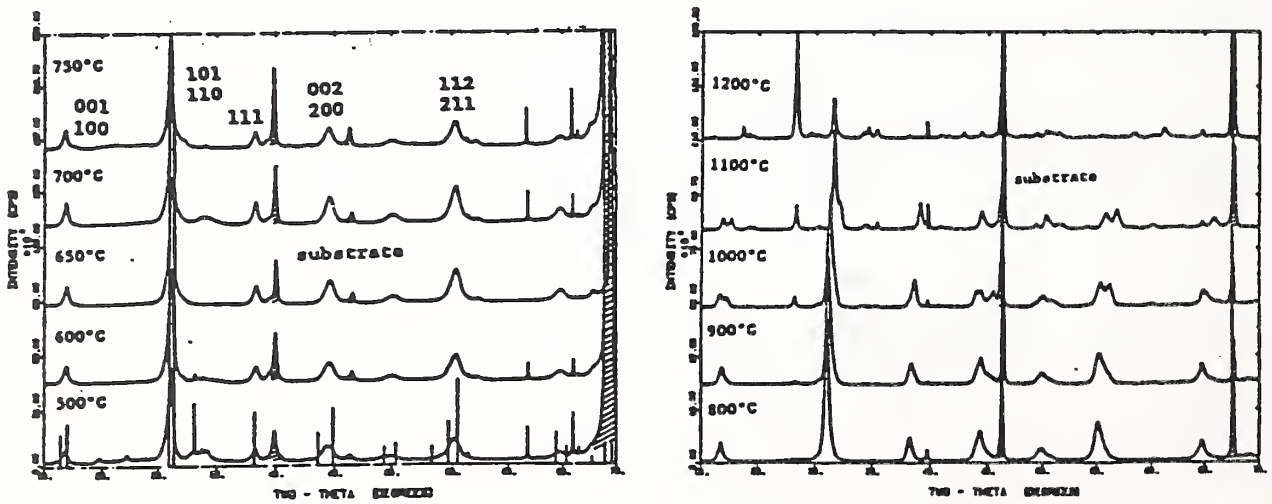

Figure 4. X-ray diffraction patterns for Nd/YAG PZT films annealed from 500 to 1200°C. Hatched peaks are due to substrate.

THERMAL PROCESSING OF LASER-DEPOSITED $BATIO_3$

L. P. Cook, W. Wong-Ng, T. Huang*, P. K. Schenck, M. D. Vaudin, C. K. Chiang, and P. S. Brody**

National Institute of Standards and Technology, Gaithersburg, MD, USA 20899
*IBM Almaden Research Center, San Jose, CA, USA
**Harry Diamond Laboratories, Adelphi, MD, USA 20783

I. Introduction

The pulsed laser deposition technique has a number of advantages for thin film deposition, including the following: a) the chemistry of complex target materials can be transferred to the deposited film; b) targets can be changed quickly without the need to break vacuum; c) a wide range of in-situ thermally processed microstructures can be produced, depending upon the temperature of the substrate; and d) deposition environment (P_{O2}, electrical field, geometry) can be easily varied.

Our early interest in pulsed laser deposition centered on the production of high T_c ceramic films [1]; shortly thereafter, we were successful in producing a wide variety of ceramic thin films by the laser deposition process, including films of refractory materials such as MgO, ZrO_2 and Al_2O_3 [2]. At the same time we realized that it was also possible to make $BaTiO_3$ by this method. Coincidentally, there existed an increasing interest in ferroelectric and dielelectric thin films for devices, and so we have continued to investigate the production of these materials by the pulsed laser deposition method. This paper summarizes our recent results for $BaTiO_3$. A companion paper in this symposium discusses results for PZT.

II. Experimental

Experimental details for this study are shown schematically in Fig. 1. A pulsed ArF excimer laser operating at 193 nm was used for this study. The essential features of laser operating conditions are: 23 ns pulse duration, 20 Hz pulse rate, fluence ~ 10 J/cm^2, 13.33 Pa (100 mT) oxygen pressure. We have found this system to give higher deposition rates and fewer particulate ejecta relative to the Nd/YAG laser system [1]. Deposition rates used in this study were typically ~ 1 μm/hr. During deposition, the pulsed laser beam impinged at ~ 35 degrees on the solid target, in this case a commercially prepared, dense ceramic of a formulation known as "$BaTiO_3$ B" which contains 5 mol % $CaTiO_3$. The target was rotated at a constant speed of 30 rpm. As the target rotated, the laser beam was rastered on the target, by moving the laser-focusing lens under computer control, so that material was removed nearly evenly from the target. Because the laser operates at 193 nm, all optics including windows were of UV grade silica, or equivalent. The films were normally deposited on a <100> silicon wafer. These wafers had a thermally grown oxide coating of several hundred nanometers, with a Ti interlayer of ~ 25 nm followed by a sputtered Pt coating of 200 nm. During $BaTiO_3$ film deposition, the substrate was rotated and heated resistively by means of d.c. current from a power supply running in the constant current mode. The amount of current was varied, depending on the size of the wafer or wafer fragment being used as the substrate, in order to give a surface temperature of ~ 750°C, based on optical pyrometer measurements. During deposition, a background pressure of 13.33 Pa oxygen was maintained by a differential pumping arrangement.

III. Results and Discussion.

When deposition took place on an unheated substrate, the resulting film was amorphous. From transmission electron microscopy (TEM) investigation, it was clear that these films formed by the gradual buildup of particulates of ~25 nm diameter (Fig. 2). With heating, crystallization was estimated to take place before 500°C was reached, based on observations from TEM hot stage microscopy and atmospheric isothermal crystallization experiments. As followed on a TEM hot stage, crystallization produced $BaTiO_3$ directly, with crystallites of roughly the same size as the deposited particles, and with no preferred orientation. On the other hand, crystallization on the hot 750°C substrates produced a very dense, completely crystalline film with a considerable degree of orientation (Fig. 3). Electron diffraction and x-ray analysis (Fig. 4) suggested cubic or near-cubic symmetry of these crystallites, which were elongated perpendicular to the substrate surface, and measured roughly 35 by at least 250 nm [3]. For these films, which were apparently not ferroelectric, a dielectric constant in the 100-200 range has been measured.

We prepared another $BaTiO_3$ film on a hot 750°C substrate by the same method, which had similar x-ray characteristics, yet which showed ferroelectric hysteresis (Fig. 5). The data in Fig. 5 were taken with a Sawyer-Tower circuit at 100 Hz using a sinusoidally applied voltage. For these measurements, 100 μm dia. Pt top electrodes were sputtered on the surface using a shadow mask. The film thickness was 100 nm. The dielectric constant calculated for this material was 1300 at 1 kHz (this agrees well with the dielectric constant of the bulk target estimated at 1200). Raman data for these films [4] indicate tetragonality, despite the lack of peak splitting on the x-ray patterns.

The reasons for the differences in ferroelectric behavior among the films prepared by the same method on the hot 750°C substrates are not known. Conceivably, such differences could be related to minor variations in the temperature of the substrate during processing, or to orientational effects, which could also explain in part the lack of observed peak splitting in the ferroelectric samples. Further measurements on these materials are in progress.

The films produced by this method are very smooth, as indicated in Fig. 6. There are practically no surface features distinguishable with the SEM. The surface roughness, as measured by profilometry, is 0.07 μm; most of this roughness is due to the presence of a few, widely scattered, larger particles.

IV. Summary.

The laser deposition method, as described here, has produced relatively smooth, dense ferroelectric thin films of $BaTiO_3$. To our knowledge, this paper is one of the first reports of ferroelectric $BaTiO_3$ produced by this method. The use of a heated substrate apparently produces dense films due to the complete coverage and growth of crystallites from the plume condensate particulates as they arrive at the surface. Films therefore do not develop the usual fissuring associated with low temperature deposition, followed by post-depositional annealing. However, modifications are necessary before production is practical, including better areal uniformity of thickness, and elimination of the remaining particulate material. Notwithstanding the possibilities for improvement, these films are of device or near-device quality. Consequently, it can be said that they have significant potential as thin film capacitors, due to their high dielectric constant, and in ferroelectric form, as materials for thin film memory.

V. References

[1] K. Moorjani, J. Bohandy, F. J. Adrian, B. F. Kim, R. D. Shull, C. K. Chiang, L. J. Swartzendruber, and L. H. Bennett, *Phys. Rev. B*, 36, p.4036-4038 (1987).

[2] L. P. Cook, P. K. Schenck, J. Zhao, E. N. Farabaugh, C. K. Chiang, and M. D. Vaudin, p. 99-107 in B. V. Hiremath, ed., *Ceramic Thin and Thick Films*, *Ceram. Trans.* Volume 11 (Amer. Ceram. Soc., 1990).

[3] L. P. Cook, M. D. Vaudin, P. K. Schenck, W. Wong-Ng, C. K. Chiang, and P. S. Brody, p. 241-246 in C. V. Thompson, J. Y. Tsao, and D. J. Srolovitz, eds., *Evolution of Thin-Film and Surface Microstructure*, *Mater. Res. Soc. Symp. Proc.*, Volume 202, 1991.

[4] L. H. Robins, NIST, unpublished data (1991).

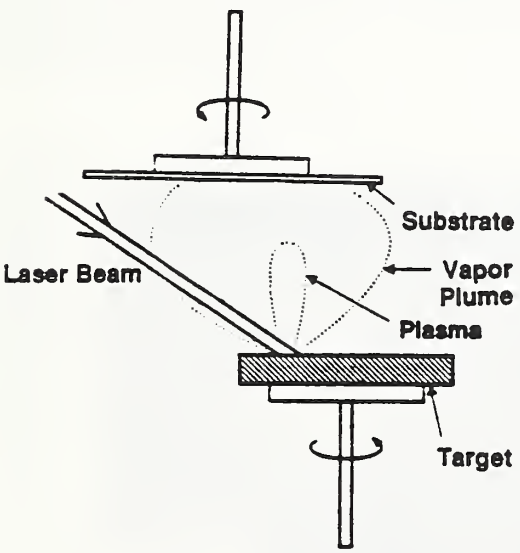

Fig. 1. Target/substrate geometry.

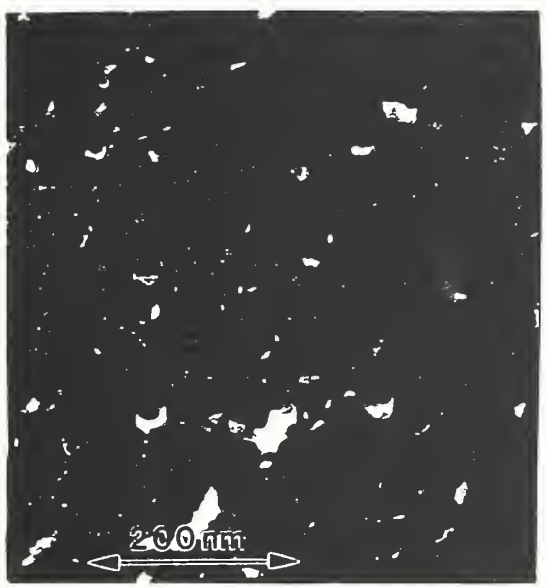

Fig. 2. As-deposited $BaTiO_3$ film (unheated substrate) (TEM).

Fig. 3. Oriented $BaTiO_3$ film (heated substrate) (TEM).

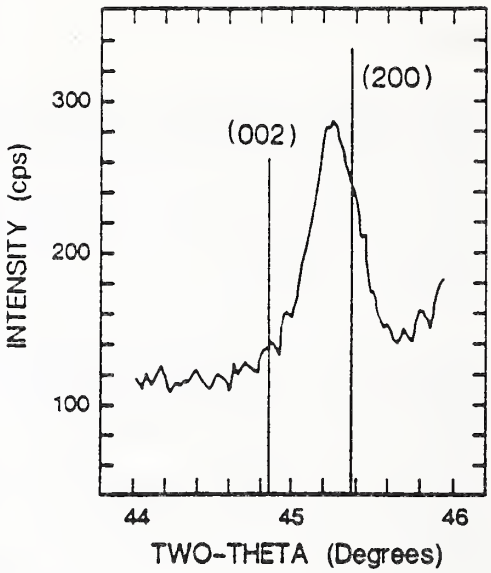

Fig. 4. X-ray data from $BaTiO_3$ thin film (heated substrate).

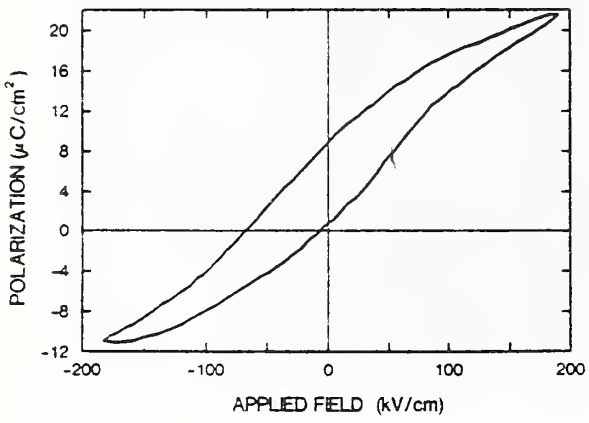

Fig. 5. Hysteresis loop for $BaTiO_3$ thin film (heated substrate).

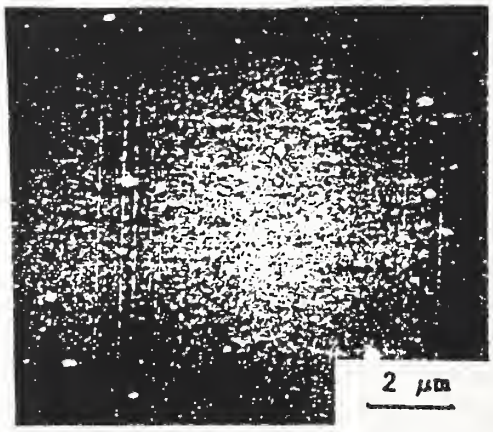

Fig. 6. Micrograph of $BaTiO_3$ thin film (heated substrate) (SEM).

Microstructure and Ferroelectric Properties of Lead Zirconate-Titanate Films Produced by Laser Evaporation

P. S. Brody, J. M. Benedetto, B. J. Rod, and K. W. Bennett
Harry Diamond Laboratories, Adelphi, MD 20783

L. P. Cook, P. K. Schenck, C. K. Chiang, and W. Wong-Ng
National Institute of Standards and Technology,
Gaithersburg MD, 20899

Abstract

Lead titanate-zirconate films were produced by laser-induced vaporization from a PZT target with the use of a focused q-switched Nd:YAG laser. Deposition was onto room-temperature platinum-covered silicon substrates. Although the films were initially amorphous as indicated by x–rays, they crystallized when annealed. EDX results showed that the film and targets were similar in composition. SEM and optical dark field micrographs showed a structure which might be interpreted as a sintered assemblage of particulate. A pattern of platinum electrodes was sputter deposited onto each sample to form parallel plate capacitors for investigating dielectric and ferroelectric properties. For a 2.5-μm-thick film annealed at 700°C, the relative dielectric constant was approximately that of the bulk target (e_r = 880). Hysteresis loops were obtained. The remanent polarization was 5.1 μC/cm² measured at a 160 kV/cm peak sinusoidal field.

Introduction

Recently, there has been increased interest in ferroelectric films on silicon substrates for silicon-integrated nonvolatile memories [1]. Laser-induced vaporization (also called laser ablation) is a film deposition technique in which a plume of ionized and ejected material is produced by high-intensity laser irradiation of a solid target [2,3]. This is a technique which could be integrated into semiconductor processing. We have applied this technique to produce films on silicon substrates using a lead zirconate-titanate (PZT) target. These films have ferroelectric properties. In this paper we report the x-ray results for crystallinity, energy dispersive x-ray (EDX) results for composition, and scanning electron microscope (SEM) and dark field optical micrographs for microstructure. We also report hysteresis loop measurements for remanent polarization and capacitance measurements for dielectric constant.

Film Preparation

The films were prepared from a commercial-source PZT ceramic disk with the use of a focused q-switched Nd:YAG pulsed laser [4]. The pulse width was 15 ns and the 1064-nm fundamental wave length was used. Pulse energies of about 100 mJ were focused to an approximately 250-μm spot. The cylindrical deposition chamber is 20 cm in diameter and 8 cm in height. The deposition geometry is one in which the ablating beam passes through a hole in the substrate (fig. 1), or a similar geometry in which a slit replaces the hole and in which the beam was moved back and forth parallel to the slit. In both arrangements, the target is rotated. The deposition chamber was continuously evacuated to less than 1 mTorr by oil free pumps. During deposition, oxygen was bled into the chamber to produce a background pressure of 100 mTorr. The substrate and target were separated by about 3 cm. The growth rate was about 2 μm per hour. Deposition was on room temperature substrates, and films were annealed after deposition in air for 1.5 to 2 hours at 650°C, 700°C, and 750°C.

Film Composition and Crystal Structure

Figure 2 shows EDX (20-kV accelerating potential) results for a 2.5-μm-thick film produced by the non-rastering method and annealed at 700°C (film No. 1). Typically, the spectrum did not vary appreciably across the film, and comparison of spectra showed that the target and the film were the same or close in composition within the limits of analytical uncertainty (5 to 10%).

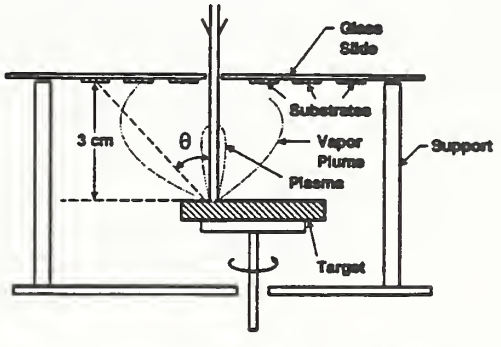

Figure 1. Schematic of laser ablation apparatus.

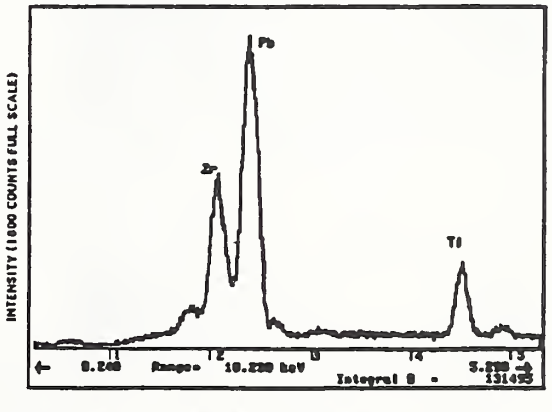

Figure 2. Energy dispersive x-ray spectrum of laser-deposited PZT film.

0-7803-0190-0/91$01.00 ©IEEE

X-ray diffraction patterns were obtained for the target and for the annealed films. The line splittings expected for the ferroelectric tetragonal or rhombohedral phase are not seen in the annealed film. The pattern for the film suggests possible cubic symmetry. Hysteresis loops and remanent polarization, however, are observed, and it is therefore likely that at least some of the material is in a ferroelectric phase. Figure 3 shows a portion of the pattern for the target, and the same portion for the annealed film.

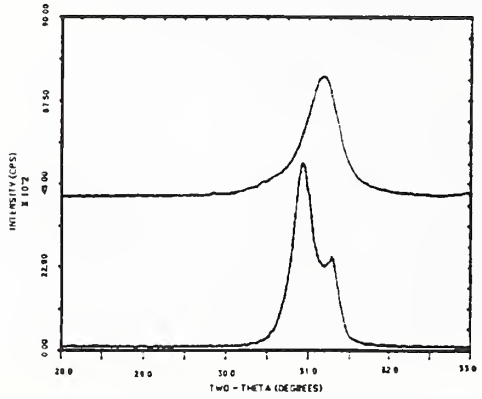

Figure 3. Portion of x-ray diffraction patterns of PZT target (bottom) and laser-deposited film annealed at 700°C (top). Characteristic tetragonal (101)/(110) splitting is seen in target but not in film.

Film Microstructure

A low-power optical dark field micrograph of an annealed film (film No. 1) is shown in figure 4. An SEM micrograph is shown in figure 5. The film appears to be an assemblage of particulate which may have originated as melted target material which was then recrystallized by the annealing process. Films annealed at 650°C and 750°C showed a similar morphology.

In the films, there is a background structure dominated by particle-like forms 0.1 µm across and less. There is also a distribution of larger particles. This kind of morphology may be characteristic of films produced by the unmodified laser ablation process. We note, however, that there may be some simple methods to reduce film coarseness [5].

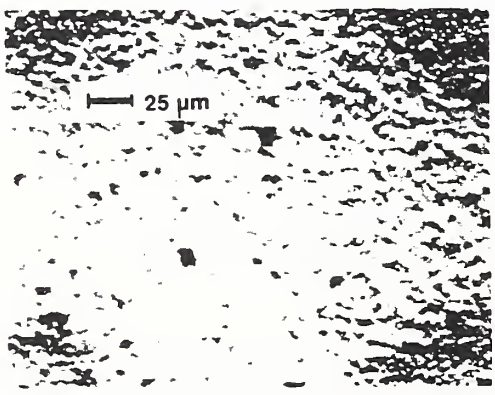

Figure 4. Dark field optical micrograph of an annealed laser-deposited film (No. 1). Dark areas in corners are portions of sputter-deposited platinum electrodes.

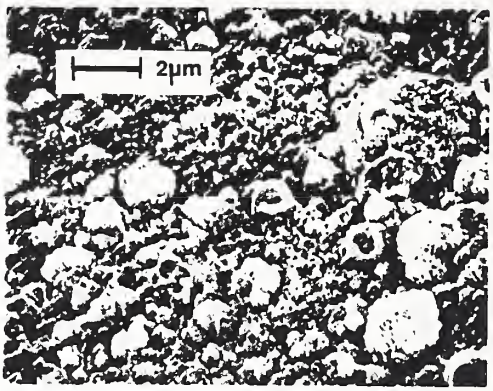

Figure 5. SEM micrograph of an annealed film (No. 1).

Dielectric and Ferroelectric Properties

Dielectric and ferroelectric properties were investigated with the use of parallel plate capacitors formed between sputtered electroded areas on the film surfaces and the platinum film covering the silicon substrate [6]. Four different films were examined: film No. 1 was annealed at 700°C; film No. 2, also at 700°C; film No. 3, at 650°C; and film No. 4, at 750°C. Electrodes on film 1 were circular, 0.010 in. in diameter; electrodes on the other films were squares, 0.006 in. on a side. Electrical contacts to electrodes were made with tungsten probes using a probe station. The films varied in thickness between 2.5 µm (film 1) and 3.2 µm (film 4). Since thickness varied across the samples and only a limited number of measurements were made on each sample, thicknesses, which were determined with a profilimeter, are only approximate. Thicknesses are also average values since the surfaces were rough and covered with particulate.

Hysteresis loops obtained with a basic Sawyer-Tower circuit and sinusoidal applied voltages (50 kHz) are shown in figure 6. From these results, it is clear that the remanent polarization is strongly dependent on the applied field. The results are for film 1. Similar loop sets were obtained for the remaining samples. Plots of remanent polarization versus applied peak field are shown for all four films in figure 7. The results are similar for the 700°C and 650°C films. The remanent polarization levels are markedly lower for the 750°C film. We note only a slight indication of saturation of remanent polarization as field levels are increased.

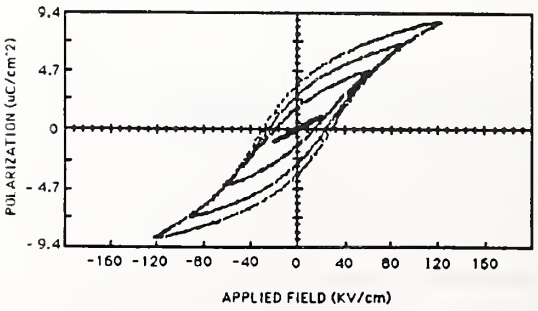

Figure 6. Nested hysteresis loops for film No. 1.

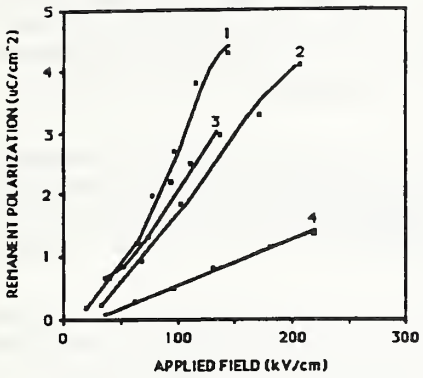

Figure 7. Plots of remanent polarization versus applied field for films 1, 2, 3, and 4.

Memory applications depend on the switching of the remanent polarization with a single pulse and the retention of the switched value with time. Figure 8 shows an oscillograph record of changes in polarization as a function of time for a test capacitor (film No. 1) switched first by a positive voltage pulse and then by a negative voltage pulse. The record was obtained using a Sawyer-Towet circuit. Note the slight decay in remanent polarization over the trace interval. Measurements determining decay over long periods of time have not yet been made. Included in the figure is a plot of the change in polarization (right scale) versus applied field (horizontal upper scale) produced by the positive pulse and negative pulse, respectively.

The dielectric constant was calculated from bridge measurements of capacitance with the assumption that the film material between the electrodes was homogeneous and using the approximate average thicknesses obtained with the profilimeter in the calculation. A value for the dielectric constant was also obtained for the bulk ceramic target. Results are shown in table 1. The values for the ceramic target and the films are reasonably close for the 650°C and 700°C annealed films. The dielectric constant of the 750°C film, however, is considerably less than that of the target. The values of dielectric constant and remanent polarization that are quoted for the films are initial values. Values of both remanent polarization and dielectric constant decreased with switching cycles, particularly for high field strengths. Results showing this decay (or fatigue) phenomenon when the electric field is cycled at 50 kHz are shown in figure 9. The fractional decrease in the value of remanent polarization and of dielectric constant after a fixed number of cycles was at least roughly the same.

Table 1. Measurements of dielectric constant at 10 kHz

Sample	Rel. dielectric constant	Temp. annealed (°C)	Thickness
Target	880	(ceramic)	5 mm (bulk)
Film no. 1	800	700	2.5 μm
Film no. 2	760	700	2.7 μm
Film no. 3	790	650	2.9 μm
Film no. 4	510	750	3.0 μm

The rapid decay with cycling, at high field strengths, of both the dielectric constant and remanent polarization and the fact that this decay occurs in a proportionate way suggest an opening of gaps (dielectric constant of air ($e_r = 1$) between the high dielectric constant particles ($e_r = 800$). The apparent decrease in the dielectric constant would result from the low dielectric constant series capacitors produced by the gaps. The appearance of gaps between particles also reduces voltages across individual particles and thus reduces the field strength within a particle. Remanent polarization is thus reduced as a result of the relation between applied field and remanent polarization (fig. 7). We speculate that such fracturing of the film material at high applied field may result from large strains (and consequent stresses) produced by *c*-domain regions nucleating or expanding within *a*-domain surroundings. Smaller strains resulting from the inverse piezoelectric effect may also contribute to the suggested fracturing. We note that separation of the electrodes from the bulk of the film could also contribute to the decay-with-cycling phenomenon.

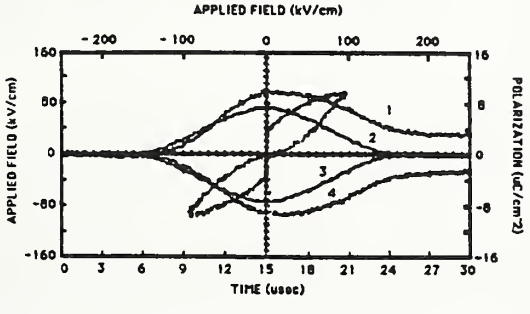

Figure 8. Changes in polarization (curve 1, right-hand scale) as a function of time for a positive pulse (curve 2, left-hand scale). Positive pulse was followed by a negative pulse (curve 3) producing polarization as a function of time (curve 4). Functional relation between electric field and polarization increment and decrement is also shown.

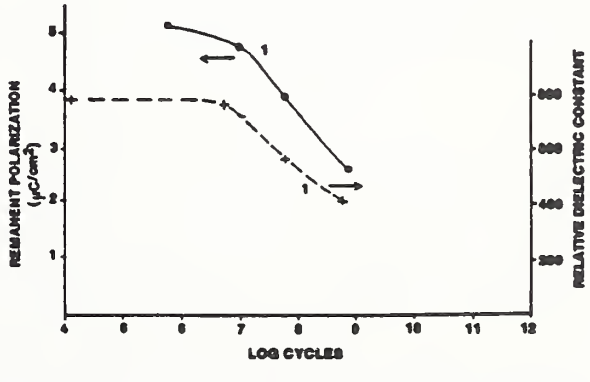

Figure 9. Results showing decay in polarization switched and apparent dielectric constant with cycling when applied field strength was 160 kV/cm.

Conclusion

Films on platinum-coated silicon substrates made by the simple process of laser evaporation from a stoichiometric PZT target were ferroelectric when post-annealed. The ferroelectric films have basic polarization-switching characteristics needed for memory applications. The films, however, presently have a coarse surface morphology which would limit applications in silicon-integrated devices. For this reason we believe primary consideration should be given to process modification directed toward both improving the smoothness of the underlying film and eliminating the large surface particulate.

References

[1] James F. Scott and Carlos A. Paz de Aroujo, "Ferroelectric Memories," *Science*, vol. 240, pp. 1400–1405, December 15, 1989.

[2] P. Krehl, F. Schwirke, and A. W. Cooper, "Correlation of Stress Wave Profiles and the Dynamics of Plasma Produced by Laser Irradiation of Plane Solid Targets," *J. Appl. Physics*, vol. 46, pp. 4400–4406, 1975.

[3] P. K. Schenck, D. W. Bonnell, and J. W. Hastie, "In Situ Analysis of Laser-Induced Vapor Plumes," *Proceedings of the Amer. Vac. Soc. Joint International Laser Science and Amer. Vac. Soc. Conf.*, Atlanta, GA, October 1988 (in press).

[4] P. K. Schenck, L. P. Cook, J. W. Hastie, E. Farabasugh, C. K. Chiang, M. D. Vaudin, and P. S. Brody, "Laser Vaporization and Deposition of Lead Zirconate-Titanate," *Proc. Symp. Beam Solid Interaction: Mat. Res. Soc.*, vol. 157A, 1990.

[5] G. Koren, R. J. Baseman, A. Gupta, M. I. Lutwyche, and R. B. Laibowitz, "Particulate Reduction in Laser-Ablated $YBa_2Cu_3O_7$-d Thin Films by Laser Induced Plume Heating," *Appl. Phys. Lett.* vol 56, pp. 2144–2146, May 21, 1990.

[6] C. K. Chiang, L. P. Cook, P. K. Schenck, P. S. Brody, and J. M. Benedetto, "Characterization of Lead Zirconate-Titanate Thin Films Prepared by Laser Ablation Technique," *Proc. Symp. Ferroelectric Thin Films: Mat. Res. Soc. Meeting*, San Francisco, CA, April 1990 (in press).

SPIE Proc. Sept. 1991 1594-41

Optical characterization of thin film laser deposition processes

P. K. Schenck, D. W. Bonnell, J. W. Hastie, L. P. Cook and C. K. Chiang

Materials Science and Engineering Laboratory
National Institute of Standards and Technology
Gaithersburg, Maryland 20899

ABSTRACT

Pulsed laser deposition (PLD) has recently been shown to be an effective means of depositing thin films from refractory targets. In this study, Nd/YAG and excimer lasers have been used to deposit thin films from refractory, high T_c superconducting, dielectric, ferroelectric and magnetic targets. Optical emission spectroscopy of the laser induced plume has been used to determine the identity and energy (temperature) of the excited state species present in the laser induced plumes. Temporally and spatially resolved optical emission spectra were obtained using a gated intensified photodiode array detector coupled to a grating spectrometer. The individual emission spectra were analyzed to identify the atomic and ionic species present. The temporal and spatial evolution of individual emission lines were used to determine the velocity of the species in the plume. These results were combined with the results from *in situ* molecular beam mass spectrometric analysis of the plumes. In addition, studies of the stoichiometry and morphology, as well as the electrical properties, of these PLD thin films were carried out for correlation with the spectroscopic observations.

1. INTRODUCTION

The vapor plumes produced by the direct interaction of high energy laser radiation with target surfaces have practical application as a material transport medium for the deposition of thin films, particularly films of ceramic and related complex materials. The literature on laser thin film deposition was reviewed by Duly[1,2], who noted that the first thin films were deposited by laser as early as 1965[3], and also by Sankur and Hall[4], who emphasized the optical applications. Most notable, however, is the recent increase in usage of the technique, as indicated by the increase in technical publications. The majority of papers are concerned with deposition of $Ba_2YCu_3O_x$, Bi-Sr-Ca-Cu-O, and related high T_c materials. This interest is due primarily to the utility of the method over conventional sputtering and other preparative methods in preparing thin films of the various high T_c ceramic superconducting phases, the first of which was discovered in 1986[5].

Laser-based sputtering systems offer a number of advantages for film deposition. Small systems suitable for research and development use require less capital investment than, for example, comparable sputtering, chemical vapor deposition (CVD), or molecular beam epitaxy (MBE) systems. Virtually any solid material can serve as a target, including those with complex multicomponent chemistries, so long as the target is relatively homogeneous. An important advantage of the PLD process is its ability to deposit thin films of essentially the same composition as the target material, even from complex mixtures. There appear to be no inherent limitations on the substrate material. Films can be deposited under a variety of conditions, including deposition in the presence of active gases and onto heated substrates.

The physical interactions occurring during laser-induced mass transport are numerous, and include, among others, melting, vaporization, particle ejection, ion etching, and plasma condensation. The absorption of the incident photons by a polycrystalline ceramic target is potentially inhomogeneous, due to the effect of grain boundaries and the optical anisotropies of the individual crystals. Ceramics vary greatly from material to material in their ability to absorb laser radiation and show strong absorption wavelength dependencies. In general, most ceramics have higher optical transmission than metals, leading to dissipation of the incident energy at greater depth in the target. Most film deposition methods utilize pulsed, rather than continuous wave excitation, as larger instantaneous incident power is possible without raising the temperature of the bulk target significantly. Time-dependent phenomena are especially important during laser irradiation. The material leaving the surface during initial plume generation may interact further with the tail of the incoming laser

pulse. The laser-generated plume typically has a strong directional component, and the optical spectra from the plume region are very complex, with both temporally and spatially varying contributions from ions as well as neutrals.

The range of laser generated plumes which have been studied in our laboratory include high T_c ceramic superconductors $Ba_2YCu_3O_x$ and $Bi_2Sr_2CaCu_2O_x$; refractory targets of graphite, SiC, TaC, HfO_2, and yttria-stabilized ZrO_2; electronic materials Si, SiO_2, MgO, Al_2O_3, and Pb_2ZrTiO_6 (PZT); and Fe_3O_4 + Ag, which form magnetic thin films. Plumes from targets of pure components, ie. Cu, Pb etc., and simpler compounds in these systems have been studied to aid in the analysis of the complex plume emission spectra.

2. EXPERMENTAL METHOD

2.1 Plused Laser Deposition Apparatus

The Laser Deposition Facility consists of a deposition chamber with target and substrate mounts, Nd/YAG and excimer high power pulsed laser systems, and ancillary analysis equipment. The Nd/YAG laser used in this work is a 20 Hz pulsed system with a typical pulse width of 15 ns. Discrete wavelengths of 355, 532, and 1064 nm, with energies up to 200 mJ per pulse at 1064 nm, are available from the Nd/YAG laser. The 1064 nm wavelength has primarily been used for optical characterization and film generation using the Nd/YAG laser for PLD, with incident energies of approximately 100 mJ focused to about 250 μm beam spot diameter. The excimer laser operates with either ArF (193 nm, 400 mJ) or KrF (248 nm, 600 mJ). The ArF 193 nm line operating at a constant energy of 100 mJ was predominantly used for excimer-produced films in this work. The laser beams were transfered to the deposition chamber through nitrogen purged channels for lab safety and, in the case of the ArF 193 nm light, to avoid energy loss by atmospheric absorption. The beams were stationary during spectroscopic observation of the plume emission. However, during thin film deposition, the beams were rastered across rotating targets obtain a larger area of uniform deposition and to facilitate uniform target removal.

The cylindrical deposition chamber was constructed of stainless steel with internal dimensions 20 cm diameter by 8 cm height. The chamber was equipped with multiple ports for mounting targets and substrates, laser access to the targets, and optical spectroscopic observations of the laser generated plumes. The chamber was normally continuously evacuated to $<.1$ Pa by oil free pumps. Sample targets were mounted on a continuously rotatable shaft which aided in minimizing cratering effects. The Nd/YAG laser was typically focused through an optical window onto the target using a 20 cm focal length lens. The laser fluence could be varied by adjusting both the laser power and lens-to-target distance.

Thin film substrates were mounted in the deposition chamber by several methods. Both stationary and rotating substrate holders were used to hold substrates at distances 1.0 - 3.0 cm from the target surface. To obtain shorter deposition distances, substrates were mounted on a microscope slide positioned directly over the target surface. A hole drilled through the slide allowed the focused laser beam to pass through to the target surface. A heated substrate holder was used during deposition of high T_c and PZT films. Background buffer/reaction gas in the deposition chamber was introduced through a micrometer-controlled needle valve. To obtain the desired background pressure, gas was supplied from a low pressure ballast tank whose pressure was servo-controlled at about one kPa.

Ports on the chamber allowed for several line-of-sight optical access paths perpendicular to the laser-plume axis. Other side ports on the chamber were provided for future access, such as electrical probing of the plume ions[6] and optical probing of the plume particulates[7].

In typical vacuum experiments, a gas-dynamically stabilized vapor plume was generated by the pulsed laser beam focused onto a target. Generated plumes have instantaneous pressures ($\sim$0.1 MPa or greater) at the surface much greater than those of classical free molecular flow ($<$10 Pa). Above the surface, rapid isentropic expansion occurs, generating a non-perturbed mass transport situation. Ideally, the laser should serve as a heat source without perturbing the vaporization and plume formation processes. Establishment of these conditions may depend on such factors as (1) laser energy, wavelength, and pulse width; (2) system geometry; (3) the optical and thermal properties of the target material; (4) local target surface morphology.

2.2 Optical Emission Spectroscopy

As shown in Fig 1., an optical multichannel analyzer (OMA) consisting of a multiple grating 0.275 meter monochromator with a gateable intensified photodiode array, was used to record the emission spectra of the plume, synchronously with the laser. One-to-one imaging of the plume on the entrance slit of the OMA is obtained using a 10 cm focal length fused silica at twice its focal length. By aperturing the entrance slits of the monochromator with a 0.5 mm horizontal slit and moving the imaging lens (L2 in Fig 1.), emission spectra from the plume can be spatially resolved. The OMA spectrometer was wavelength calibrated using a Hg pen lamp. The actual spectral sensitivity of the spectrometer system was calibrated by mounting spectral radiance standards (D_2 lamp for the UV and a tungsten ribbon lamp for the visible) inside the deposition chamber. This insured that the spectral response calibration included window, lens and filter (used to block second order) effects.

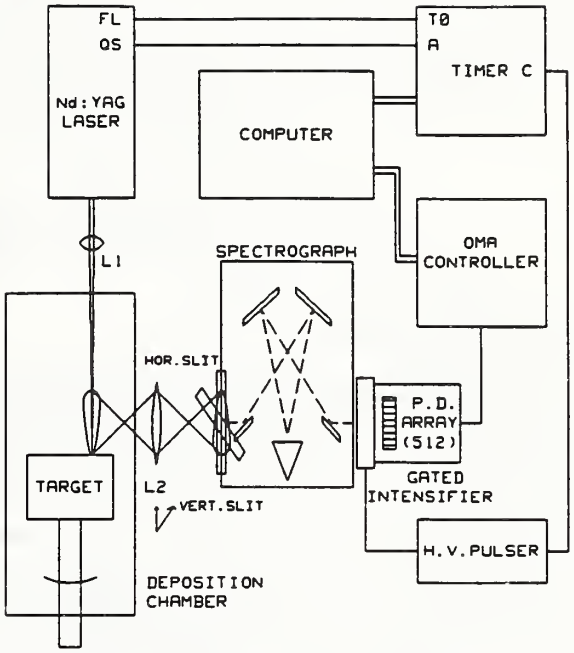

Figure 1 Schematic of apparatus for temporally and spatially resolved optical emission spectra of the laser induced plume.

The timing of the laser firing and OMA gate were controlled by a laboratory computer. When the Nd/YAG laser was used, as depicted in Fig 1., the computer controlled both the flashlamp (FL) and Q-switch (QS) firing. Since the Q-switch firing set the exact time of the laser firing, the gate of the OMA was referenced directly to the Q-switch time. In the case of the excimer laser operating in a constant energy mode, the actual firing of the laser relative to the timing trigger varied with laser internal temperature and the voltage required to maintain the constant energy. Because of this, the actual firing time of the excimer laser was measured relative to the laser trigger using a photodiode and time interval counter. This measured time was used by the computer to adjust the actual OMA gate time. Two OMA detection time schemes were used. In the first approach, the detector gate was 100 ns long and fixed in time after the laser pulse to avoid saturating the detector array. This technique was used when higher resolution spectra were obtained from weakly emitting plumes. In the second approach, the gate was 10 ns wide and was swept under computer control from before the laser onset to several hundred nanoseconds after the laser firing in order to resolve the plume emission spectra in time. Typically, 28 discrete gate times were used to map the temporal evolution of the emission spectra. The interval between gate times was adjusted to cover the duration of observable emission. The OMA controller averaged the detector array spectra from 100 to 1000 laser pulses and subtracted from the emission spectrum a previously stored dark current signal prior to transfer to the laboratory computer. The laboratory computer was used to plot the data and perform wavelength or spectral sensitivity corrections.

2.3 Spectral Analysis

The OMA-obtained emission spectra from the laser generated plumes were complex, containing not only lines from highly excited neutral and ionic species, but also broad band emission from the plasma portion of the plume. The analysis of the spectra was difficult, since the plume temperature greatly exceeds the source temperatures in standard wavelength reference lists. In addition, the volume of spectral data, 28 gate times, 512 spectral elements repeated at several spatial locations makes manual analysis impossible. Most of the spectra obtained were at low spectral resolution ($\sim$1 nm), thus emission line overlap in spectra from multi-element targets was inevitable. Emission spectra taken of laser induced plumes from single element targets were used to generate a reference library of emission spectra obtained under conditions similiar to those of the multi-element targets used in film depositions. Higher resolution spectra ($\sim$0.1 nm) also helped identify lines with individual neutral or ionic species.

The analysis of the plume emission spectra was aided by an in-house computer spectral search program created specifically to help analyze the OMA data. This program used a 33 element data base based on a standard reference wavelength table[8]. The database contained 11,363 lines from 190 to 900 nm. Both manual and automatic peak search and identify with adjustable search sensitivity and width is available. Wavelength calibration can also be based on known line locations. The time resolved spectra were plotted versus time and wavelength. Spectral features identified by the computer were then plotted as a function of time to yield information on the creation, velocity, and temperature of the species.

3. RESULTS AND DISCUSSION

3.1 Emission Spectroscopy of Graphite Targets

Optical emission spectra generated from laser vaporization of graphite targets depended dramatically upon the focus conditions of the laser spot (20 mJ at 532 nm) on the sample. With a tight focus, and hence high local laser fluence, the plume emission was dominated by line spectra, due primarily to C^+ and C^{++}. Defocussing the laser, and thereby reducing the laser fluence, resulted in spectra dominated by C_2 emission. Fig. 2 shows a low resolution spectrum of the C_2 plume emission obtained with a 100 ns OMA gate set just after the laser pulse. The well known Swan system ($A^3\Pi_g$ - $X'^3\Pi_u$) is apparent in Fig. 2. The $\Delta\nu$ = -2, -1, 0, +1, +2 vibrational bands at 436.5, 473.7, 516.5, 563.5 and 619.1 nm, respectively, dominate the spectrum. Additional features at 387.6 nm and 426.7 nm are due to a strong emission from C^+. A small amount of residual laser scattering is also observable at 532 nm. Fig. 3 is a higher resolution spectrum of the 1→0, 2→1, 3→2 and 4→3 transitions (running red to blue). The intensity ratios of these vibrational transitions provides information on the vibrational temperature of the C_2 molecule in the plume, assuming local equilibration of vibrational states. A preliminary analysis of this spectrum indicates vibrational temperatures of 6000-8000 K. The rotational temperatures are substantially lower, 3000-4000 K, due to the expected more facile collisional rotational cooling of the C_2 molecules in the expanding plume. This emission spectrum is neither time nor spatially resolved and it is unlikely that a single rotational or vibrational temperature can be assigned since both rotational and vibrational cooling will occur during the plume expansion. These vibrational and rotational temperatures are also higher than the terminal kinetic (translational) temperatures of the neutral species obtained from the mass spectrometric time-of-arrival data[9,10].

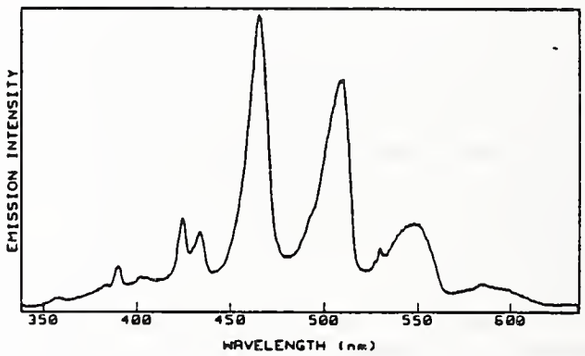

Figure 2 Low resolution (0.6 nm) emission spectra from laser-generated plume from a graphite target showing the C_2 Swan bands.

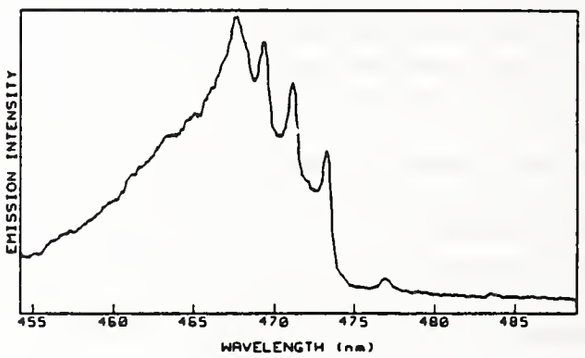

Figure 3 High resolution emission spectrum from the laser-generated plume from a graphite target.

Time and spatially resolved emission spectra were obtained by using a 10 ns gate on the OMA and aperturing the entrance slit of the OMA's monchomator as described above. The time and spatially resolved emission spectra shown in Fig. 4 were obtained using a 1 mm aperture and imaging the target surface at the aperture . Normally the spectra are accumulated every 10 ns from just prior to the laser pulse to 400 ns after the laser pulse, but for clarity in Fig. 4, only the spectra taken every 20 ns from 70 to 190 ns after the laser are shown. The strong emission line from C^+ at 426.7 nm rapidly decreases in time due to the short radiative lifetime of the transition (~5 ns) and the fact that ion production within the plume falls off sharply 50-100 ns after the laser pulse. This narrow production time effect may also be seen

in the narrow ion peaks in mass spectral time of arrival profiles[9,10]. The C_2 Swan band emission intensity falls off more slowly due to its longer radiative lifetime (170 ns) and possible creation in the plume after the laser pulse has ended. The relative heights and widths of these bands depend on both the C_2 vibrational and rotational temperatures, however, the relative heights are more sensitive to the vibrational temperature, and the relative widths to the rotational temperature. The ratio of the Δv = -1 vibrational band at 473.7 nm to the Δv = 0 band at 516.5 nm can provide a C_2 vibrational temperature. Likewise, the width of these bands provides a measure of the C_2 rotational temperature. Both the rotational and vibrational temperatures of C_2 decrease with time, as one would expect.

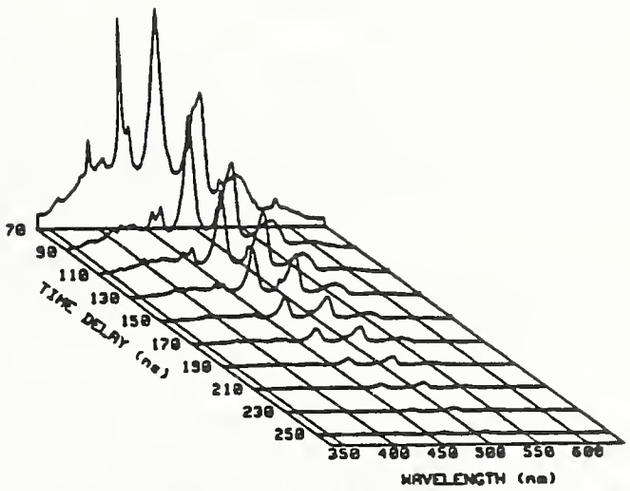

Figure 4 Time and spatially resolved emission spectra of the C_2 Swan bands in the laser-generated plume.

3.2 Emission Spectroscopy of $Ba_2YCu_3O_x$ Targets

Fig. 5 shows two representative OMA emission spectra obtained from the $Ba_2YCu_3O_x$ target plume. The plumes were generated using 20 mJ of 532 nm Nd/YAG laser light focused to a 250 μm spot with a background gas pressure of ~13 Pa of O_2. In Fig. 5 the sample position was static, and the spectrum of Fig. 5A was obtained with a fresh target, while Fig. 3B shows the spectrum after cratering of the surface had occurred from repeated laser impact. Note the dependence of relative intensities on the number of accumulated laser shots. The more volatile Y and Ba species have been depleted, relative to Cu, after 5000 laser shots in the emission spectra of the plume. This result is consistent with the observation by Sudarsen et. al[11] that films deposited with higher fluence are deficient in Cu and rich in Ba and Y.

Mass spectrometric studies of the laser-induced plumes were carried out in collaboration with other workers in our laboratory[10]. The major plume species observed from the high temperature superconductor target, $Ba_2YCu_3O_x$, were Y, Ba, Cu, Cu^+, CuO^+, O_2, and O. In addition to these species, mass spectrometric signals identified as H_2O, CO_2, BaO, YO, Na^+, K^+ and bimetallic species (CuBa, YCu) were also observed in the plume. Elemental assignments were confirmed by isotopic ratio measurements. Oxygen atoms and ions, which are known to be present from the optical emission spectra, were not detectable in the mass spectrometer.

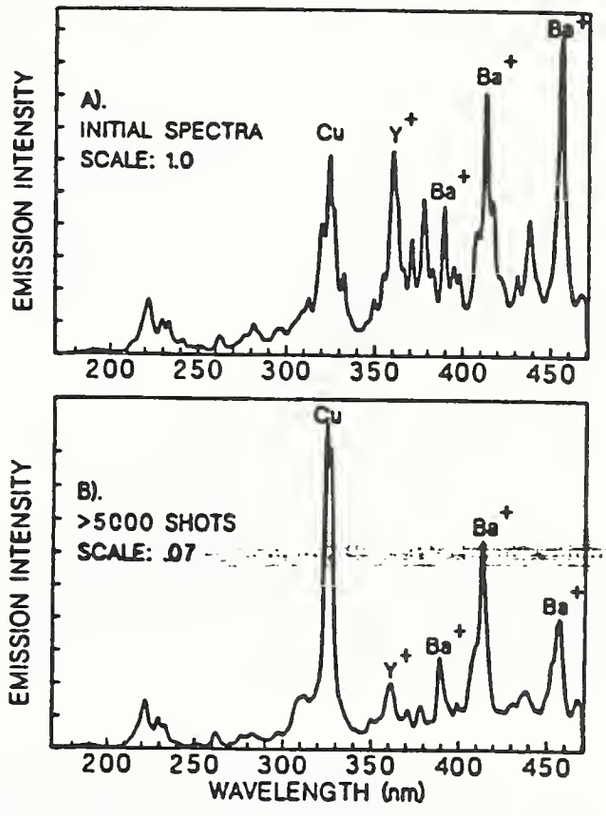

Figure 5 Emission spectra from the laser-generated plume from a $Ba_2YCu_3O_x$ target.Fig. A. shows average spectra from first 1000 shots and Fig. B shows the average spectra of 1000 shots after 5000 shots.

The films deposited using the 1.06 μ Nd/YAG laser light and $Ba_2YCu_3O_x$ targets with a background pressure of ~13 Pa O_2 were found to be oxygen deficient. Post annealing in an O_2 atmosphere did not result in a superconducting thin film. However, thin films made using 193 nm excimer light, ~13 Pa O_2 background pressure and $Bi_2Sr_2CaCu_2O_x$ targets were superconducting (T_c= 80 K) after annealing (810-850°C, 24-72 hours in air).

3.3 Emission Spectroscopy of PZT Targets

Fig. 6 and Fig 7 show representative emission spectra from the excimer (100 mJ, 193 nm) laser-induced plume at 2.0-2.5 mm and 7.0-7.5 mm above the PZT target with a background pressure of 13 Pa O_2. These spectra are part of a series of spectra taken with 0.5 mm spatial resolution in two dimensions relative to the laser impact point. Spectra were taken at each location at 10 ns intervals (near the time of the laser pulse) and 20 ns intervals (100 ns after the laser pulse). In Fig. 6 and Fig. 7 only every other spectrum is plotted for clarity.

The PZT plume emission spectra were compared with emission spectra from laser-induced plumes above pure Ti, Zr, and Pb targets to aid in their analysis. Emission from the PZT targets occured at early times (<100 ns) by emission from singly, doubly and triply ionized Ti and Zr, and with singly ionized Pb emission to a lesser extent. At longer times the spectral features were due to singly ionized and neutral species. Fig. 7 shows this to be particularly true 7mm above the target surface compared to nearer the target surface. The strong ionic emission is consistent with the formation of a plasma extending from the laser impact point to about 12 mm above the target in the center of the laser-induced plume. The velocities of the various ionic and neutral species were estimated from the most probable arrival times at various heights above the PZT target. Species with higher states of ionization have greater observed velocities. Ti^{+++} and Zr^{+++} have velocities in excess of 10^7 cm/s. These velocities and those of the other ionic species present correspond to kinetic energies of from 50 to >100 ev. The role of these highly energetic species in the deposition process is unclear and is under study by adjusting the laser fluence which in turn alters the ratio of higher ionized species to singly ionized/neutral species.

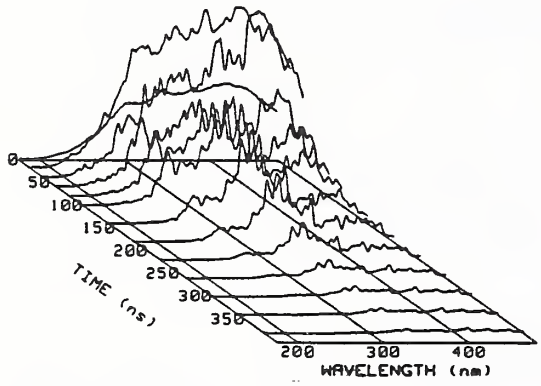

Figure 6 Time-resolved emission spectra from the laser-induced plume 2.0-2.5 mm above the PZT target (Vertical Scale:256048 counts).

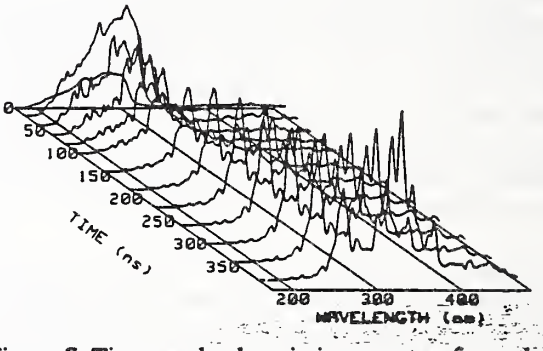

Figure 7 Time-resolved emission spectra from the laser-induced plume 7.0-7.5 mm above the PZT target (Vertical Scale:18186 counts).

PZT films were deposited on Pt-coated silicon substrates using both the Nd/YAG 1.06 μ line and the excimer 193 nm line (conditions as for Figs. 6-7). The as-deposited films were amorphous and required post-deposition annealing at $\sim$550°C to obtain the required ferroelectric perovskite phase. The PZT films deposited using the excimer laser have much better microstructure, i.e. less ejected particles and a smoother surface, and exhibit better ferroelectric properties than those obtained using the Nd/YAG laser. The excimer PZT films were patterned and ferroelectric hysteresis loops were obtained using a Sawyer-Tower circuit. Further optical and mass spectrometric work is planned to study the role of laser wavelength and fluence on the PZT deposition process.

4. COMMENTS AND CONCLUSIONS

The techniques of time-resolved optical emission spectroscopy and mass spectrometry (MS) complement each other in the *in-situ* analysis of laser-induced vapor plumes. Optical emission spectroscopy is well suited to monitoring the evolution of highly excited species formed during plume development while mass spectrometry is more suited to analysis of the cooler post expansion species. Together, the two techniques provide a more complete picture of plume composition, temperature, dynamics, and thin film laser deposition processes than either one alone. A significant problem in comparing MS and optical results is the dichotomy between observable species of the two techniques.

In future studies, methods will be developed and applied to time-resolved optical measurement of surface and plume temperatures. The results will be used to test models, under development, of the laser heating and plume formation process.

5. ACKNOWLEDGEMENTS

The authors would like to acknowledge the asistance of Jianrong Zhao in the analysis of the OMA spectra, W. G. Mallard for computer simulation of the C_2 spectra; E. N. Farabaugh, M. Vaudin, J. Kelly and A. J. Paul for characterization of the thin films; and P. S. Brody for electrical characterization of PZT thin films. This work was supported in part (graphite) by the Air Force Office of Scientific Research.

6. REFERENCES

1. W. W. Duley, *CO_2 Lasers: Effects and Applications*, Academic Press, New York, 1976.

2. W. W. Duley, *Laser Processing and Analysis of Materials*, pp. 171-172, Plenum Press, New York, 1983.

3. H. M. Smith and A.F. Turner, "Vacuum Deposited Thin Films using a Ruby Laser", *Appl. Opt.*, Vol. 4, No. 1, pp. 147-148, 1965.

4. H. Sankur and R. Hall, "Thin-Film Deposition by Laser-Assisted Evaporation", *Appl. Opt.*, Vol. 24, No. 20, pp. 3343-3347, 1985.

5. J. G. Bednorz and K.A. Muller, "Possible High T_c Superconductivity in the Ba-La-Cu-O System", *Z. Phys. B*, Vol. 64, pp. 189-193, 1986.

6. P. Krehl, F. Schwirke and A.W. Cooper, "Correlation of Stress-Wave Profiles and the Dynamics of the Plasma Produced by Laser Irradiation of Plane Solid Targets", *J. Appl. Phys.*, Vol. 46, No. 10, pp. 4400-4406, October 1975.

7. G. Shen and E.S. Yeung, "A Spatial and Temporal Probe for Laser-Generated Plumes Based on Density Gradients", *Anal. Chem.*, Vol. 60, No. 9, pp. 864-868, May 1, 1988.

8. J. Reader, C. H. Corliss, W. L. Wiese and G. A. Martin, *Wavelengths and Transition Probabilities for Atoms and Atomic Ions*, NSRDS-NBS 68, U. S. Goverment Printing Office, 1980.

9. J. W. Hastie, D. W. Bonnell and P. K. Schenck, "Thermochemistry of Materials by Laser Vaporization Mass Spectrometry: 2. Graphite, *High Temp. High Press.*, Vol. 20, pp. 73-89, 1988.

10. P.K. Schenck, D.W. Bonnell, and J.W. Hastie, "*In situ* Analysis of Laser-Induced Vapor Plumes", *High Temp. Sci.*, Vol. 27, pp. 483-501, 1990.

11. U. Sudarsan, N. W. Cody, M. J. Bozack and R. Solanki, "Excimer laser-induced sputtering of $Yba_2Cu_3O_{7-x}$", *J. Mater. Res.*, Vol. 3, No. 5, pp.825-829, Sept./Oct. 1988.

Preparation, Microstructure, and Ferroelectric Properties of Laser-Deposited Thin $BaTiO_3$ and Lead Zirconate-Titanate Films

P. S. Brody, B. J. Rod, K. W. Bennett
Harry Diamond Laboratories, Adelphi, MD 20783-1197

L. P. Cook, P. K. Schenck, M. D. Vaudin, W. Wong-Ng, and C. K. Chiang
National Institute of Standards and Technology
Gaithersburg, MD 20899

Abstract: Ferroelectric thin films of $BaTiO_3$ and lead zirconate titanate, $PbZr_{0.53}Ti_{0.47}O_3$ (PZT), have been prepared by pulsed excimer laser deposition. The microstructure and crystallography of these films have been studied by scanning electron microscopy (SEM), energy dispersive x-ray spectrometry (EDX), transmission electron microscopy (TEM), x-ray diffraction (XRD), and differential scanning calorimetry (DSC). Electrical properties, including remanent polarization, dielectric loss, and dielectric constant, have been measured. Also, switched remanent polarization has been measured under conditions of continuous cycling.

Introduction

Interest in ferroelectric thin films has increased recently, due to the realization that the use of these materials may provide practical and improved nonvolatile silicon integrated random access memory (RAM).[1] Ferroelectric thin films have other applications as well, including optical switches and waveguides, and sensors and actuators. The tetragonally distorted perovskite forms of lead zirconate titanate (PZT) and $BaTiO_3$ are the most extensively studied and used bulk ferroelectric materials, and have also become leading candidates for thin film applications.

In a series of papers[2-10] we have described progress in the use of the laser deposition method to produce ferroelectric thin films. Our earliest studies demonstrated that PZT films could be deposited using the Nd/YAG laser.[2,3] Subsequently, we were able to show that these films, although characterized by a rough surface morphology, could be made ferroelectric.[4,5] Next, we applied the excimer laser to thin film deposition, and were able to produce films having markedly smoother surfaces,[6] although these were not ferroelectric. Most recently, we have succeeded in producing excimer-deposited films having both improved surfaces as well as ferroelectric properties.[7-10] The present paper builds upon these results and reports new results on the characterization of PZT and $BaTiO_3$ thin films produced by the excimer laser deposition method. Laser deposition presents, we believe, a very important route for the preparation of ferroelectric thin films.

Thin Film Deposition and Processing

Pulsed laser deposition was used to prepare thin films of $BaTiO_3$ and PZT from dense stoichiometric ceramic targets. The laser was operated at 193 nm (ArF). Films were deposited on <100> silicon substrates which had been coated with a titanium bond layer about 25 nm thick, followed by a 200-nm-thick platinum layer. Depositions took place in an evacuated chamber, with a background oxygen pressure of 13.33 Pa. This pressure was maintained by a continuously metered oxygen flow combined with a differential pumping arrangement. The laser beam was brought into the chamber and onto the target at an incidence angle of ~35° through a windowed vacuum port. The laser was pulsed at 20 Hz, with 23-ns pulse duration. Fluence was ~30 J/cm^2, with 100 mJ per pulse. The substrate-to-target distance was 2 to 3 cm. The geometry of the deposition system is shown in Fig. 1. During deposition, a luminous plume was produced, the axis of which was perpendicular to the target surface. The laser beam was scanned across the rotating target by an external focusing lens, which was moved under computer control at the rate necessary to ensure comparable exposures on each area of the target. Using this arrangement it was possible to avoid production of deep troughs in the target surface, and instead, material was removed relatively evenly from the surface, thereby prolonging the useful life of the target. Deposition times ranged up to 1 hr at deposition rates of ~2 μm/hr. The as-deposited films showed optical interference fringes, indicating a variation in thickness near the edges. Rotation of the substrate during deposition promoted increased uniformity of film thickness, and resulted in films without interference fringes over a central 1 to 1.5-cm^2 region. While the use of this effect was limited by the size of our chamber, we believe the idea of dual nonconcentric rotation axes for target and substrate could be applied to produce films uniform over much larger areas.

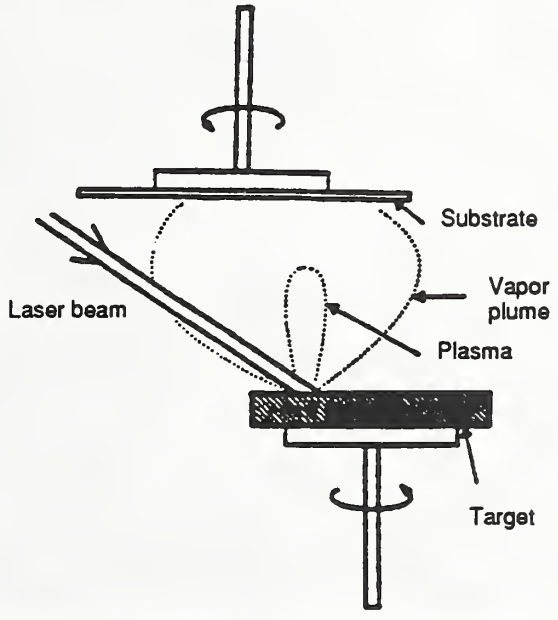

Figure 1. Arrangement for deposition of films using excimer laser.

In the present study films were deposited on both unheated and heated substrates. The substrate heater used a geometry similar to Fig. 1, in which the rotating Si substrate was resistively heated by passing 1.5 to 2.5 A through it at an applied potential of 6 to 12 V. The temperature was maintained during the depositions by operating the heating power source, a dc supply, in the constant current mode. At first the temperature was slowly raised to the desired point manually to avoid thermal runaway. Temperatures were estimated by optical pyrometry at incandescent temperatures (i.e., T > 550°C).

Due to Pb volatility, it was not possible to deposit PZT on substrates heated to incandescent temperatures. Instead, substrates were heated to a temperature below incandescence—estimated, as above, to be at ~400°C. Other films were deposited on unheated substrates. To complete a post-depositional annealing step for all PZT films, the wafer substrate was inserted into a preheated box furnace for times ranging from 15 min to several hours.

Microstructural Characterization

General

Before the electrical measurements, the laser-deposited films were examined by SEM/EDX, TEM (including hot stage work), Raman scattering, profilometry, and XRD (Ni-filtered Cu Ka radiation, theta/two-theta diffractometer).

In the as-deposited state on unheated substrates, all films were amorphous, based on both x-ray and electron diffraction. By comparison with films prepared by the Nd/YAG method (Fig. 2), we found the surfaces of the excimer films were relatively smooth (Fig. 3), with only a few widely scattered ejecta present (e.g., at upper left of Fig. 3). Profilometry measurements on the excimer-deposited films

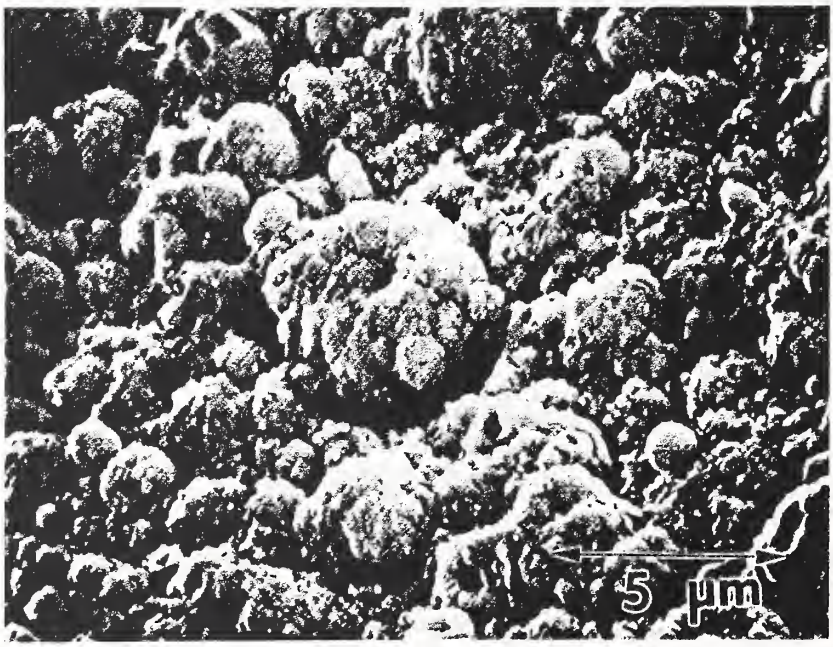

Figure 2. Microstructure of Nd/YAG-deposited PZT film (SEM).

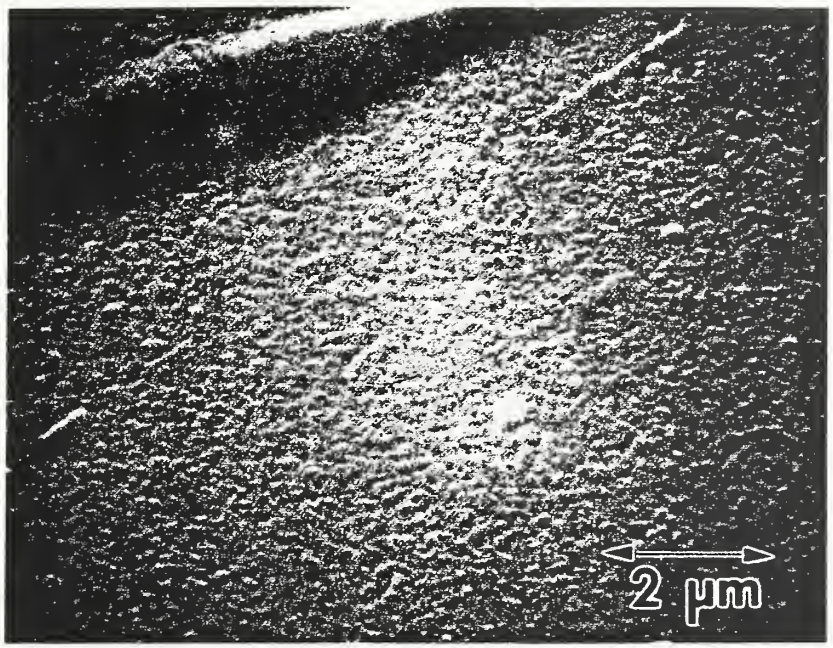

Figure 3. Microstructure of excimer-deposited PZT thin film (SEM).

indicated an average surface roughness of nearly 0.07 μm for both $BaTiO_3$ and PZT films. Most of this roughness was caused by a few widely scattered ejecta.

$BaTiO_3$

Excimer-deposited thin films were prepared from a dense ceramic target of a commercial formulation known as ceramic "B," which contained 5 mol% $CaTiO_3$. Preliminary TEM-hot-stage experiments were completed on very thin excimer-deposited films which had been formed directly on electron-transparent carbon substrates. Most of the results of this study have been described in ref. 6, where it was noted that, with heating, amorphous $BaTiO_3$ particulates crystallized directly to tetragonal $BaTiO_3$. On the basis of this information, we decided to deposit $BaTiO_3$ directly on a heated substrate, with the aim of causing crystallization to occur at the vapor plume/film interface, as film growth proceeded. Using the heated substrate assembly described above, we deposited a film at dull red heat, estimated at 750 °C. This crystalline $BaTiO_3$ film had a very dense microstructure, and showed apparent cubic (rather than tetragonal) symmetry, on the basis of both XRD and TEM-electron diffraction. It also had considerable preferred orientation, with <100> perpendicular to the substrate surface. The grains were elongated parallel to the crystallographic alignment axis. A TEM micrograph for a section perpendicular to the alignment axis is shown in Fig. 4, where it can be seen that the average grain size in this section is in the range 25 to 50 nm. The grains were rodlike and measured at least 250 nm in the elongated direction. This film was not ferroelectric, and was found to have a dielectric constant of ~100. Another film deposited in similar fashion, although also having apparent cubic symmetry on the basis of the x-ray pattern (Fig. 5), was ferroelectric (to be described below). Raman data for this ferroelectric thin film showed that in spite of an apparently

cubic x-ray pattern which did not exhibit splitting, the material had Raman lines at wavenumbers characteristic of tetragonal symmetry.[11]

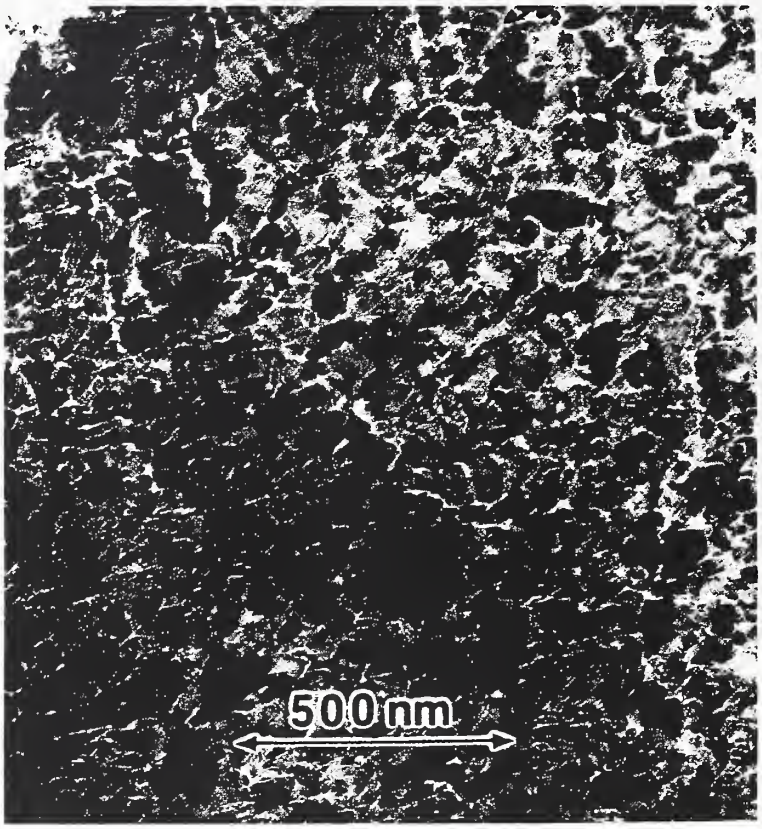

Figure 4. Microstructure of excimer-deposited $BaTiO_3$ thin film deposited on heated substrate (~750°C) (TEM).

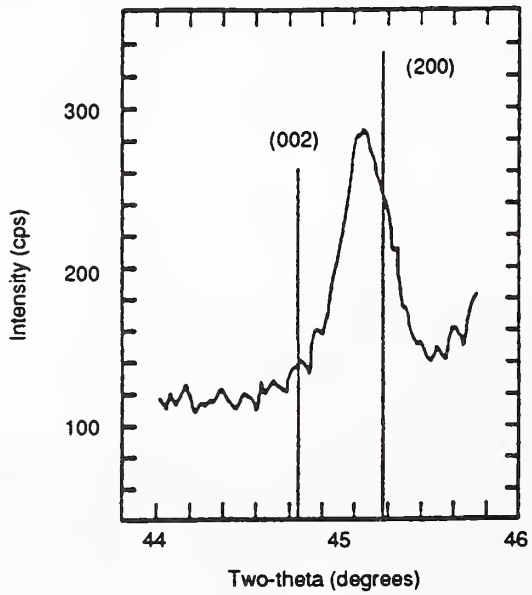

Figure 5. XRD data for ferroelectric excimer-deposited $BaTiO_3$ thin film. Note lack of tetragonal splitting.

PZT

To prepare PZT thin films, we used a dense ceramic of a commercial formulation known as "PZT 5A." Initial TEM studies[6] indicated lead loss due to electron beam heating, so crystallization studies were not completed in the TEM. However, noting that the as-deposited PZT films were amorphous, we carried out studies to investigate the crystallization process by DSC,[6,9] a method commonly employed for glassy materials. The DSC data suggested a glass transition near 300°C. We then attempted to deposit films at a substrate temperature of ~400°C (i.e., above the glass transition temperature), so that the mobility of deposited material would permit good densification. Crystallization was then completed after deposition by annealing in air under isothermal conditions. Since the DSC data indicated a broad crystallization maximum near 500°C, we chose an annealing temperature of 600°C. This yielded unexpectedly large crystallites, as shown in Fig. 6, where it can be seen that the individual crystallites averaged 4 to 5 μm across. On the basis of EDX analyses, production of correct film stoichiometries using the excimer system was more of a problem for PZT than for $BaTiO_3$. The portions of the films deposited away from the vapor plume axis could not be crystallized completely; rather, they contained PZT crystals in a lead-depleted, glassy matrix. Areas of the film deposited directly in front of the plume could be crystallized completely, however, and so these areas were used for the electrical measurements reported below. XRD patterns for films prepared in this fashion were similar to those for the $BaTiO_3$, in that they showed a lack of tetragonal splitting (Fig. 7).

Figure 6. Microstructure of partially crystallized excimer-deposited PZT thin film (reflected light microscope).

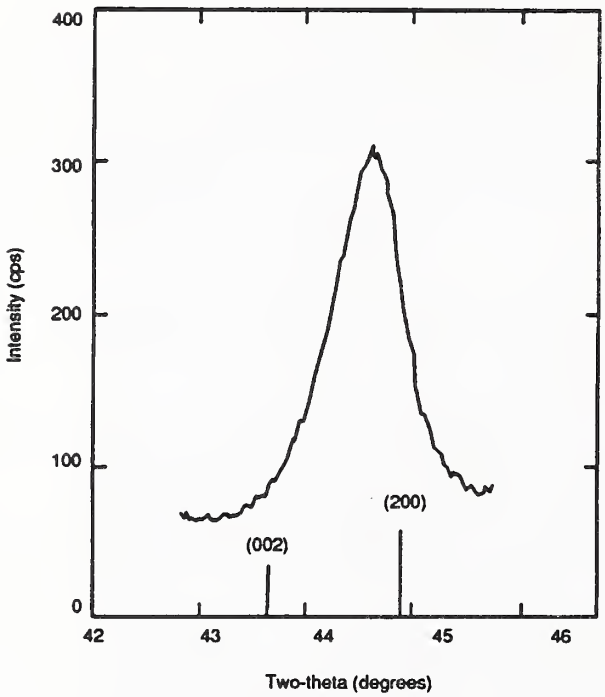

Figure 7. XRD data for ferroelectric excimer-deposited PZT thin film. Note again the lack of tetragonal splitting.

Dielectric and Ferroelectric Properties

General

Dielectric and ferroelectric properties were studied using parallel plate capacitor structures. To form these structures we deposited an array of square Pt electrodes on the surface of the film by sputtering using a shadow mask. The resulting capacitors were investigated using a Hewlett-Packard 4275A LCR meter* and a four-probe technique; capacitance and dissipation factors were measured at 1 mV. Ferroelectric hysteresis measurements for determining remanent polarization were made using a Sawyer-Tower circuit and a Hewlett-Packard 8116A pulse/function generator at sinusoidal applied voltages of ±5 V. We measured decay of remanent polarization and dielectric constant with cycling at 200 kHz.

$BaTiO_3$

A 2-μm-thick $BaTiO_3$ film, with microstructural and crystallographic characteristics as described in the previous section, was measured and shown to give a ferroelectric hysteresis loop (Fig. 8) with a remanent polarization of 4.3 $\mu C/cm^2$ at an applied field of 180 kV/cm. Because of the thickness of this film it was not possible to fully investigate the dependence of remanent polarization on applied field. The dielectric constant for this film was calculated to be ~1300, a value close to the bulk dielectric constant for $BaTiO_3$ ceramic "B."

**Certain commercial equipment, instruments, or materials are identified in this paper in order to adequately specify the experimental procedure. Such identification does not imply recommendation or endorsement by the U.S. Government.*

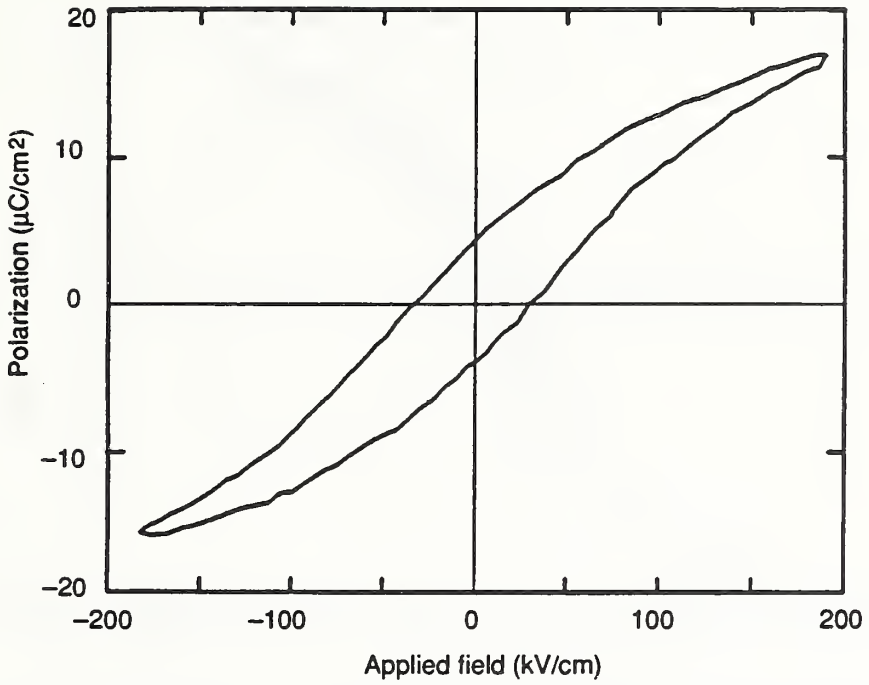

Figure 8. Polarization vs. applied field for 2-μm excimer-deposited $BaTiO_3$ thin film measured at 10 kHz.

PZT

A 180-nm-thick PZT film was shown to give ferroelectric hysteresis loops as indicated in Fig. 9. There is no clear tendency for saturation of the remanent polarization in Fig. 9. Fig. 10 indicates the effect of applied field on remanent polarization. The highest measured remanent polarization was 13.5 $\mu C/cm^2$ at 600 kV/cm. The switching behavior was measured for single 8-V negative and positive pulses as shown in Fig. 11.

The remanent polarization shows no indication of decay over the time interval of Fig. 11. Fig. 12 shows decay of the switched remanent polarization as a function of switching cycles (fatigue), as determined from hysteresis loop measurements. It appears that the decay begins to level off at 10^{10} cycles. The value of the dielectric constant, as determined from the measured capacitance and by assuming a homogeneous film, also decayed with cycling (Fig. 12). The dissipation factor (Fig. 13) showed relatively less change with cycling. These fatiguing data are similar to those obtained on PZT films prepared by other methods.

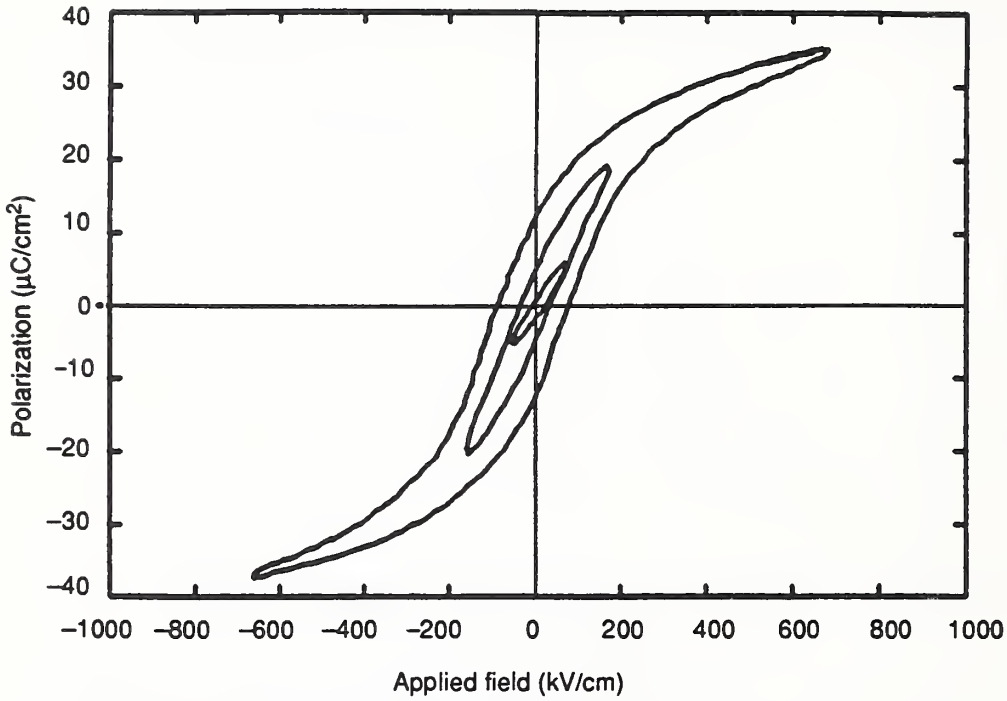

Figure 9. Polarization vs. applied field, showing nested hysteresis loops, for 180-nm excimer-deposited PZT film (annealed at 600°C); measured at 10 kHz.

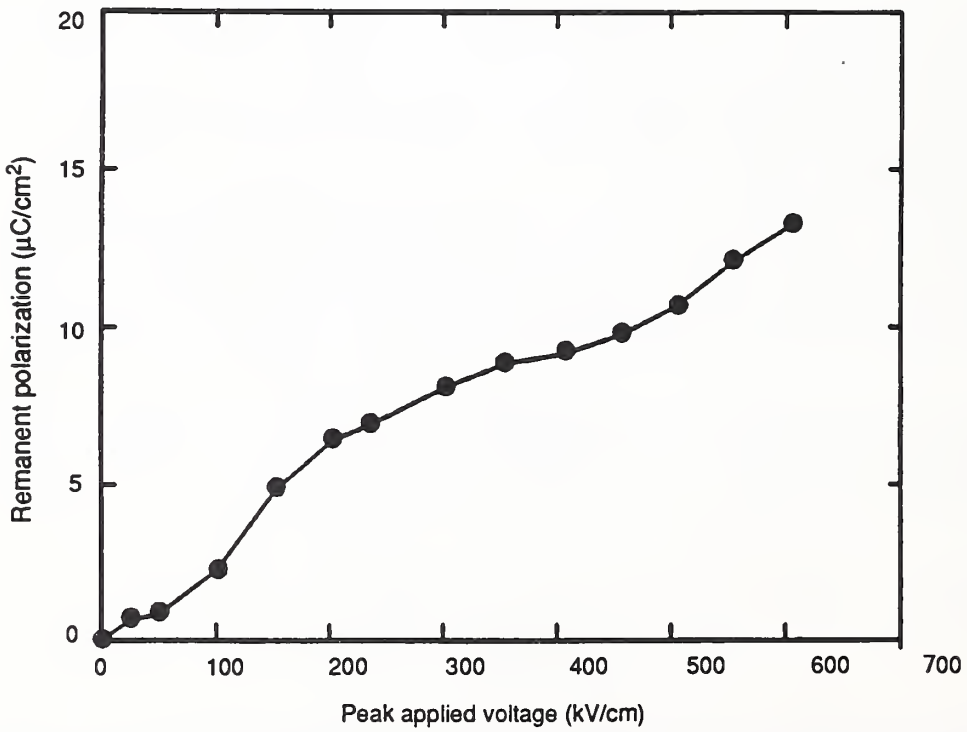

Figure 10. Remanent polarization vs. applied field for same film as in Fig. 9.

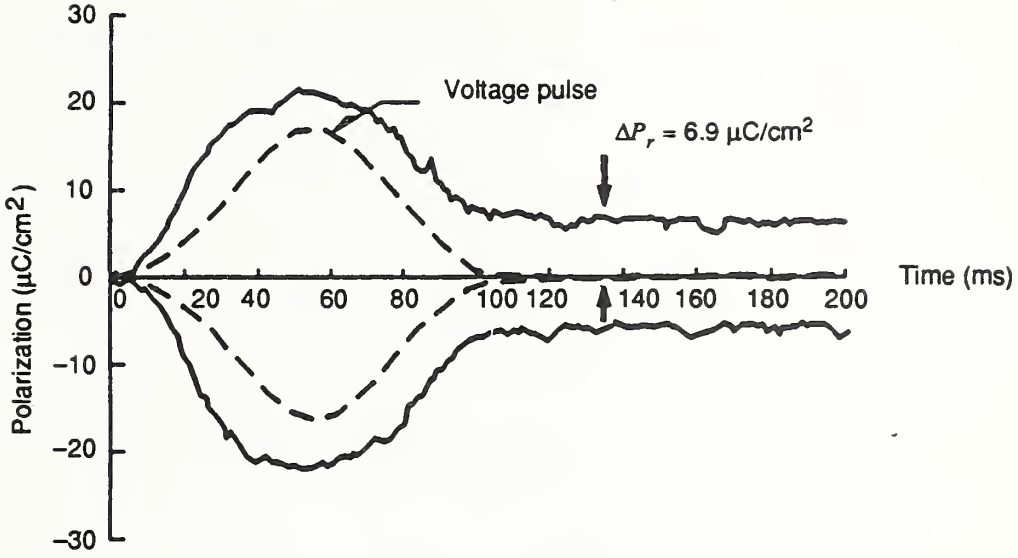

Figure 11. Polarization vs. time for 8-V positive and negative pulses for same film as Fig. 9.

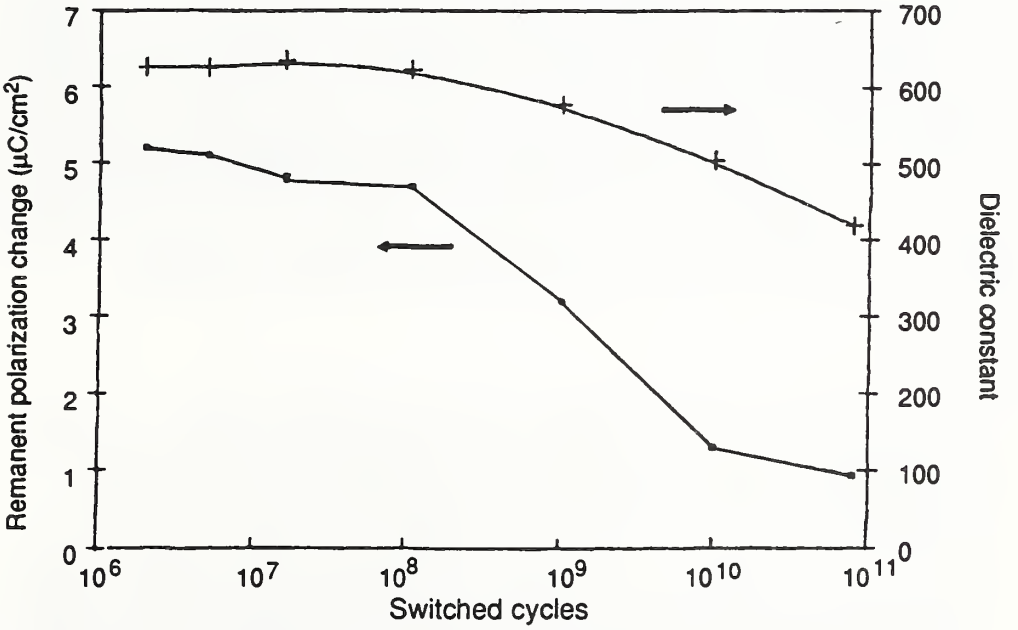

Figure 12. Remanent polarization and dielectric constant vs. cumulative switching cycles at 200 kHz for same film as Fig. 9.

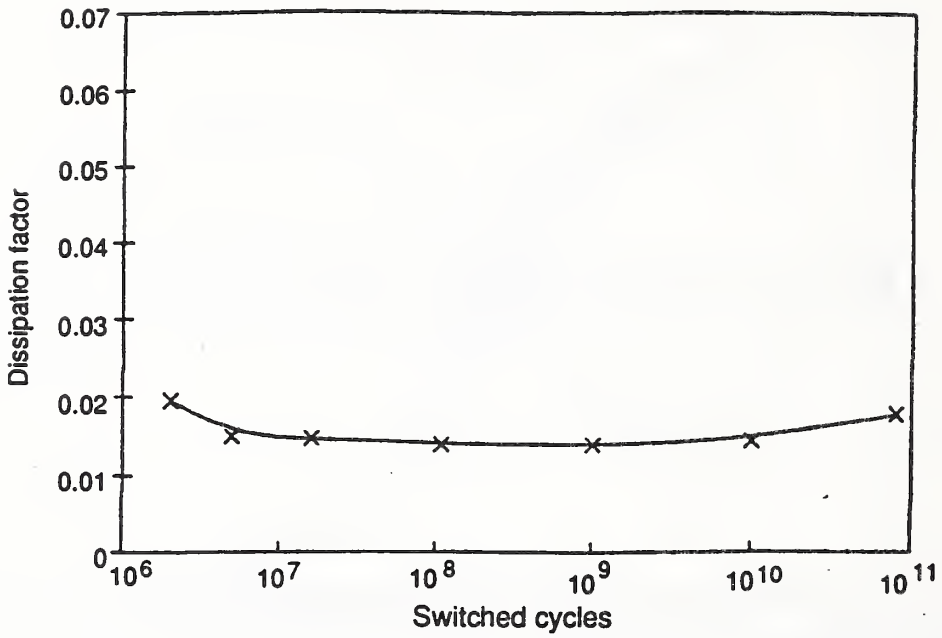

Figure 13. Dissipation factor as a function of cumulative switching cycles at 200 kHz for same film as in Fig. 9.

Conclusions

Dense smooth thin films of $BaTiO_3$ and PZT were prepared on Pt-coated silicon using the pulsed excimer laser deposition technique. Ferroelectric $BaTiO_3$ films can be formed directly on substrates heated at dull red heat. To produce ferroelectric PZT films, however, it was necessary to use a lower substrate deposition temperature, followed by post-deposition annealing. The PZT ferroelectric thin films have polarization/switching characteristics required for memory applications; the $BaTiO_3$ thin films have not been fully investigated. Fatigue properties of the PZT thin films are similar to those prepared by other methods.

References

1. J. F. Scott and C. A. Paz de Aroujo, *Science*, **240** (1989), 1400.
2. L. P. Cook, P. K. Schenck, J. Zhao, E. N. Farabaugh, C. K. Chiang, and M. D. Vaudin, in *Ceramic Thin and Thick Films*, Ceramic Trans. **11**, B. V. Hiremath, editor (Amer. Ceram. Soc., Westerville, OH, 1990), 99-107.
3. P. K. Schenck, L. P. Cook, J. Zhao, J. W. Hastie, E. N. Farabaugh, C. K. Chiang, M. D. Vaudin, and P.S. Brody, in *Beam-Solid Interactions: Physical Phenomena*, Mater. Res. Soc. Symp. Proc., **157**, J. A. Knapp, P. Borgesen, and R. A. Zuhr, editors (Mater. Res. Soc., Pittsburgh, PA, 1990), 587-592.
4. P. S. Brody, J. M. Benedetto, B. J. Rod, K. W. Bennett, L. P. Cook, P. K. Schenck, C. K. Chiang, and W. Wong-Ng, "Microstructure and Ferroelectric Properties of Lead Zirconate-Titanate Films Produced by Laser Evaporation," to be published in *Proceedings of the 7th International Symposium on Applications of Ferroelectrics (ISAF)* (IEEE, Univ. Illinois,

Champaign-Urbana, 6-8 June 1990).

5. C. K. Chiang, L. P. Cook, P. S. Brody, and J. M. Benedetto, in *Ferroelectric Thin Films*, Mater. Res. Soc. Symp. Proc. **200**, E. R. Myers and A. I. Kingon, editors (Mater. Res. Soc., Pittsburgh, PA, 1990), 133-138.
6. L. P. Cook, M. D. Vaudin, P. K. Schenck, W. Wong-Ng, C. K. Chiang, and P. S. Brody, in *Evolution of Thin-Film and Surface Microstructure*, Mater. Res. Soc. Symp. Proc. **202**, C. V. Thompson, J. Y. Tsao, and D. J. Srolovitz, editors (Mater. Res. Soc., Pittsburgh, PA, 1991), 241-246.
7. W. Wong-Ng, T. C. Huang, L. P. Cook, P. K. Schenck, M. D. Vaudin, C. K. Chiang, and P. S. Brody, "PZT Films Prepared by the Pulsed Laser Deposition Technique," to be published in *Proceedings of the International Conference on Materials and Process Characterization for VLSI (ICMPC '91)*, R. C. McDonald and T. C. Huang, editors.
8. L. P. Cook, W. Wong-Ng, T. Huang, P. K. Schenck, M. D. Vaudin, C. K. Chiang, and P. S. Brody, *Thermal Processing of Laser-Deposited* $BaTiO_3$, **ibid.**
9. L. P. Cook, P. K. Schenck, M. K. Vaudin, C. K. Chiang, W. Wong-Ng, "Processing of Laser-Deposited Thin Films of $BaTiO_3$ and PZT," to be published in *Ferroelectric Films*, Proc. AcerS Symp. Cincinnati, OH (April 1991), A. S. Bhalla and K. M. Nair, editors (Amer. Ceram. Soc., Westerville, OH, 1991).
10. C. K. Chiang, W. Wong-Ng, P. K. Schenck, L. P. Cook, M. D. Vaudin, P. S. Brody, B. J. Rod, and K. W. Bennett, "Characterization of Lead Zirconate-Titanate Thin Films Prepared by Pulsed Laser Deposition," to be published in *Phase Transformation Kinetics in Thin Films*, Mater. Sci. Symp. Proc. **230** , ed. by M. Chen, M. Thompson, R. Schwartz, and M. Libera (Mater. Res. Soc., Pittsburgh, PA, 1991).
11. L. H. Robins, unpublished data, NIST, 1991.

POWDER X-RAY DIFFRACTION CHARACTERIZATION OF LASER DEPOSITED FERROELECTRIC THIN FILMS

W. Wong-Ng, T.C. Huang*, L.P. Cook, P.K. Schenck, M.D. Vaudin, C.K. Chiang, L.H. Robins and P.S. Brody**

National Institute of Standards and Technology (NIST), Gaithersburg, MD 20899

*IBM Almaden Research Center, San Jose, CA, USA

**Harry Diamond Laboratory (HDL), Adelphi, MD, USA.

ABSTRACT

Thin films of $BaTiO_3$ and $Pb(Zr_{.53}Ti_{.47})O_3$ (PZT) have been deposited on Pt and Pt-coated silicon substrates using both Nd-YAG and excimer lasers. The $BaTiO_3$ films were prepared using heated substrates and were crystalline. The PZT films were deposited at room temperature and were amorphous; on annealing, they crystallized and gave rise to well-defined powder x-ray diffraction patterns.

To compare and correlate the properties and processing conditions of these thin films, characterizations were performed using a variety of analytical techniques including x-ray diffraction, TEM, SEM/EDX and ferroelectric and dielectric property measurements. The x-ray diffraction technique was used for identifying the various phases formed and also for analyzing the profiles of the diffraction peaks. Both the PZT films annealed below 800°C and the $BaTiO_3$ films typically show polycrystalline x-ray diffraction patterns corresponding to a pseudo-cubic structure (i.e no peak splitting) instead of the tetragonal patterns characteristic of the target materials. It was found that for the $BaTiO_3$ films the pseudosymmetry was due to crystallographic alignment of the longer c-axis in the substrate surface to relieve strain. In the PZT films annealed below 900°C, it is suggested that the residual surface strain and/or small crystallite size of these materials may have precluded the peak splitting; at higher annealing temperatures, the tetragonal symmetry was recovered.

INTRODUCTION

In recent years, ferroelectric $Pb(Zr_{.53}Ti_{.47})O_3$ (PZT) and $BaTiO_3$ films on silicon wafers have become increasingly important for silicon-integrated nonvolatile memories. Laser-induced vaporization (also called pulsed laser deposition) is a technique in which a plume of ionized and ejected material is produced by high-intensity laser irradiation of a solid target, and the plume is deposited on a substrate. This technique has been applied using two different types of lasers, Nd/YAG and excimer, to produce films on Pt-coated Si wafers and Pt foil substrates, by laser irradiation of

commercially prepared lead zirconate-titanate (PZT(Zr/Ti = 53/47)) and $BaTiO_3$ (5% $CaTiO_3$) targets.

In the structure of a cubic perovskite ABO_3 (Figure 1), the B^{4+} ions occupy the centers of each unit cell while the A^{2+} ions are located at the corners. In the corresponding distorted ferroelectric structure, the B^{4+} ions move parallel to the c-axis, giving rise to a tetragonal crystal structure with two polarization states; a permanent electric dipole parallel or antiparallel to $\underline{c}$ is produced primarily by the up or down displacement of the B^{4+} ions with respect to the other ions. The high temperature form of $BaTiO_3$ is cubic, and as it cools to room temperature a phase transformation to a tetragonal structure takes place at the Curie temperature ($\approx$ 120°C) [1]. In the case of PZT, although $PbZrO_3$ is antiferroelectric, its solid solutions with more than about 10 mole percent $PbTiO_3$ are ferroelectric [2] and show rhombohedral and tetragonal distortion from the ideal cubic perovskite structure at room temperature. A morphotropic phase boundary occurs near 55 mole % $PbZrO_3$. Solid solutions richer in $PbZrO_3$ are rhombohedral (pseudocubic with slight extension along a body diagonal), while those richer in PbTi03 are tetragonal with c/a a few percent greater than 1. Both the rhombohedral and the tetragonal phase are ferroelectric.

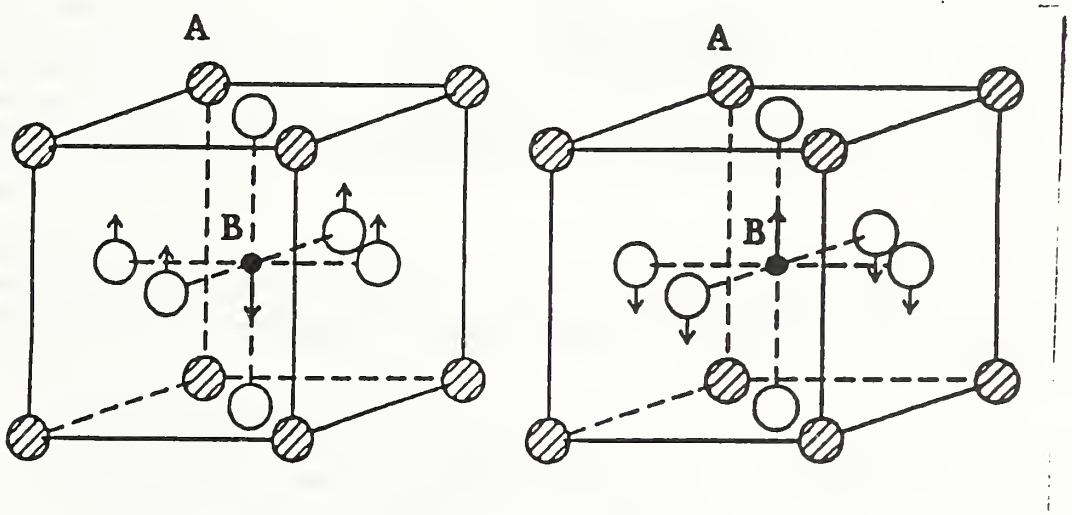

Fig. 1 Polarization states in a ferroelectric ABO_3 structure

Since knowledge of the crystallization process in thin films is fundamental to thin-film processing technology, the goals of this continuous joint effort [3-6] are: to investigate the optimum conditions for preparing PZT films; to understand the phase formation at various heat treatment conditions; to understand the crystallography of the thin film materials; to characterize the properties of these films by using a variety of techniques including x-ray diffraction, scanning and transmission electron microscopy (SEM and TEM) and electrical measurements; and to compare properties of films prepared with the Nd/YAG and the excimer lasers. This paper emphasizes the results of x-ray diffraction studies.

EXPERIMENTAL

Fully dense PZT and $BaTiO_3$ target disks for film preparation were obtained commercially. Films were produced with the use of both a focused Q-

switched Nd/YAG pulsed laser and a focused ArF excimer laser. The schematic of the Nd/YAG laser deposition apparatus is shown in Figure 2. A laser beam was passed through a hole in the substrate holder and was focused onto a rotating target in a vacuum chamber to produce a plume which deposited onto the substrate. The pulse width was 15 ns and the 1064 nm fundamental wave length was used. Although the excimer laser deposition apparatus was similar to the Nd/YAG apparatus, the 192 nm laser beam did not pass through a hole in the substrate. Instead, it impinged on the target surface at about 65° to the surface normal. In both laser systems

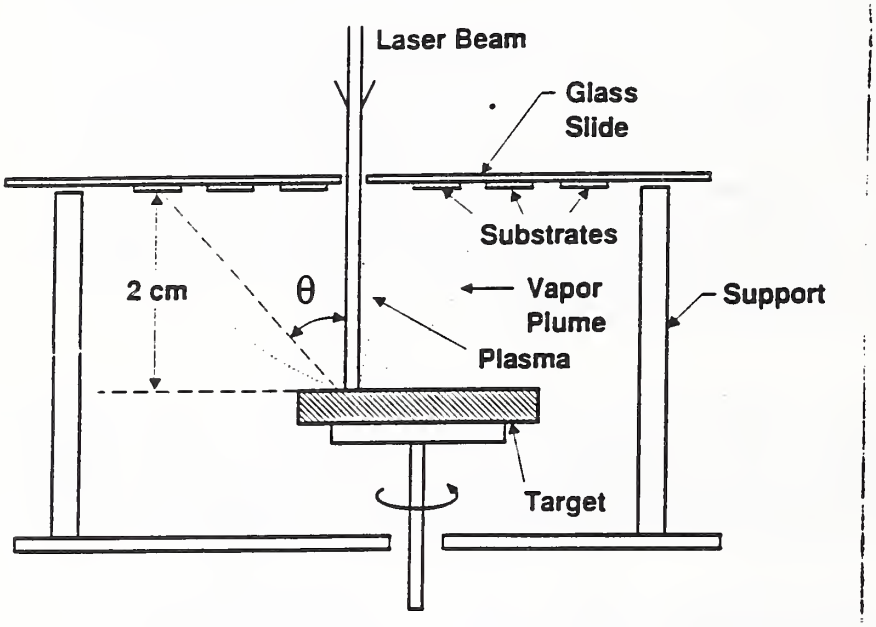

Fig. 2 Schematic of the Nd/YAG laser deposition apparatus

analytical diagnostics were available for the plume and deposition process, including mass spectroscopy, optical spectroscopy, electrical probes and optical scattering. We have reported optical spectra from the PZT plume in an earlier reference [3]. During deposition, oxygen was metered into the chamber to produce a background pressure of 13.33 Pa (100 mTorr). The growth rate of the film was about 1-2 μm per hour, and the distance between the target and the substrate was about two centimeters.

The $BaTiO_3$ films were deposited using an excimer laser on a heated substrate whose temperature was estimated to be around 750°C. The PZT films reported here were deposited onto room temperature substrates and post-annealed at various temperatures up to 1200°C. Two substrates were used, Pt metal foil and Pt-coated silicon wafers. In the case of the Nd/YAG films, heat-treatments were performed at 500, 600, 650, 700 and 750°C in air, and also at higher temperatures of 800, 900, 1000, 1100 and 1200°C by using a lead-buffered cell. The PZT films produced by the excimer laser were heat-treated at 357, 398, 450, 500, 550 and 602°C. The average thickness of the films was estimated by profilometry.

X-ray data were measured with a computer-controlled diffractometer equipped with a graphite crystal monochromater operating at 40KV and 30MA. $CuK_{\alpha 1}$ radiation was used for data collection. In general, the 2θ scanning range was 3°-72°.

A $BaTiO_3$ film was prepared for TEM observation by cutting a 3 mm disk and ion milling the disk from the substrate side with a glass cover on the film side to avoid sputtering from the substrate onto the film. Once the film had been perforated, the specimen was milled briefly from both sides to remove any glass that was sputtered from the cover slip onto the film.

RESULTS AND DISCUSSION

$BaTiO_3$ Thin Films

The average thickness of the $BaTiO_3$ films is about 1 μm. X-ray powder patterns from these films do not show obvious evidence of peak splitting in Figure 3a, where the stick pattern of the tetragonal reference pattern of $BaTiO_3$ from the JCPDS-ICDD File 5-626 [8] is included for comparison. It is seen that despite the presence of only one experimental peak for each doublet in the tetragonal standard, the experimental peaks align with the higher 2θ peak in the standard as shown clearly in the 001/100 diffraction peak in Figure 3b. This suggests that the film is crystallographically textured with the a-axis of the tetragonal cell normal to the surface of the film. Detailed examination of the 002/200 diffraction peak in Figure 3c showed a partially resolved splitting, which yielded a tetragonal cell of a = 3.993(1) and c = 4.013(3) Å.

TEM observation of a $BaTiO_3$ film at many different orientations showed it to consist of rod-shaped crystals with their long axes approximately normal to the plane of the film. The rods are 25 to 50 nm in diameter. Their average length cannot be accurately determined but has been estimated to be around 250 nm. Figure 4a is a TEM image of the $BaTiO_3$ film taken when the film was tilted 65° from normal to the electron beam so that the rods are nearly side-on.

The crystallographic alignment of the rods of $BaTiO_3$ relative to the film was observed with electron diffraction. Figure 4b is a diffraction pattern from a selected area of Figure 5a correctly oriented with respect to the image. The arcs of intensity in a number of the diffraction rings indicate

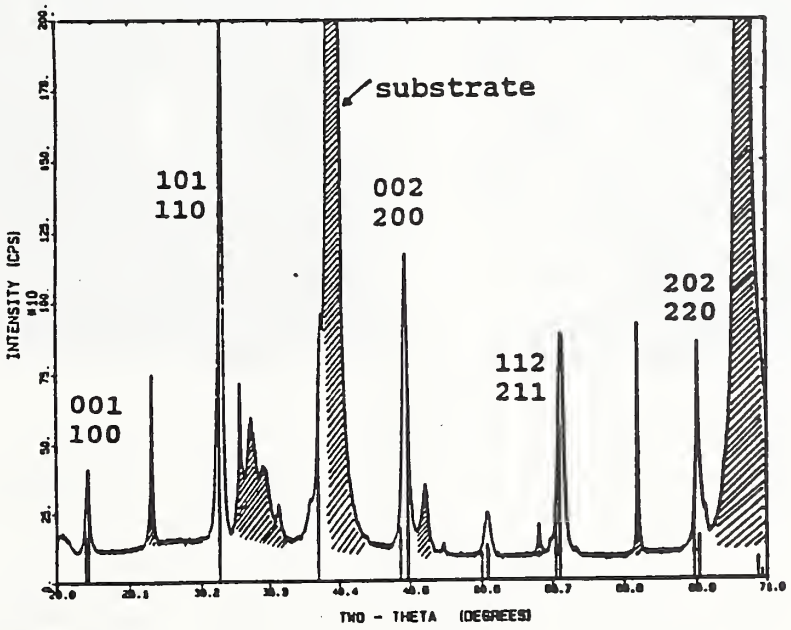

Fig. 3a X-ray diffraction pattern of $BaTiO_3$, the stick pattern from the JCPDS File is included for comparison.

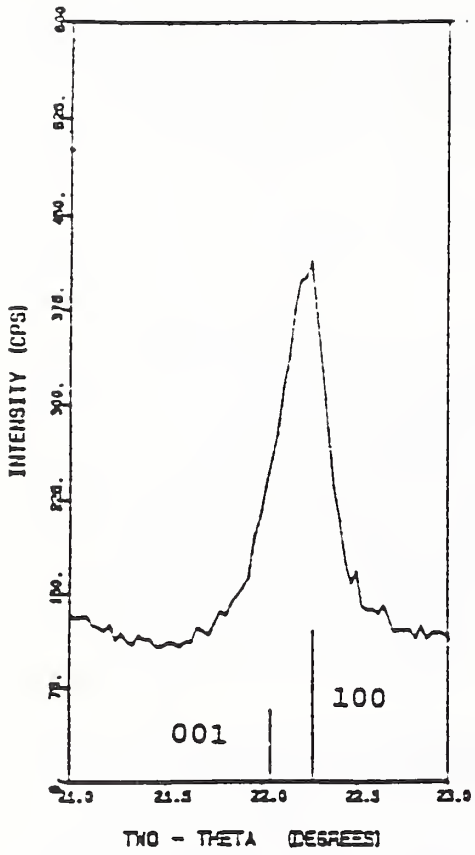

Fig. 3b X-ray pattern showing alignment of a-axis.

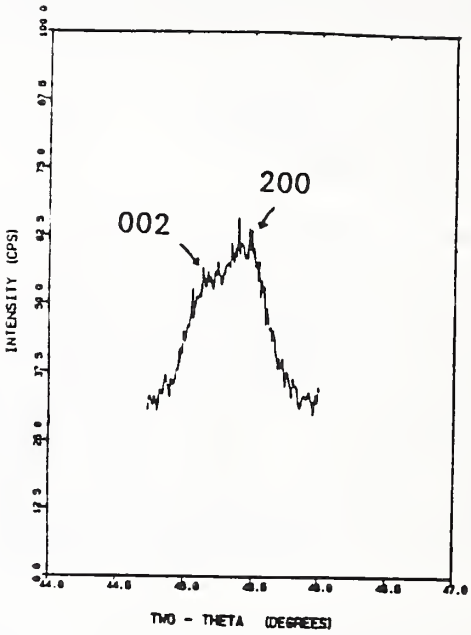

Fig. 3c X-ray pattern showing a-axis incipient splitting.

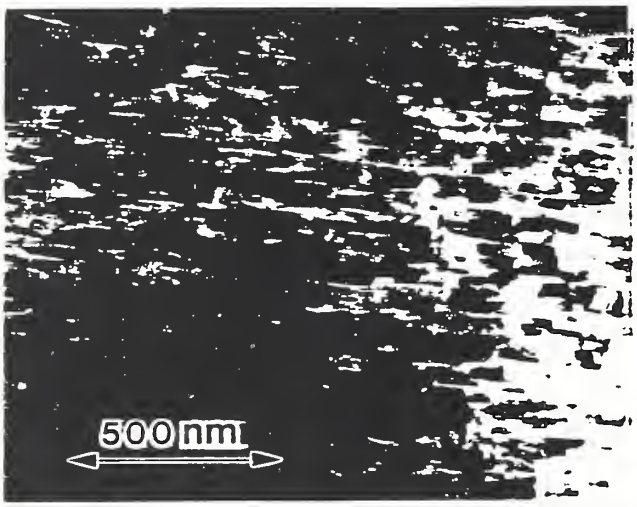

Fig. 4a TEM micrograph of excimer $BaTiO_3$ on heated Pt/Si substrate.

Fig. 4b Selected area electron diffraction from area in Figure 4a.

crystalline texture in the film. For example, the first ring, 100/001, and the fourth ring, 200/002, have sharp, relatively intense arcs centered on a line parallel to the direction of the rods in the image. With electron diffraction it is not possible to differentiate between 100 and 001 diffraction. However, the x-ray results showed a tendency for the a-axis

of the tetragonal cell to be normal to the film, indicating the rods are mostly a-axis aligned. During the growth of the film, the fastest growing rods will come to dominate the microstructure. This suggests that during deposition at ≈750°C, when the material is cubic, <100> is the fast growth direction.

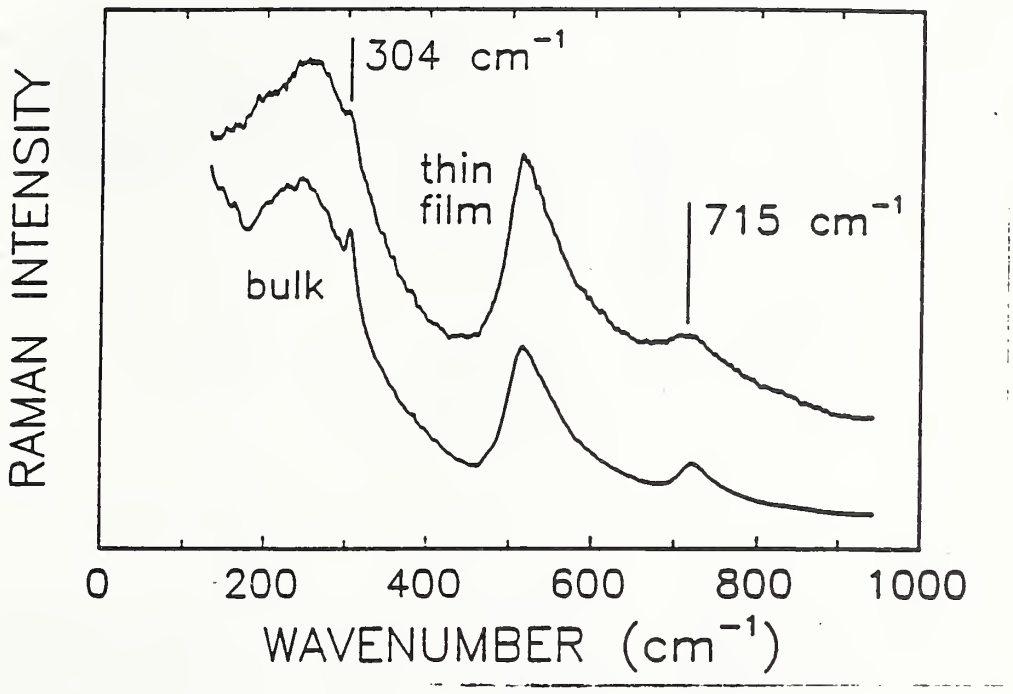

Fig. 5 Raman spectrum of $BaTiO_3$

An explanation for the c-axis orientation of $BaTiO_3$ in the plane of the film can be suggested as follows. On cooling from the deposition temperature of ≈750°C, the film developed tensile stresses in the plane of the substrate. When the $BaTiO_3$ cooled through the Curie temperature of about ≈120°C [1], it underwent a cubic to tetragonal phase transformation. It has been shown that cooling from 727°C (1000K) to 127°C (400K) Pt and $BaTiO_3$ contract by 0.613% and 0.712% respectively [1]. The $BaTiO_3$ film, being constrained by the Pt substrate, experiences a thermal expansion mismatch of about 0.1%. Alignment of the larger tetragonal c-axis parallel with the substrate surface reduced the magnitude of the tensile stresses in the plane of the substrate. This is consistent with the alignment of the a-axis with the substrate normal that is observed in the x-ray diffraction patterns.

The tetragonal symmetry of the $BaTiO_3$ film was also implied by the similar Raman spectra of the film and the ceramic target. Figure 5 shows a section of the spectrum up to 1000 cm^{-1}. The narrow lines at 304 and 715 cm^{-1} are an indication that the film has cryatallized in the tetragonal form. These lines, however, are weaker and broader in the film than in the target. Possibly this is because the magnitude of the tetragonal distortion is smaller in the film than in the substrate [8], or, alternatively, because residual strain in the film causes inhomogeneous broadening of the lines.

PZT thin films

X-ray diffraction results show that both the Nd/YAG and the excimer lasers produced amorphous PZT films at room temperature, and that under

appropriate heat-treatment the ferroelectric perovskite PZT phase was formed. The average thickness of the films was about 2 μm. The energy dispersive x-ray spectra of these films show compositions similar to the target.

Thin-films of $Pb(Zr_{.53}Ti_{.47})O_3$ were prepared with the Nd/YAG laser and annealed at various temperatures and times ranging from 15 minutes at 1200°C to 6 hours at 500°C. X-ray diffraction patterns from these films are shown in Figure 6. The perovskite PZT phase appears to form at a temperature as low as 500°C (the stick pattern of PZT from the JCPDS Powder Diffraction File 33-784 [8] is shown for comparison). The diffraction patterns for films annealed at temperatures between 500 and 750°C appear to be characteristic of cubic symmetry. For example, the film annealed at 750°C can be indexed by a pseudo-cubic unit cell with a_o = 4.067(2)Å). For comparison, the hkl indices are illustrated for the tetragonal case.

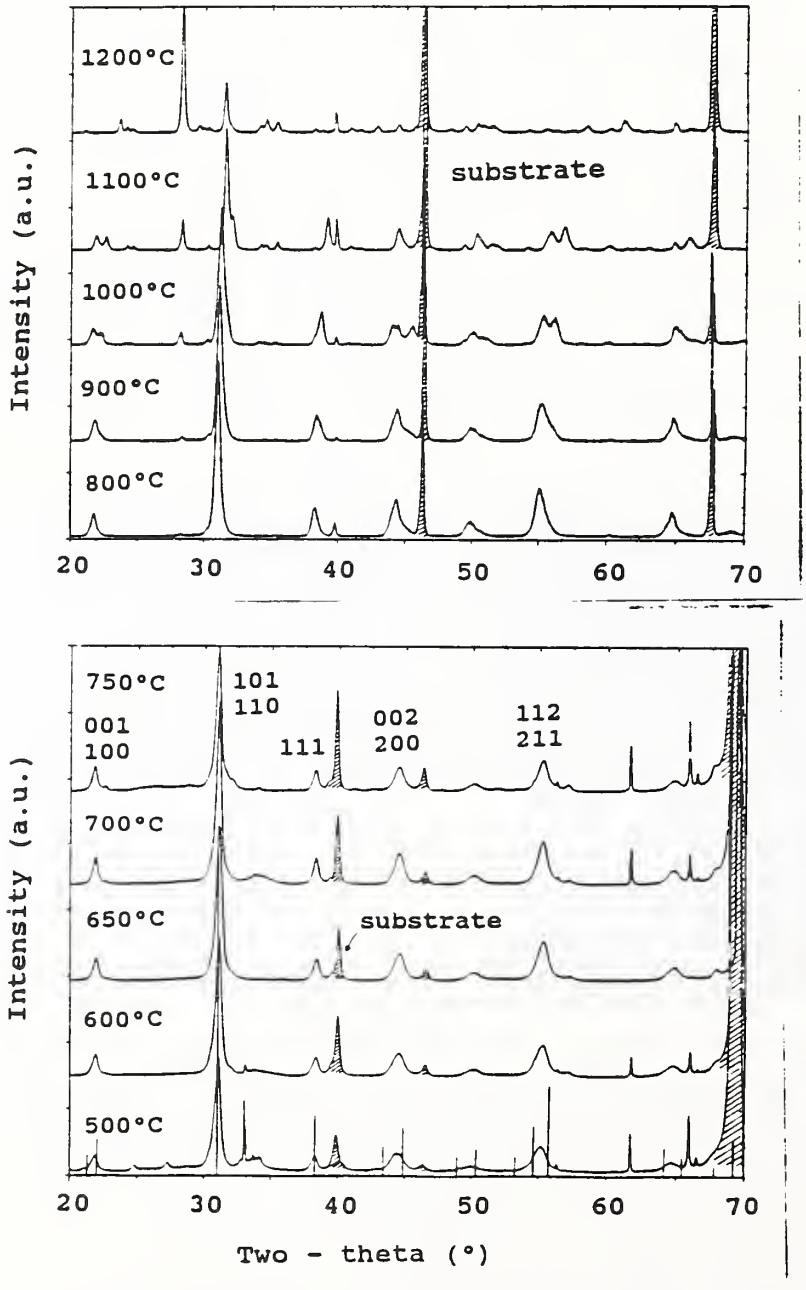

Fig. 6 X-ray diffraction patterns for annealed Nd/YAG PZT films produced by excimer laser

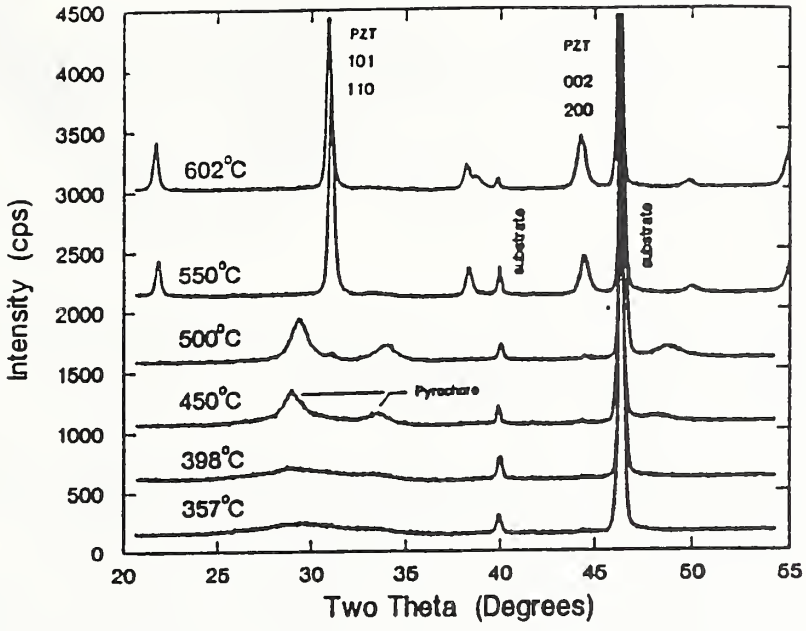

Fig. 7 X-ray diffraction patterns for annealed excimer PZT films.

At higher annealing temperatures (800-1200°C), splitting of the pseudo-cubic peaks was observed at a temperature > 900°C. The patterns taken at 750°C and 800°C are rather similar. The apparent splitting of the diffraction peaks occurs at an annealing temperature slightly below the temperature for the onset of chemical decomposition. At 1100°C, a tetragonal cell of ≈ a=3.937(4) and c=4.068(5)Å can be used to index the diffracsion peaks. In these films annealed at high-temperature, small amounts of other phases such as ZrO_2 appear to be present. At 1200°C, the pattern was drastically different; the peaks corresponding to PZT diminished and the presence of a much larger amount of ZrO_2 was identified. The possible presence of $ZrTiO_4$, PbO and $Pb_2Ti_2O_6$, was also noted. Some unknown peaks still remain to be identified.

X-ray results (Figure 7) from a set of films produced by the excimer laser show the formation of the pyrochlore phase at low annealing temperatures and the formation of a pervoskite PZT phase between 500 and 550°C. Again, the pseudocubic symmetry was observed from these PZT patterns.

The ferroelectric nature of some of these films was demonstrated by the hysteresis loops relating the remanent polarization and the applied field. Figures 9a and 9b are hysterisis loops from PZT films, one deposited by the Nd/YAG laser and annealed at 700°C, and the other deposited by the excimer laser and annealed at 600°C. Annealing above 550°C has been found necessary to produce the PZT phase.

The ferroelectric properties, shown in Figure 8, of the film annealed at 700°C require the presence of non-cubic symmetry. Unlike the $BaTiO_3$ film which was deposited at high temperature, the PZT films do not appear to be crystallographically aligned. The pseudo-cubic x-ray peaks lie at positions intermediate between the tetragonal doublets of the target materials, instead of aligning with either peak of the doublets. The apparent difference between the observed cubic symmetry and the lower symmetry

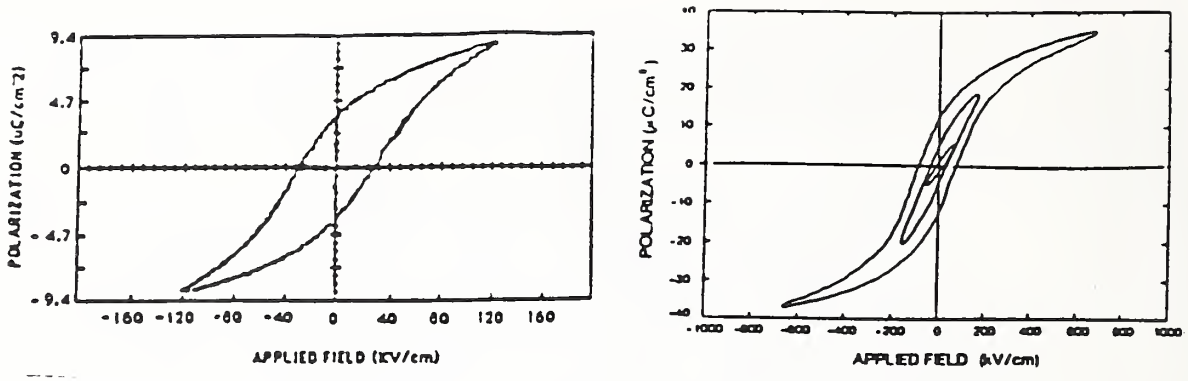

Fig. 8 Applied field vs. polarization for PZT (a) Nd/YAG annealed at 700°C and (b) excimer, annealed at 600°C.

required for ferroelectric behavior is possibly due to the presence of interfacial stress as a result of thermal mismatch between PZT and the substrate, and/or the small crystallite size of the material.

The x-ray full width half maxima values (FWHM) of the major diffraction peaks from the Nd-YAG PZT film annealed at 750°C, as well as for a $BaTiO_3$ film, have been measured. While these FWHM values are all greater than those of the standard profile reference material LaB_6 (average ≈ 0.1°) [9], the PZT peaks are substantially broader (average 0.4°) than the $BaTiO_3$ values (average 0.2°). This indicates that unlike the $BaTiO_3$ film which was deposited on a heated substrate at a temperature of ≈850°C (from which grains can orient to partially relieve strain during cooling), the PZT films may still have a certain amount of surface residual strain (apparent shift of XRD peaks as compared with the tetragonal standard) . Only when these films were annealed at high enough temperature, i.e. at >900°C, was the residual stress relieved (which also allowed grain growth). Efforts are continuing in the x-ray profile analysis of the films annealed at around 700°C to investigate the residual strain and crystallite size contribution to the diffraction peak broadening.

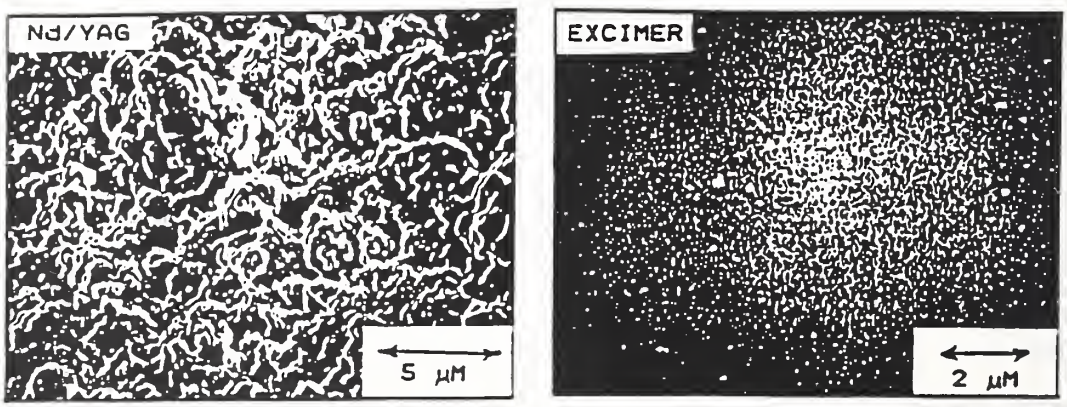

Fig. 9 SEM micrograph of PZT films (a) ND/YAG, annealed at 700°C and (b) excimer, annealed at 600°C.

In general, the excimer laser appears to produce films with finer microstructures. The SEM micrographs of the films annealed at around 600°C are shown in Figure 9a for the Nd/YAG and in Figure 9b for the excimer laser. The Nd/YAG film shows the presence of large particles, presumably produced by ejection of melted material from the surface of the target. The grain size is smaller and more uniform in the excimer-produced films.

SUMMARY

Thin films of PZT deposited on Pt and Pt-coated silicon substrates using laser deposition techniques (Nd/YAG and excimer) produced amorphous films at room temperature. Upon annealing, these films crystallized and gave rise to well-defined x-ray powder patterns with pseudocubic symmetry. Surface stress on the film and/or small crystallite size presumably precluded the splitting of these peaks. Higher annealing temperatures appeared to relieve the strain and allowed the tetragonal PZT symmetry to appear. The $BaTiO_3$ films were deposited at high temperature and alignment of the tetragonal a-axis normal to the substrate was observed in both x-ray diffraction (pseudo-cubic symmetry) and TEM. This alignment presumably reduces the tensile stress due to the thermal mismatch between the film and the substrate. In general the excimer laser produced films with better surface morphology.

ACKNOWLEDGEMENT

Dr. R. Gates is thanked for his measurement of the thickness of the film. Dr. G. White, J. Carpenter, J. Stalick and H.F. McMurdie for their critical review of this manuscript.

REFERENCES

1. Y.S. Touloukian, R.K. Kirby, R.E. Taylor and T.Y.R. Lee, Thermophysical Properties of Matter (Thermal Expansion, Nonmetallic, 12, 254, and 13 554 (1977).

2. B. Jaffe, R.S. Roth and S. Marzullo, J. Res. Nat'l Bur. Stds, 55, (1955).

3. P.K. Schenck, L.P. Cook, J.W. Hastie, E. Farabaugh, C.K. Chiang, M.D. Vaudin and P.S. Brody, Proc. Symp. Beam Solid Interaction; Mat. Res. Soc., vol. 157A, (1990).

4. P.S. Brody, J.M. Benedetto, B.S. Rod, K.W. Bennett, L.P. Cook, P.K. Schenck, C.K. Chiang and W. Wong-Ng, Proc. Seventh Int'l Symp. on Applic. of Ferroelectrics, (1990), Univ. Illinois, Urbana-Champaign.

5. L.P. Cook, M.D. Vaudin, P.K. Schenck, W. Wong-Ng, C.K. Chiang and P.S. Brody, Proceeding of Symposium on Evolution of Thin film and Surface Microstructure, Mat. Res. Soc. Fall Meeting, Boston, November, (1990), in press.

6. C.K. Chiang, W. Wong-Ng, P.K. Schenck, L.P. Cook, M.D. Vaudin, P.S. Brody, B.J. Rod and J.M. Benedetto, to be published in Phase Transformation Kinetics in Thin Films, Mater. Sci. Symp. Proc. v. 230, ed. by M. Chen, M. Thompson, R. Schwartz and M. Libera (Mater. Res. Soc., Pittsburg, PA, 1991)

7. J.J. Parsons and J. Rimai, Solid State Comm. 5, 423 (1967)

8. Powder Diffraction File (PDF), JCPDS-ICDD, 1601, Park Lane, Swarthmore, PA 19081.

9. Standard Reference Material 660, Instrument Line Position and Profile Shape Standard For x-ray Powder Diffraction, obtainable from the Natl. Inst. Stand. and Tech., Office of Standard Reference Materials, Gaithersburg, MD 20899. Current price will be quoted on request (1989).

POST-PROCESSING OF PULSED LASER-DEPOSITED PZT THIN FILMS

C. K. CHIANG, W.WONG-NG, L. P. COOK, P. K. SCHENCK, and H. M. LEE*
National Institute of Standards and Technology
Gaithersburg, MD 20899

P. S. BRODY, K. W. BENNETT, and B. J. ROD
Harry Diamond Laboratories
Adelphi, MD 20783

ABSTRACT

PZT thin films were prepared by pulsed laser deposition on unheated Pt-coated Si substrates. As deposited, the films were amorphous. Films crystallized at 550 - 600 °C to produce predominantly crystalline ferroelectric PZT. Crystallization of the amorphous material was accompanied by a linear shrinkage of ~2 %, as manifested in development of cracks in the film. Spacing, width and morphology of larger cracks followed a regular progression with decreasing film thickness. For film thicknesses less than 500 nm, much of the shrinkage was taken up by small, closely-spaced cracks of local extent. Implications for measurement of PZT thin film ferroelectric properties and processing are discussed.

INTRODUCTION

The laser deposition method is an important alternative route for processing thin film lead zirconate-titanate (PZT) because it can be made compatible with silicon wafer processing, and it is a practical way of transferring material with known bulk properties to thin film form.[1,2] Using a pulsed excimer laser, dense, smooth PZT thin films have been successfully deposited on platinum coated silicon wafers.[3] When the substrate was held at ambient temperature, the as-deposited films were amorphous. Post depositional heat-treatment or the use of heated substrates is therefore needed to form crystalline PZT films with ferroelectric properties.

In previous studies[3], we used differential scanning calorimetry to show that amorphous PZT films have a glass transition at ~300 °C, and that crystalline phases form in the temperature range from 350°C to 650°C. The amorphous to crystalline transition of the film was also investigated using the x-ray diffraction method. For processing PZT films deposited on silicon substrates, the optimum temperature for heat-treatment was tentatively shown to be near 550°C.

In this paper we report confirmatory results on the post-depositional crystallization of PZT films and provide new data on the structural changes associated with the crystallization process.

EXPERIMENTAL

PZT thin films were prepared by using an ArF excimer laser (193 nm). The deposition was done at a repetition rate of 10 Hz and nominal pulse width

---

*Guest scientist from Department of Materials and Nuclear Engineering, University of Maryland, College Park, MD.

of 23 ns. The laser beam was focused to produce a fluence of 10-30 J/cm^2. A commercial PZT ceramic (PZT 5A, 47% $PbTiO_3$ and 53% $PbZrO_3$, , from Morgan Matroc, Inc., Vernitron Div., Bedford, OH**) was used as target. During the deposition, the target was rotated and the laser beam was rastered across the target to maintain uniform material removal. A rotating substrate holder was used to hold substrates directly over the target surface at distances 2.0-3.0 cm from the target surface. The reaction chamber was continuously evacuated by oil free pumps to a background pressure of <1 mTorr. During deposition, oxygen was metered into the chamber to produce a background pressure of 100 mTorr. The growth rate of the PZT films was about 50 nm/min.

We used silicon <100> single crystal wafers as substrates which were coated with 200-500 nm platinum. The substrates were held at ambient temperature during the deposition. After deposition, the films were heat-treated in air at various temperatures. Typical heat-treatment time was one hour.

The annealed films were examined by x-ray powder diffraction (Cu $K\alpha_1$ radiation) to determine the formation of the crystalline PZT phase. Reflected light microscopy was used to examine the gross features of the films, and a scanning electron microscope (SEM) was used to examine the microstructure of the films. Circular platinum electrodes of 2.5 X 10^{-3} cm^2 area were sputtered on the surfaces of the annealed films using a shadow mask to study ferroelectric properties. Ferroelectric hysteresis loops were measured with a balanced Sawyer-Tower circuit operated at 200 kHz.

RESULTS AND DISCUSSION

Fig. 1 shows the x-ray patterns of PZT thin films on Pt/Si heat-treated at 450, 550, and 600 °C. In the 450 °C film, there is no definite indication of crystalline PZT, whereas in the 550 °C film, the (101/100) PZT peak is visible, but weak. The 600 °C film shows a well-developed PZT diffraction pattern. The broad pyrochlore peak is present in all three films. The PZT pattern shows no tetragonal peak splitting, suggesting cubic symmetry - nonetheless we have observed ferrolelectricity in these films. The test for ferroelectricity was, however, greatly hindered by the difficulty in obtaining non-shorted electrodes.

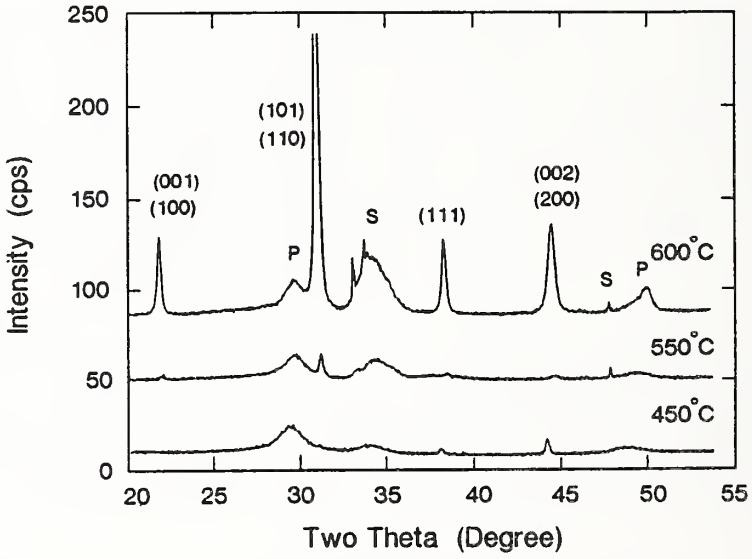

Fig. 1 X-ray diffraction patterns of PZT films on Pt/Si deposited on unheated Pt/Si substrates and post-annealed at various temperatures for one hour. PZT peaks are indexed; P = pyrochlore; S = substrate.

**Identification of items by explicit reference to an individual manufacturer are given for completeness, and are not meant to indicate that the US government recommends these specific items for this application.

Undoubtedly, much of this difficulty was caused by microcracks produced in the films by the annealing process. These microcracks were observed by light microscopy in most films annealed above 500 °C, and were more pronounced in thicker films; with decreasing thickness, the cracks appeared to diminish, and ultimately to disappear. Results of more detailed SEM observations on films of various thickness annealed at 600 °C, 1 hr, are shown in Figs. 2-4.

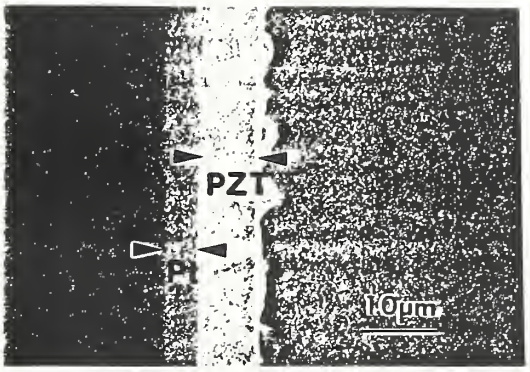

Fig. 2 Edge-on view of substrate with 0.8 μm film.

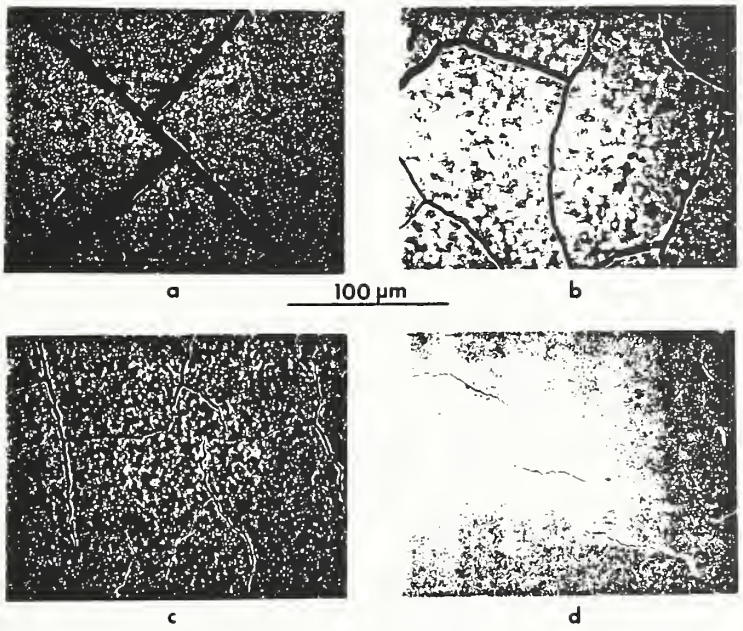

Fig. 3 Plan view of films; a) rectilinear cracks in 1.3 μm film; b) network of irregular cracks in 0.6 μm film; c) discontinuous cracks in 0.4 μm film; d) widely spaced thin cracks in 50 nm film.

Fig. 2 shows a cross section of a relatively thick film (0.8 μm), which appeared to be continuous. As the plan view in Fig. 3a indicates, however, the 1.3 μm film was traversed by a relatively regular, rectilinear network of cracks. In a thinner film of thickness ~0.6 μm (Fig. 3b), the cracks did not have straight sides and instead formed an irregular, yet continuous network. For a film thickness of ~0.4 μm (Fig. 3c) the network was not continuous and the cracks terminated themselves by closing, rather than by intersecting other cracks. In films of ~50 nm thickness (Fig. 3d), the major cracks did not extend far enough to intersect and these cracks were thin and widely spaced. However higher magnification (Fig. 4) indicates that these very thin films, while having few large cracks, contained myriad closely-spaced, submicron-wide fissures extending less than a micrometer.

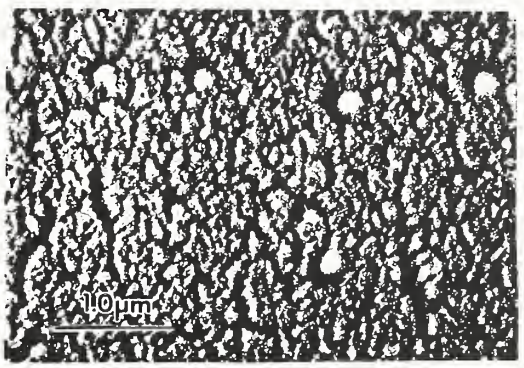

Fig. 4 Plan view of 50 nm film at higher magnification

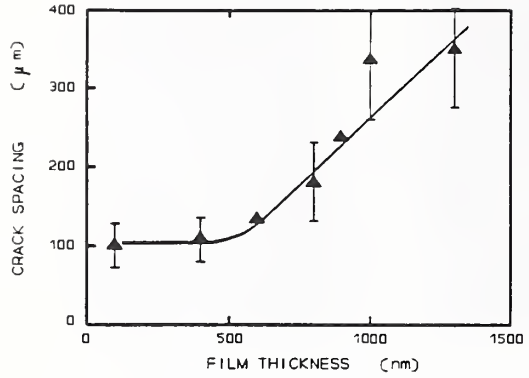

Fig. 5 Average spacing between cracks as a function of film thickness

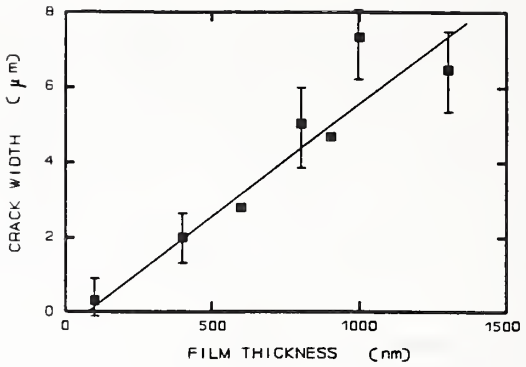

Fig. 6 Average crack width as a function of film thickness

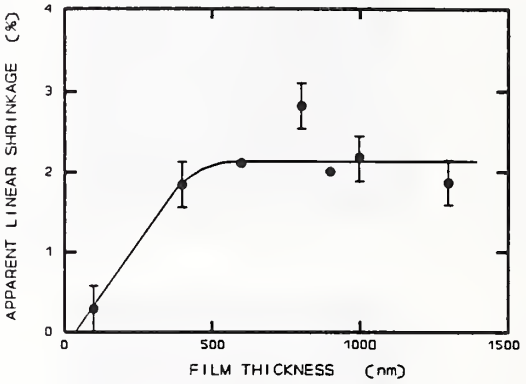

Fig. 7 Apparent linear shrinkage as computed from data in Figs. 5 and 6

Data on crack spacing and crack widths obtained from SEM studies are shown in Figs. 5 and 6, respectively. Crack spacing showed a definite decrease from ~350 μm to ~100 μm as film thickness decreased from ~1.3 μm to ~0.5 μm; below this there was no further decrease. Crack width showed a similar decrease, from ~7 μm at ~1.3 μm thickness to ~0.3 μm at ~0.5 μm thickness. By combining data in Figs. 5 and 6, an estimate of the linear shrinkage in these films was obtained, as indicated in Fig. 7. Based on this, shrinkage was ~2 % for most film thicknesses, a reasonable value by comparison with other crystallized glasses[5]. Films less than 0.5 μm thick showed lower apparent shrinkage, because the large cracks did not account for shrinkage due to microfissures of the type illustrated in Fig. 4, which became dominant as film thickness decreased.

The transition from a rectilinear network of cracks to an irregular, more polygonal arrangement took place at a film thickness of ~1.0 μm. The transition from this continuous, roughly polygonal, network to discontinuous cracks with closed ends began at a film thickness of ~0.5 μm. At this point the films may have become too weak to support the long range stress field necessary to produce a network of large cracks. Fracture mechanics analysis of simple shrinkage of an isotropic sheetlike body ideally produces an array of hexagonal polygons separated by a regular hexagonal crack pattern . The existence of the rectilinear pattern noted above for the thicker films suggests that this ideal situation was complicated there by additional factors, possibly including a preferred orientation of PZT crystallites, and a mechanical interaction with the substrate. For films below ~0.5 μm the influence of microfissures was increasingly important and the rectilinear pattern was accordingly affected.

It should be noted that the one-step heat treatment used to post-process the films consisted of putting a cool sample directly in a hot furnace or, alternatively, heating it up with the furnace. We have also prepared films by both air quenching and furnace cooling. All procedures involving crystallization resulted in cracks. Although there was some variation in the severity of cracking, no significant improvement was found among the alternative heating and cooling schemes. Similarly, a prolonged annealing did

not affect the cracks. Only films not heated above 500°C were crack-free; however, these did not contain ferroelectric crystalline PZT. One method to eliminate the cracking problem should be to deposit PZT on heated substrates so that it crystallizes directly, without the need for post-depositional annealing.

With cracks existing in the PZT film, the electrical characterization was very difficult[4]. Some cracks simply shorted the electrodes and others severely distorted the result of the measurements. The electrical measurements could be performed only if the electrode area was less than the area between the cracks. Using an electrode 560 μm in diameter we were able to verify the ferroelectric hysteresis of the films in a few areas as shown in Fig. 8.

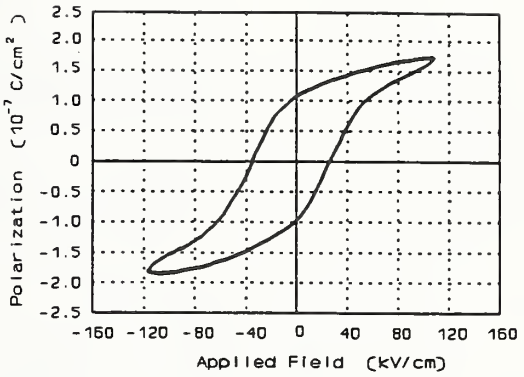

Fig. 8 A typical hysteresis loop of a PZT film after post-depositional heat-treatment at 600°C for one hour in air. The diameter of circular electrode was 560 μm.

CONCLUSIONS

Post-depositional experiments on laser-deposited amorphous PZT thin films have confirmed that crystallization to ferroelectric PZT occurs between 550-600°C. The ~2 % shrinkage accompanying crystallization causes cracks to form, with a geometry which depends upon film thickness.

REFERENCES

1. P. K. Schenck, L. P. Cook, J. Zhao, E. N. Farabaugh, and C. K. Chiang, Proc. Symposium on Beam Solid Interaction: Physical Phenomena, Mat. Res. Soc., 157A, 587, (1990)

2. P.S.Brody, B.S.Rod, J.M.Benedetto, K.W.Bennett, L.P.Cook, P.K. Schenck, C.K.Chiang and W.Wong-Ng, Proc. Seventh Intl Symp. on Applic. of Ferroelectrics, Univ. Ill, Urbana-Champaign, IL., (1990).

3. L. P. Cook, M. D. Vaudin, P. K. Schenck, W. Wong-Ng, C. K. Chiang, and P. S. Brody, p. 241-246 in C. V. Thompson, J. Y. Tsao, and D. J. Srolovitz, eds., "Evolution of Thin-Film and Surface Microstructure", Mater. Res. Soc. Symp. Proc., 202, (1991).

4. C.K.Chiang, L.P.Cook, P.K.Schenck, "Ferroelectric Thin Films", Mat. Res. Soc., 200, 133, (1990).

5. P. W. McMillan, "Glass-Ceramics", London, Academic Press, p. 110, (1979).

CRYSTALLOGRAPHIC ASPECTS OF FERROELECTRIC PZT THIN FILMS PREPARED BY LASER DEPOSITION TECHNIQUE

Winnie Wong-Ng, Ting C. Huang*, Lawrence P. Cook, Peter K. Schenck, M.D. Vaudin, Chwan K. Chiang, and P.S. Brody**
National Institute of Standards and Technology, Gaithersburg, MD, USA.

*IBM Almaden Research Center, San Jose, CA, USA
**Harry Diamond Laboratory, Adelphi, MD, USA.

ABSTRACT

X-ray diffraction techniques were used to study the crystallography of PZT thin films prepared by the laser deposition technique. This investigation included identification of phases formed during the annealing process and also the analysis of the profiles of selected diffraction peaks. The PZT films annealed below 800°C typically showed powder x-ray diffraction patterns corresponding to a cubic structure (i.e no peak splitting) instead of the tetragonal patterns characteristic of the target materials. The upper bound contribution of the macro and micro strain to the observed X-ray peak profile and positions was estimated. It was believed that the combined effect of small crystallite size together with residual strain, and possible local inhomogeneity gave rise to the broadening and displacement of the x-ray peaks, which subsequently masked off the splittings. At this stage the physical effect of high temperature annealing is not known. It is possible that as the annealing temperature increased, grain growth took place along with relaxation of residual strain, allowing peak splitting to be observed.

INTRODUCTION

Knowledge of the crystallography of ferroelectric thin films is fundamental to thin-film processing technology. To make useful devices using these films, information on crystal symmetry, lattice parameters and detailed structure must be correlated with electrical properties. The x-ray powder diffraction technique was employed in this study to obtain crystallographic information. By comparing the positions, profiles and relative intensities of diffraction peaks from the film with those from the target material, and also with the reference pattern provided by ICDD Powder Diffraction File (PDF) [1], information on the phase purity, structure, preferred orientation, residual strain and crystallite size of the material was obtained.

In general, strain can be classified into two types, namely, macrostrain and microstrain. Residual strain causes x-ray diffraction peak displacement and is calculated by

$$\delta d/d_o = (d_f - d_o)/d_o \qquad (1)$$

where d_o is the unstrained spacing and d_f is the corresponding strained value. The possible causes of diffraction peak broadening are microstrain, small crystallite size, stacking faults and compositional inhomogeneity. One of the fastest approximate ways to determine the crystallite size value, D (equation (2)) by assuming the microstrain to be negligible, is to use the breadth B of a peak corrected for instrumental broadening and to apply the Scherrer equation:

$$B = K\lambda/(D\cos\theta) \qquad (2)$$

In this equation K is a dimensionless constant depending on a number of factors including the crystallite shape and size distribution [2] and generally can be set to unity, λ is the X-ray wavelength and θ is the Bragg angle. The most widely used method for measuring the peak (line) breadth is the width at half peak maximum. In this study, B was obtained using the relation $B^2 = B_o^2 - B_i^2$, where B_o and B_i are the widths of the observed peak profile and the instrumental broadening profile, respectively. Crystallite sizes obtained by substituting the value B into equation (2) have been found to be within 20% of those of the Warren-Averbach and the integral breadth methods that take into account possible contributions from microstrains [3].

The primary goal of this paper, which is part of a continuing study [4-8], is to compare the crystallography of PZT films produced using the laser deposition technique with that of the target, and to study the profile and peak position of selected peaks in order to estimate the upper bound contribution of crystallite size and residual strain to the observed diffraction peaks.

EXPERIMENTAL

The laser-induced vaporization (also called pulsed laser deposition) technique was used to produce PZT films on Pt-coated Si wafers and Pt foil substrates at temperatures higher than 800°C. Pt-coated Si wafers were used because of the smoother surfaces which were more suitable for patterning in order to study the electric properties. However, at high temperature, ie. 800°C, oxidation of Si and delamination of the Pt coating took place, and therefore Pt was used instead. Fully dense PZT target disks for film preparation were obtained commercially[1]. A focused Q-switched Nd/YAG pulsed laser and an ArF excimer laser were both used to produce the films. Energy dispersive x-ray spectrometry was used to study the composition of films. The details of the laser and deposition chamber have been described elsewhere [4-8].

All PZT films reported here were deposited onto room temperature substrates and post-annealed at temperatures up to 1200°C. In the case of the Nd/YAG films, sequential heat-treatments were performed at 500, 600, 650, 700 and 750°C in air, and with a different film prepared under the same deposition conditions at 800, 900, 1000, 1100 and 1200°C using a PZT cell to maintain the proper lead pressure. Since the results of subsequent annealings of these films showed the PZT formation to be around 600°C, the films produced by the excimer laser were heat-treated at lower temperatures of 357, 398, 450, 500, 550 and 600°C to investigate phase formation. The average thickness of the films was measured by profilometry by using a masked area of the film as a reference.

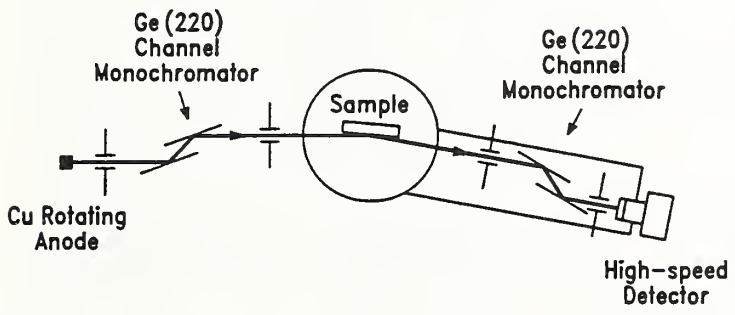

Fig 1. Schematic of parallel beam x-ray optics

Phase identification was conducted using a computer-controlled diffractometer. X-ray profile analysis was performed at IBM using a high resolution x-ray parallel beam double crystal diffractometer with a rotating anode and $CuK\alpha_1$ line source. A high-speed scintillation counter[2] was used. Figure 1 is a schematic drawing showing the arrangement of the parallel beam geometry of the x-ray optics. The details of the x-ray optics have been described elsewhere [9]. To avoid interference from overlapping peaks from the substrate, the (101)/(110) and the (112)/(121) peaks were used for the crystallite size calculation.

X-ray diffraction results show that both the Nd/YAG and the excimer lasers produced amorphous PZT films at room temperature, and that under appropriate heat-treatment the ferroelectric perovskite PZT phase was formed. Energy dispersive x-ray spectra from these films show compositions similar to the target. From profilometry, the films were of ≈ 2 μm thickness. The ferroelectric nature of the selected films was demonstrated by hysteresis loops relating the remanent polarization and the applied field [8].

X-ray patterns of PZT films prepared with the Nd/YAG laser and the excimer laser are shown in Fig. 2 and 3. These results demonstrate the formation of a perovskite PZT phase between 500 and 600°C for both the Nd/YAG and the excimer deposited films; at lower temperatures a pyrochlore phase was observed in the excimer laser film which could be converted into PZT at higher annealing temperatures. The lack of obvious differences in the intensity distribution between the PZT film and the reference pattern of PDF 33-784 [1] indicates that preferred orientation is not significant and the PZT film is not crystallographically aligned.

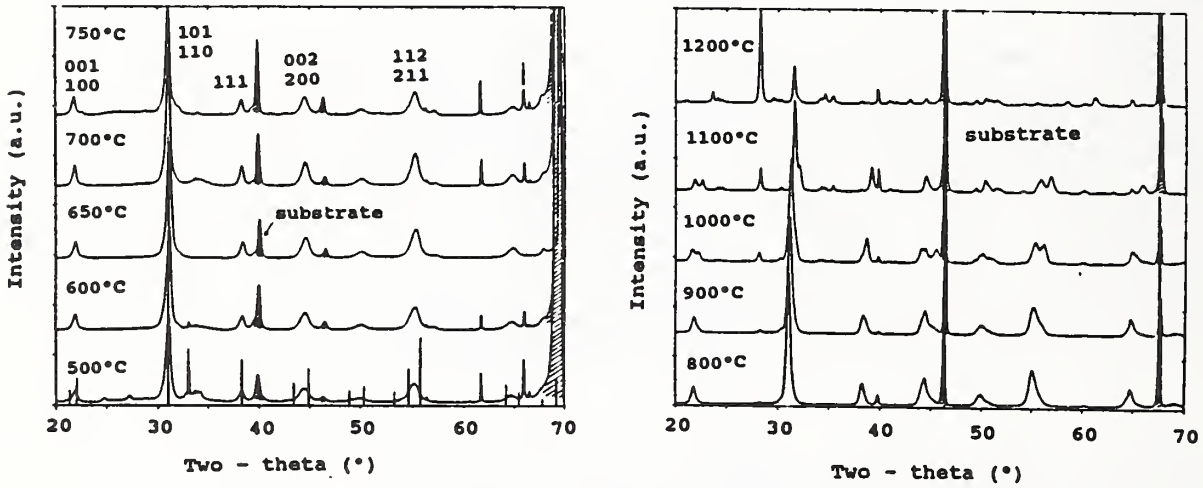

Fig. 2. X-ray diffraction patterns for the annealed Nd/YAG PZT films. The reference pattern of PDF 33-784 [1] is included for comparison.

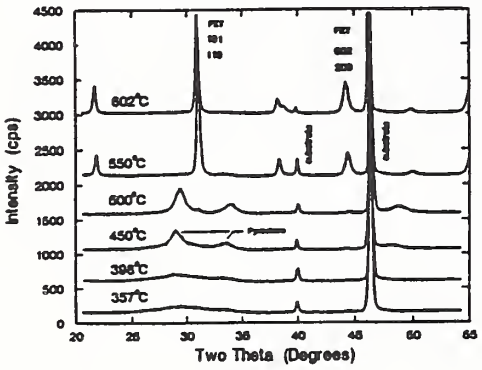

Fig. 3. X-ray diffraction patterns for excimer PZT films

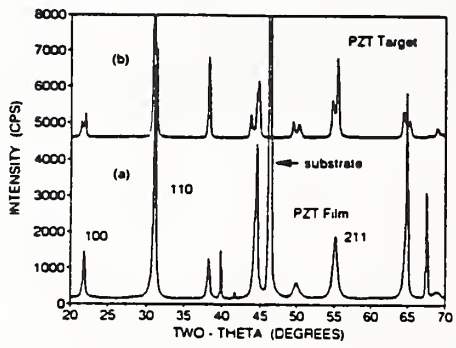

Fig. 4. X-ray patterns of (a) PZT target and (b) film annealed at 750°C

Figure 4 shows a comparison of the X-ray diffraction pattern of the Nd/YAG film annealed at 750°C with the pattern from the target material. We see substantial differences between these patterns: the diffraction peaks from the film are rather broad with no peak splitting and the pattern can be indexed

using a cubic unit cell (with a_o = 4.067(2)Å), whereas the pattern from the target has tetragonal symmetry; the peak positions match those of the JCPDS stick pattern very closely and correspond to a cell with a = 4.036Å, c = 4.146Å. All the diffraction patterns for films annealed at temperatures between 500 and 800°C appear to be characteristic of cubic symmetry. The splitting of the diffraction peaks occurs at an annealing temperature slightly below the temperature for the onset of chemical decomposition. At 1100°C, a tetragonal cell of a=3.937(4) and c=4.068(5)Å (c/a = 1.033) can be used to index the diffraction peaks. At this stage the physical process of annealing at high temperature is not known.

The diffraction pattern from the Nd/YAG film annealed at 750°C was analyzed in terms of crystallite size and strain. The widths, B, of the 110/101 and 112/121 diffraction peaks, 0.29° and 0.38°, were used to calculate the crystallite size using equation (2), giving results of 315 and 260 Å. The strain in the a and c directions required to transform the tetragonal cell of the target to the cubic cell of the film was calculated:

$$\delta d_c/d_{c(target)} = (d_{c(film)} - d_{c(target)})/d_{c(target)} = -1.91\times10^{-2}$$

$$\delta d_a/d_{a(target)} = (d_{a(film)} - d_{a(target)})/d_{a(target)} = 7.68\times10^{-3}$$

DISCUSSION

Figure 5 shows the $PbTiO_3$-$PbZrO_3$ sub-solidus phase diagram [11]. $PbZrO_3$ has a perovskite structure and is antiferroelectric, however its solid solutions with more than about 10 mole percent $PbTiO_3$ are ferroelectric [10]. In the structure of a cubic perovskite ABO_3 (Figure 6), the B^{4+} ions occupy the centers of each unit cell while the A^{2+} ions are located at the corners. In the corresponding distorted ferroelectric tetragonal structure, with cell parameters c and a such that c/a is a few percent greater than 1, the B^{4+} ions move parallel to the c-axis, giving rise to a crystal structure with two polarization states; a permanent electric dipole parallel or antiparallel to c is produced primarily by the up or down displacement of the B^{4+} ions with respect to the other ions. Another ferroelectric phase has a rhombohedral R3m symmetry [11, 12]. This can be considered as a pseudocubic structure with slight extension along a body diagonal.

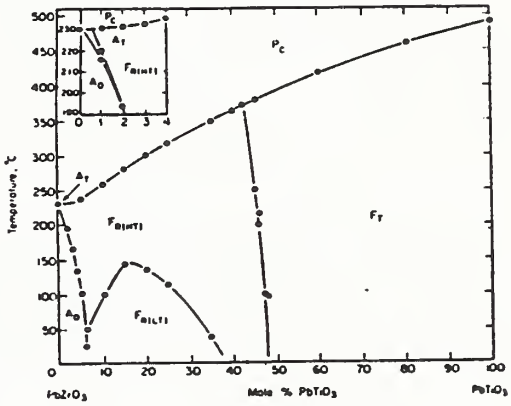

Fig. 5 The $PbTiO_3$-$PbZrO_3$ subsolidus phase diagram [11]

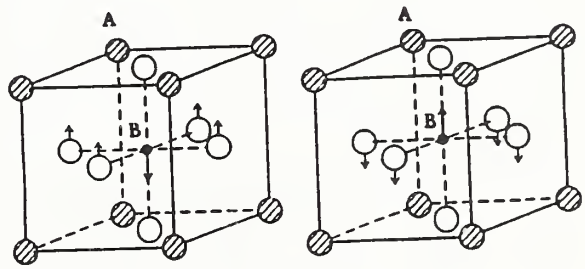

Fig. 6. Polarization states in a ferroelectric ABO_3 structure

Figure 5 also illustrates the crystallographic transformation temperature and composition of $PbTiO_3$-$PbZrO_3$. The high temperature form of PZT is cubic, and as it cools to room temperature a phase transformation to a tetragonal or rhombohedral structure takes place at the Curie temperature which ranges from ≈ 250 to 480°C depending on composition. A morphotropic phase boundary (an abrupt structural change within a solid solution with variation in composition) occurs near 55 mole % $PbZrO_3$ and is nearly independent of

temperature[10]. Solid solutions richer in $PbTiO_3$ are tetragonal, while those richer in $PbZrO_3$ are rhombohedral. Previous work [13] on the measurements of electrical and thermal expansion properties, x-ray and neutron diffraction studies have found that the rhombohedral region contains two phases.

It is thought that the PZT films in this study are not cubic at room temperature but rather tetragonal for the following 2 reasons: (1) the presence of a remanent polarization loop; (2) according to the phase diagram as shown in Figure 5, the cubic phase is not stable at room temperature for these compositions.

Possible reasons for the apparent conflict between the observed cubic symmetry and the lower symmetry required for ferroelectric behavior include small crystallite size, the presence of macro and microstrain, and inhomogeneous composition. In general, small crystallite size of ≈100 to 1000Å in a material will cause peak broadening [14]. In tetragonal materials with c/a close to one, peaks may broaden to the extent that closely separated doublets corresponding to two d spacings, d and $d+\delta d$, can no longer be distinguished, giving the appearance of a single peak at a position intermediate between the two. This occurs when the total broadening from microstrain, particle size effects (equation (1)) and instrumental broadening, B_i, is greater than the peak separation, $2\delta d\tan\theta/d$. The separations for the 101/110 and 112/211 doublets for the reference PDF pattern 33-784 [1] (with c/a = 1.033) were 0.4° and 0.8° respectively, considerably greater than the measured peak widths for the cubic film annealed at 750°C. Therefore, unless the PZT initially crystallizes in a tetragonal structure with c/a close to one, the 110 and 112 cubic peaks can not be the result of purely broadened doublets due to small crystallite size.

Macro strains may be caused by the mismatch in thermal contraction between the film and the Pt substrate while cooling from the annealing temperature and also by phase transformation. On cooling from 1000K to the Curie temperature of about 650K, unconstrained Pt contracts by 0.07% more than unconstrained PZT (in the cubic perovskite form). At the Curie temperature the cube axes transform such that a is about 1% less than the cubic parameter and c is 2% more; the stresses generated by this transformation are partially accommodated by domain formation and rearrangement. From the Curie temperature down to room temperature Pt contracts by about 0.35% more than PZT and therefore the PZT film experiences compressive stress as it cools. The calculated values of 7.68 x 10-3 and -1.91 x 10-2 for the a and c strains for the present film which are necessary for changing the doublets into singlets are however too large to be realistic for room temperature deposited laser films. These values are comparable to the values for epitaxially prepared films which are known to have relatively high residual strains. From this estimate, it is therefore likely that the residual strain could not be the sole factor which caused the doublets to converge to one.

Another possible reason for peak broadening is that the individual particles in the sample may not be compositionally homogeneous which would give rise to a variation of lattice constant. However, this is not believed to be the main cause of the observed cubic symmetry because as the annealing temperature increases, peak splittings were observed.

It is tentatively concluded that not any one of the above factors alone, but a combination of them contribute to the observed profile and peak position. We cannot, however, exclude the possibility that a portion of the film did crystallize in the cubic form. Current work continues on the investigation of the individual contribution of the macro and microstrain, crystallite size and compositional inhomogeneity to the diffraction profile.

Thin films of PZT were deposited on Pt and Pt-coated silicon substrates using laser deposition techniques (Nd/YAG and excimer). The films were amorphous at room temperature but, on annealing, they crystallized and gave rise to well-defined x-ray powder patterns with cubic symmetry; however, the films were ferroelectric which requires a lower symmetry. It is suggested that the characteristic tetragonal peak splitting is not observed because of peak broadening and shifting due to a combined result of the presence of residual strain (and microstrain), small crystallite size and local inhomogeneity. At higher annealing temperatures, grain-growth and/or strain annealing possibly occur and allow the tetragonal PZT symmetry to appear.

[1] Morgan Matroc Inc., Vernitron Division, Bedford, Ohio. The name of the manufacturer was cited in this paper for the purpose of explaining experimental procedures only. NIST does not endorse it for public use.

[2] Rigaku Instrument Inc., Japan.

REFERENCES

[1] Powder Diffraction File (PDF), JCPDS-ICDD, Swarthmore, PA 19081.

[2] J.I. Langford and A.J.C. Wilson, J. Appl. Cryst. 11 (1978) 102

[3] T.C. Huang, G. Lim, F. Parmigiani and E. Kay, J. Vac. Sci. Technol. A3 (1985) 2161

[4] P.K. Schenck, L.P. Cook, J.W. Hastie, E. Farabaugh, C.K. Chiang, M.D. Vaudin and P.S. Brody, Proc. Symp. Beam Solid Interaction; Mat. Res. Soc., 157A (1990).

[5] P.S. Brody, J.M. Benedetto, B.S. Rod, K.W. Bennett, L.P. Cook, P.K. Schenck, C.K. Chiang and W. Wong-Ng, Proc. Seventh Int'l Symp. on Applic. of Ferroelectrics (1990), Univ. Illinois, Urbana-Champaign.

[6] L.P. Cook, M.D. Vaudin, P.K. Schenck, W. Wong-Ng, C.K. Chiang and P.S. Brody, Proceeding of Symposium on Evolution of Thin film and Surface Microstructure, Mat. Res. Soc. Fall Meeting, Boston, November (1990) in press.

[7] C.K. Chiang, W. Wong-Ng, P.K. Schenck, L.P. Cook, M.K. Vaudin, P.S. Brody, B.J. Rod and J.M. Benedetto, to be published in Phase Transformation Kinetics in Thin Films, Mater. Sci. Symp. Proc. 230 (1991), ed. by M. Chen, M. Thompson, R. Schwartz and M. Libera (Mater. Res. Soc., Pittsburgh, PA)

[8] W. Wong-Ng, L.P. Cook, P.K. Schenck, M.D. Vaudin, C.K. Chiang, L.H. Robins, T.C. Huang and P.S. Brody, Adv. X-ray Analy. (1992), to be published.

[9] W. Parrish, C. Erickson, T.C. Huang, M. Hart, B. Gilles and H. Toraya, Mat. Res. Soc. Symp. Proc. 208 (1991) 327

[10] B. Jaffe, R.S. Roth and S. Marzullo, J. Res. Nat'l Bur. Stds. (1955) 55

[11] G. Shirane and K. Suzuki, J. Phys. Soc. Japan 7 (1952) 333

[12] E. Sawaguchi, J. Phys. Soc. Japan 8 (1953) 615

[13] C. Michel, J. M. Moreau, G.D. Achenbach, R. Gerson and W.J. James, Solid State Commun. 7 (1969) 865

[14] H.P. Klug and L.E. Alexander, X-ray Diffraction Procedure for Crystalline and Amorphous Materials, 2nd edition, Wiley-Intersceience, (1974) 643.

TEXTURING AND DIELECTRIC PROPERTIES OF LASER DEPOSITED $BaTiO_3$ THIN FILMS GROWN ON HEATED SUBSTRATES

M.D. VAUDIN*, L.P. COOK*, W. WONG-NG*, P.K. SCHENCK*, P.S. BRODY**, B.J. ROD** and K.W. BENNET**
*National Institute of Standards and Technology, Gaithersburg, MD 20899.
**Harry Diamond Laboratories, Adelphi, MD 20783

ABSTRACT

Thin films of $BaTiO_3$ were deposited on platinum-coated silicon substrates using pulsed laser deposition and characterized using electron microscopy, powder x-ray diffraction and electrical measurements. The microstructure consisted of columnar $BaTiO_3$ grains oriented normal to the substrate. Two preferred orientations were observed, with either the (001) or (111) planes of $BaTiO_3$ being parallel to the substrate. The electrical properties of two films were measured and it was found that the (111) film was ferroelectric and the (001) film was not. Possible reasons for this are discussed.

BACKGROUND

The envisaged applications of $BaTiO_3$ thin films make use of the desirable electrical properties of this material. The large electro-optic effect displayed by $BaTiO_3$ enables it to be used in photonic switching devices. Non-ferroelectric $BaTiO_3$ could be used in thin-film capacitors for dynamic random-access memory (DRAM). Ferroelectric $BaTiO_3$ would find application as long-term, radiation-hard, non-volatile memory. For all these applications, the grain size, shape and crystallographic texture of the films must be controlled for optimum properties. Careful characterization of the microstructure of $BaTiO_3$ thin films as a function of processing conditions is a vital part of any research program that leads to useful devices. In this paper we report progress on relating the structural characterization of these films to their electrical properties.

EXPERIMENTAL METHODS

Thin films of $BaTiO_3$ were deposited onto a platinum-coated silicon wafer by pulsed laser deposition using an ArF excimer laser (wavelength 193 nm) in a chamber containing oxygen at 13.3 Pa (100 mTorr)[1-5]. The target was commercial $BaTiO_3$ containing 5% $CaTiO_3$. The substrates used were (001) Si wafers with a thin coating of thermally grown amorphous silicon oxide followed by a 25 nm interlayer of Ti to improve adhesion between the silicon oxide and the 200-250 nm thick layer of Pt. The laser was pulsed at 10 Hz with each pulse lasting about 23 ns and typically containing 100 mJ of energy. The laser was focussed on the target producing a luminous plume; the fluence varied from 10 to 60 J/cm^2 per pulse. The substrate was heated by passing a controlled current through it. In early designs electrical contact was made with a simple alligator clip and the temperature was not uniform across the wafer. Recent improvements in the design of the contact have produced a more uniform distribution of the surface temperature which is measured using optical pyrometry. Deposition times up to 1 h were used and the maximum film thickness deposited varied from 500 to 1000 nm; however, the thickness varied significantly over the wafer because the distance from the plume source to the substrate varied over the wafer surface. No heat treatments were carried out on the specimens after removal from the deposition chamber.

Microstructural characterization of the films was carried out using transmission electron microscopy (TEM). Some specimens were studied in cross section and some in plan-view. Cross-section specimens were prepared by gluing 1 to 2 mm wide strips of coated substrate together in the face-to-face orientation, cutting cross sections, supporting them with Cu disks containing a 600 μm hole, grinding them to 20 to 30 μm thick and ion milling. Further characterization was performed using powder X-ray diffraction to assess phase purity and crystallographic texture, i.e. preferred orientation. Electrical measurements were made on several of the films to determine whether they were ferroelectric and, if so, to obtain a value for the remanent polarization.

RESULTS

In this study, three specimens which will be denoted A, B and C were studied in either cross section or plan view. Fig. 1(a) is a cross-section TEM micrograph of specimen A showing only the $BaTiO_3$ film; the Pt/Si substrate has been milled away along with a part of the film. The film consists of columnar grains that have grown normal to the substrate. These grains are about 40 to 100 nm in cross section and extend across the thickness of the film which was measured to be 550 nm in a thicker part of the specimen where the film was complete. An electron diffraction pattern was recorded with the electron beam parallel to the $(001)_{Si}$ substrate plane (Fig. 1(b)) and contains diffraction spots from the Si and diffraction rings from the $BaTiO_3$ thin film. Because c/a for tetragonal $BaTiO_3$ is 1.01 (very close to one), the separation of, for example, the 002 and 200 rings is too small to be detectable by electron diffraction. Thus, from this pattern, we cannot determine whether the $BaTiO_3$ is tetragonal, and cubic indexing is given. The 111 ring is strong and the 110 and 002 rings are weak in the direction normal to the $(001)_{Si}$ substrate indicating preferred orientation of the (111) $BaTiO_3$ planes parallel to the substrate. The Pt/$BaTiO_3$ interface region of this specimen is shown in Fig. 2; a lighter band 15 to 25 nm wide can be seen between the $BaTiO_3$ and the polycrystalline Pt and there is some penetration of this lighter region into the Pt film. Energy dispersive x-ray spectra from this band and from the bulk $BaTiO_3$ show that the lighter band is Ti-rich in comparison with the $BaTiO_3$ and electron diffraction from this region suggests that it is amorphous.

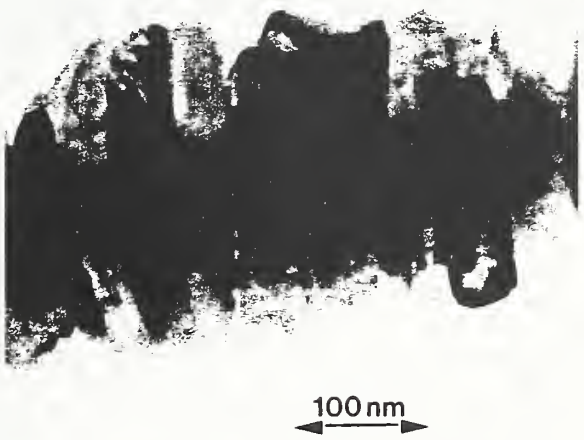

Fig. 1(a). Cross-sectional TEM micrograph of specimen A showing columnar grains

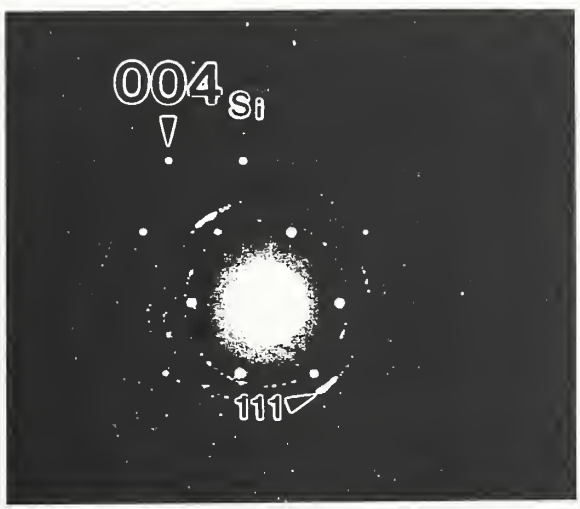

Fig. 1(b). Electron diffraction pattern from specimen A showing strong 111 ring

Specimen B had a similar microstructure to A with a slightly smaller grain size, 20 to 70 nm. However, a diffraction pattern (Fig. 3) taken at the same

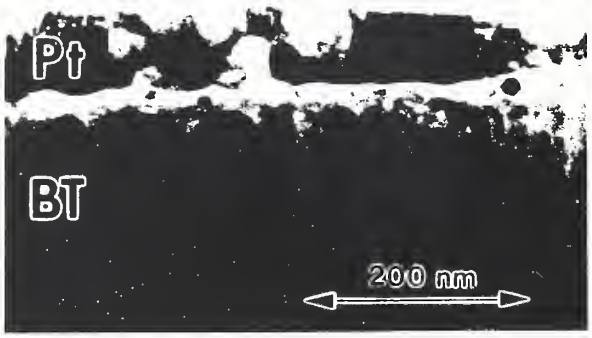

Fig. 2. $BaTiO_3$/Pt interface region of specimen A showing light region at interface

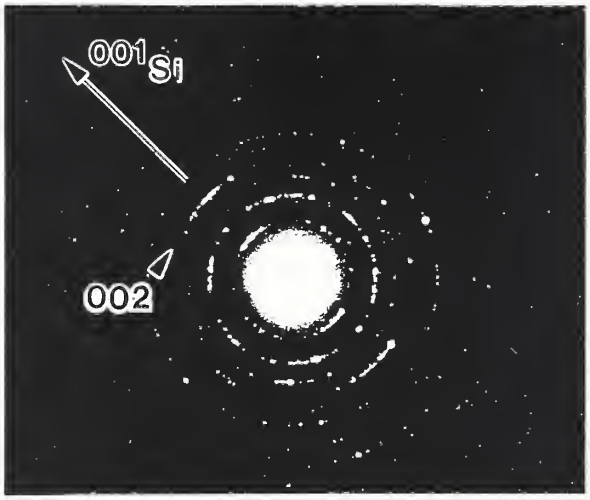

Fig. 3. Electron diffraction pattern from specimen B, showing strong 001 and 002 rings. $[001]_{Si}$ is marked

orientation as Fig. 1(b) showed a different preferred orientation to A, with the 001 and 002 rings being strong and other rings weak in the $[001]_{Si}$ direction. Thus two different preferred orientations parallel to the substrate plane have been detected, (001) and (111). The temperature of the substrate during deposition varied between 700 and 750°C for specimen B. The temperature for specimen A could not be measured. Specimen C was studied in plan-view and a TEM micrograph taken normal to the film is shown in Fig. 4. The grains are equiaxed in cross section with a grain size of 20 to 80 nm which is similar to that of specimens A and B. Previously published micrographs and diffraction patterns[3] show that this film also consists of columnar grains of $BaTiO_3$ normal to the substrate, and has (001) preferred orientation like specimen B. Fig. 4 also shows that between the grains of $BaTiO_3$ there is a lighter layer typically 10 nm thick. The contrast behavior of this material during specimen tilting suggests that it is amorphous. Fig. 5 is an electron diffraction pattern taken with the beam parallel to the film normal of specimen C and shows that there is no preferred orientation within the plane of the film.

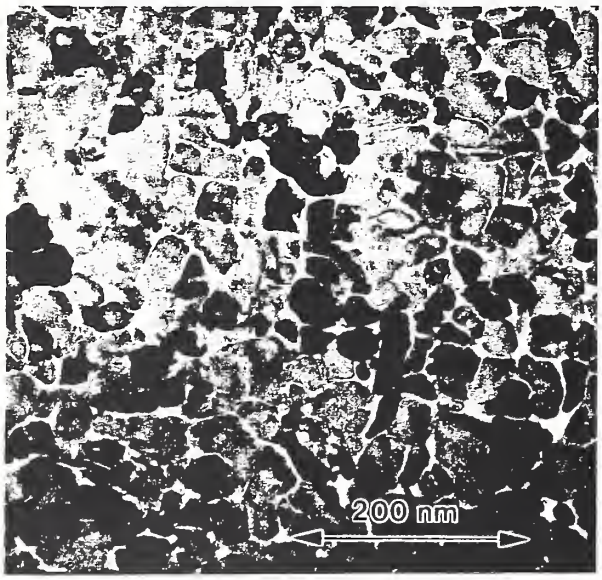

Fig. 4. Plan-view TEM micrograph of specimen C

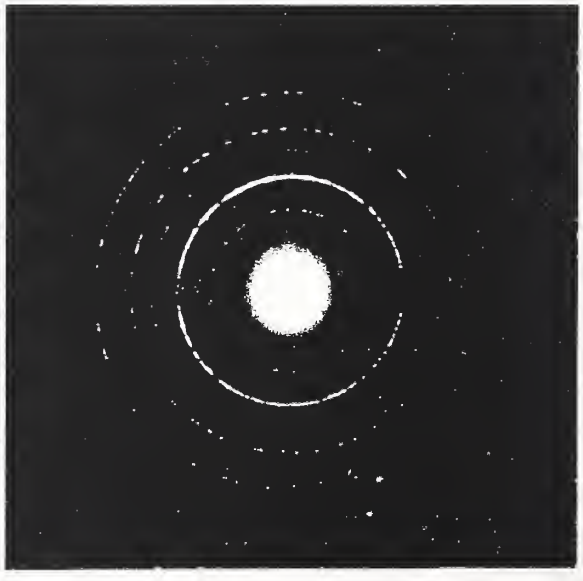

Fig. 5. Electron diffraction pattern from specimen C, showing lack of preferred orientation in film plane

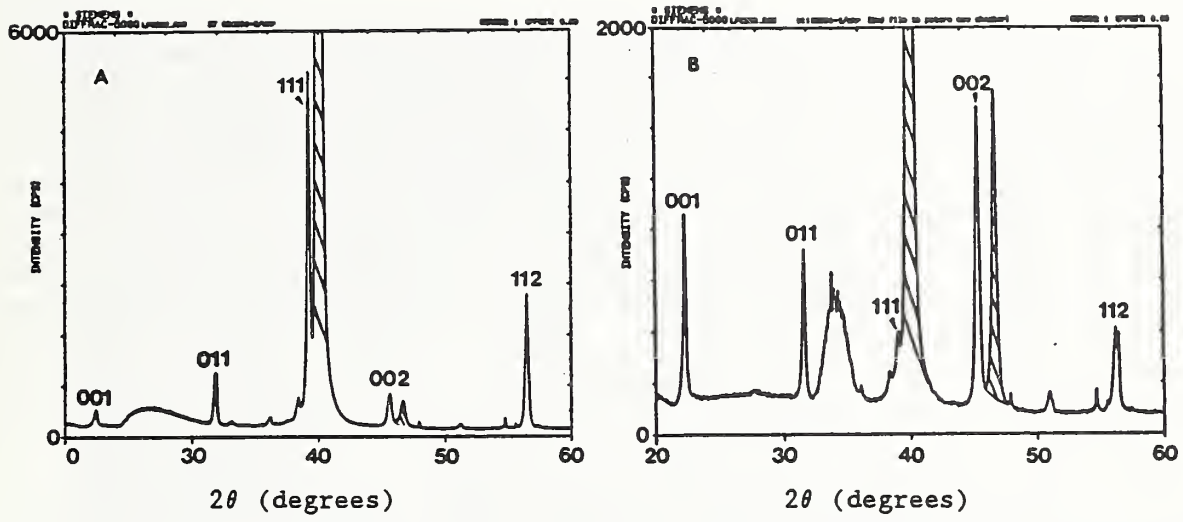

Fig. 6. X-ray powder diffraction patterns from specimens A and B showing (A) (111) and (B) (001) crystalline texture

Powder x-ray diffraction patterns from specimens A and B are shown in Fig. 6 and corroborate the electron diffraction findings: the 111 peak for specimen A is strong and 001 and 002 are relatively weak whereas for specimen B the situation is reversed. Six specimens were made on the same day as specimen A and diffraction patterns obtained from these films all show (111) preferred orientation, and the two other specimens made during the same week as specimen B both showed (001) preferred orientation. Electrical measurements made on films A and C showed that film A was ferroelectric with a remanent polarization of 4.3 $\mu C/cm^2$ at a coercive field of 180 kV/cm whereas film C was not ferroelectric. The results for the three films are summarized in Table 1.

Table 1

Summary of data for $BaTiO_3$ films A, B and C

Specimen	A	B	C
Fluence (J/cm^2)	≈10	≈60	≈20
Crystal plane parallel to film	(111)	(001)	(001)
Grain size (nm)	40 - 100	20 - 70	20 - 80
Interface region	Ti-rich, amorphous	Ti-rich, amorphous	Not observable in plan view
Ferroelectric properties	4.3 $\mu C/cm^2$ at 180 kV/cm	Not measured	Not ferroelectric

DISCUSSION

The relationship between (001) preferred orientation and the absence of ferroelectricity can be rationalized using a strain energy argument which will be briefly presented here. During cooling from the deposition temperature of 727°C (1000K) to the Curie temperature 127°C (400K), unconstrained Si, Pt and $BaTiO_3$ contract by 0.23%, 0.60% and 0.71% respectively[6]. Thus the Pt and $BaTiO_3$ thin films are both under tensile stress in the plane of the film at the Curie temperature. We estimate the elastic strain, δ, in the $BaTiO_3$ at the Curie point as the sum of two terms: (1) an elastic tensile strain in the Pt due to the thermal contraction mismatch between Si and Pt (0.37%) which is only partially relieved by plastic deformation of the Pt; (2) the difference between the thermal contractions of the $BaTiO_3$ and the Pt (0.11%). The first term cannot easily be calculated but a lower bound of 0.05% is used which yields an estimate for the unrelieved elastic strain in the $BaTiO_3$ of 0.16%. At the Curie temperature, the cubic $BaTiO_3$ unit cell transforms to a tetragonal cell by strains of ϵ_c in the c direction and ϵ_a in the two a directions. Assuming small strains and zero volume chage associated with the transformation (both valid assumptions for $BaTiO_3$), then $\epsilon_a = -\epsilon_c/2$ and the tetragonal cell has a c/a ratio of $1+\epsilon$ where $\epsilon = \epsilon_c - \epsilon_a$. Just below the Curie temperature, ϵ is 0.0045 and it increases with decreasing temperature[7].

In the case where the (001) plane of the cubic $BaTiO_3$ is parallel to the substrate plane (specimens B and C), the fraction, f_n, of c axes normal to the substrate will be a function of δ. We assume that the c axes are oriented to create a transformation strain in the substrate plane which, if possible, is equal to δ, such that:

$$\delta = f_p(\epsilon_a + \epsilon_c)/2 + f_n\epsilon_a \qquad (1)$$

where f_p is the fraction of c axes parallel to the substrate. Substituting $f_p = 1-f_n$ and rearranging gives

$$f_n = 1/3 - 2\delta/\epsilon \quad \text{for } \delta < \epsilon/6; \quad f_n = 0 \quad \text{for } \delta \geq \epsilon/6 \qquad (2)$$

where $\epsilon = \epsilon_c - \epsilon_a$ and we ignore second order and higher terms. On cooling from the Curie temperature to room temperature, ϵ increases to 0.01, and for the δ value of 0.16% calculated above, this strain minimization model predicts $f_n = 0$, i.e. complete preferred orientation of the c axes parallel to the substrate and hence zero remanent polarization normal to the substrate. In the (111) case (specimen A) all the c axes lie at angles of about 35° to the substrate leading to non-zero remanent polarization normal to the substrate. Note also that since, on average, all the cube axes are at the same angle to the substrate before the Curie transformation, the driving force for preferred orientation is zero. Thus the differences in electrical behavior of the (001) and (111) textured films can be explained as the result of thermal contraction mismatch.

The presence of (001) and (111) preferred orientation in different films cannot be explained at present because the substrate temperature, which is believed to be a critical deposition parameter, is not well known for all the films. All the films made around the same time had the same preferred orientation (i.e. the texturing is repeatable) and were made with the same laser fluence which varied between specimens as shown in Table 1. The (111) films were made with about $10J/cm^2$ fluence, whereas the (001) films were made with fluences two or more times larger, suggesting that the laser fluence may also be one of the controlling factors for the crystalline texture.

The grains imaged in Fig. 4 were equiaxed in cross section and their size (about 50 nm) did not vary significantly from that of the other films. In earlier experiments, a thin film of $BaTiO_3$ was laser deposited onto room temperature carbon films supported on TEM grids[3]. The film consisted of amorphous, approximately spherical particles about 20 nm in diameter, loosely

agglomerated; this particle size is smaller than the crystalline grains in the films studied. We suggest that as each amorphous particle hits the heated Pt surface, its temperature rises above the glass transition temperature and it flattens out due to surface tension; on further heating, it crystallizes and becomes the nucleus for a single grain. Much work remains to be done on relating processing conditions, microstructure and properties. However, this work has shown that if the crystallographic texture of a thin film can be controlled, it may be possible to tailor the electrical properties in useful ways, in some cases producing ferroelectric thin films for non-volatile memory and photonic applications and in others producing high dielectric constant, non-ferroelectric material for thin film capacitors and dynamic, random-access memory.

CONCLUSION

Observations of (111) and (001) crystalline texture in thin films of $BaTiO_3$ deposited by pulsed laser ablation have been linked with the presence and absence, respectively, of ferroelectricity. A model to explain these results is proposed in which strains induced by thermal contraction mismatch are relieved in the (001) case by preferred orientation of the tetragonal c axis parallel to the plane of the film leading to zero remanent polarization; in the (111) case there is no driving force for preferred orientation and, in addition, the c axis of the majority of the grains lies out of the film plane leading to useful ferroelectric properties.

REFERENCES

1. P.K. Schenck, L.P. Cook, J. Zhao, J.W. Hastie, E.N. Farabaugh, C.K. Chiang, M.D. Vaudin and P.S. Brody in Beam Solid Interaction: Physical Phenomena, edited by J.A. Knapp, P. Borgesen and R.A. Zuhr (Mater. Res. Soc. Proc. 157A, Pittsburgh, PA 1990) pp. 587-592.
2. P.S. Brody, J.M. Benedetto, B.S. Rod, K.W. Bennett, L.P. Cook, P.K. Schenck, C.K. Chiang and W. Wong-Ng, Proc. Seventh International Symposium on Application of Ferroelectrics (1990), Univ. Illinois, Urbana-Champaign.
3. L.P. Cook, M.D. Vaudin, P.K. Schenck, W. Wong-Ng, C.K. Chiang and P.S. Brody, in Evolution of Thin-Film and Surface Microstructure, edited by C.V. Thompson, J.Y. Tsao and D.J. Srolovitz (Mater. Res. Soc. Proc. 202, Pittsburgh, PA 1990) pp. 241-246.
4. C.K. Chiang, W. Wong-Ng, P.K. Schenck, L.P. Cook, M.D. Vaudin, P.S Brody, B.J. Rod and J.M. Benedetto in Phase Transformation Kinetics in Thin Films, edited by M. Chen, M. Thompson, R. Schwartz and M. Libera (Mater. Res. Soc. Proc. 230, Pittsburgh, PA 1991).
5. W. Wong-Ng, L.P. Cook, P.K. Schenck, M.D. Vaudin, C.K. Chiang, L.H. Robins, T.C. Huang, and P.S. Brody, Advances in X-ray Analysis (1992), accepted for publication.
6. Y.S. Touloukian, R.K. Kirby, R.E. Taylor and P.D. Desai, Thermophysical Properties of Matter 12, IFI/Plenum, New York, 1970.
7. H.F. Kay and P. Vousdan, Philos. Mag. 7 (40), 1019 (1949).

Dielectric Constant and Hysteresis Loop Remanent Polarization from 100 Hz to 2 MHz for Thin Ferroelectric Films

K. W. Bennett,* P. S. Brody,* B J. Rod,* L .P. Cook,** P. K. Schenck,**and S. Dey***
*Harry Diamond Laboratories, Adelphi, MD 20783-1197
**National Institute of Standards and Technology, Gaithersburg, MD 20899
***Arizona State University, Tempe, AZ 85287-6006

Abstract

A modification of the standard Sawyer-Tower circuit method of displaying ferroelectric hysteresis allowed the technique to be extended to sinusoidal switching frequencies of 2 MHz. Using this method, probe station measurements of switched remanent polarization were made for two films: excimer-laser-deposited lead zirconate titanate (PZT) and sol-gel PZT. Switched remanent polarization and dielectric constant were measured as a function of frequency between 100 Hz and 2 MHz and as a function of elapsed switching cycles at the 1-MHz rate. Both films showed decreasing switched remanent polarization and dielectric constant with increasing frequencies. This effect is attributed to limitations in domain wall velocity.

1. Introduction

Knowledge of the intrinsic frequency dependence of switched remanent polarization in ferroelectric films is important for the development of nonvolatile silicon integrated random-access memories, since these ideally would operate under conditions of continuous cycling at relatively high frequency rates (in the megahertz range). It is also important to be able to measure switched remanent polarization at high switching rates, both to cover the frequency range at which switching will occur in memory devices and to accumulate, in tests, a number of switched cycles that would be representative of the number that would accumulate in the actual operation of a device.

An easily implemented method of obtaining the switched remanent polarization is from a Sawyer-Tower circuit hysteresis loop display of polarization versus applied sinusoidal field [1]. Such measurements are typically made at low frequencies (of 1 kHz and less) because of the distorting effects on the loop display of inductive-capacitive resonances at higher frequencies. This is particularly true when measurements are made directly on a substrate with probes, because of uncompensated circuit inductance from the long leads required when probe stations are used.

To study the frequency dependence of the films at higher frequencies, we modified the basic hysteresis measurement arrangement to decrease the size of the charge-measuring capacitor, while still retaining the ability to determine the field across the ferroelectric film. The effect of reducing the capacitor size is to increase the resonance frequency and thus increase the maximum frequency at which measurements could be made. Using the modified circuit, we could measure relatively large film capacitor structures on a substrate over a frequency range extending to 2 MHz. We could also measure remanent polarization as a function of elapsed switching cycles at up to a 2-MHz rate while continually monitoring the switched remanent polarization.

In this paper we describe the modified circuit and results obtained with this circuit. Two lead zirconate titanate (PZT) films of similar composition were examined. One was produced by excimer laser evaporation (laser ablation), the other by the sol-gel process. In addition to switched remanent polarization from hysteresis loops, we measured film capacitor dielectric constant and loss as a function of frequency to 2 MHz, using a Hewlett-Packard 4194A impedance/gain phase analyzer which used a four-probe technique.

The results for switched remanent polarization showed an intrinsic dependence on the frequency of the applied field, that is, one which did not depend on the ability of the testing circuitry to supply adequate charge during a switching cycle. A simple test in which measure-

ments were made at two different source impedances confirmed this conclusion. This intrinsic frequency dependence is probably a result of limitations in domain wall velocity and pinning at grain boundaries. Some brief discussion of how such mechanisms would operate to produce observed dependencies is included in this paper (see sect. 6).

2. Modified Sawyer-Tower Circuit

In the standard Sawyer-Tower circuit, most of the voltage from the source is dropped across the ferroelectric capacitor because the ferroelectric capacitance is always much smaller than that of the series-measuring capacitor, C_m; that is, a large measuring capacitor is always used. This results in a low resonant frequency in the Sawyer-Tower loop circuit and undesirable ringing at low frequencies. If the large measuring capacitor is replaced with a smaller capacitor, the resonant frequency of the circuit increases by a factor equal to the square root of L_1C_1/L_2C_2, where L_1 equals the circuit inductance with the larger capacitor, C_1 equals the capacitance of the larger capacitor, L_2 equals the circuit inductance with the smaller capacitor, and C_2 equals the capacitance of the smaller capacitor. Since one can now no longer assume the voltage drop across the measuring capacitor to be small compared to the voltage drop across the ferroelectric capacitor, we must measure the drop across the ferroelectric capacitor directly.

At low frequencies (i.e., 100 Hz), leakage across the measuring capacitor through the input resistance of the oscilloscope input can no longer be ignored if the measuring capacitor is small. We approached this problem by increasing the value of the measuring capacitor for lower frequency measurements. An experimental check ascertained that changing the value of this capacitor did not change the measured remanent polarization at the change point. That is, measurements made with either capacitor produced the same result.

The arrangement for the hysteresis loop measurements is shown in figure 1. The films were deposited onto platinum-coated oxide-buffered silicon substrates. Platinum electrodes, 150 × 150 μm square, were sputter deposited onto the surface of the film with a micromachined silicon shadow mask. The capacitor that formed between the top electrode and the substrate electrode constituted a parallel-plate capacitor. A probe station was used, with four shielded probes contacting electrodes: Probe 1 contacted the top electrode and applied the switching voltage, V_a. Probe 2 also contacted the top electrode and was used to determine the voltage $V_{m(high)}$ on the electrode. Probe 3 contacted the base electrode through an etched window and provided a contact which was used to determine the voltage $V_{m(low)}$ on the base electrode. Probe 4 also contacted the bottom electrode and was used to place a capacitor C_m between that electrode and ground. A digital oscilloscope recorded voltages at probe points 2 and 3 and digitally subtracted the two to obtain the voltage applied to the ferroelectric capacitor. The voltage at probe point 3 is proportional to the polarization charge. The loop formed by displaying this quantity versus the applied field (as computed from the digital data by the oscilloscope) is the hysteresis loop, from which the switched remanent polarization versus frequency results were obtained.

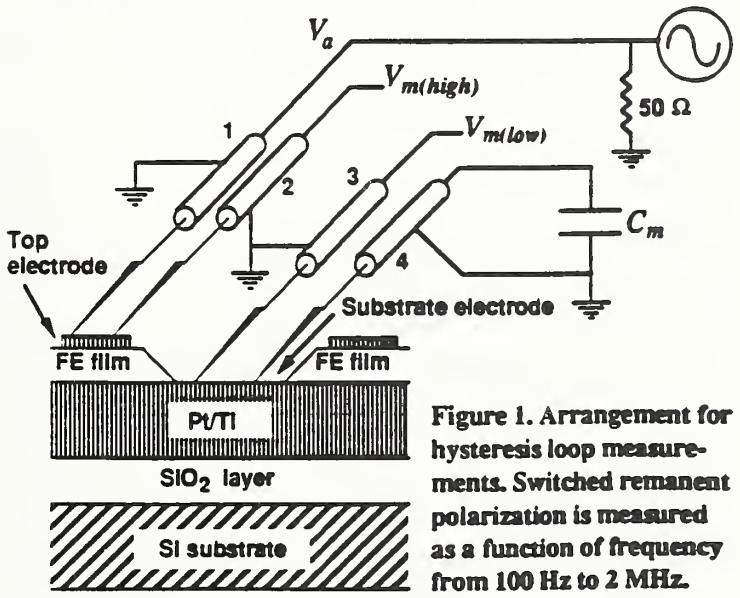

Figure 1. Arrangement for hysteresis loop measurements. Switched remanent polarization is measured as a function of frequency from 100 Hz to 2 MHz.

3. Measurements of Dielectric Constant and Loss

A Hewlett-Packard 4194A impedance/gain phase analyzer incorporating a four-probe measurement setup is used to measure capacitance and dissipation factor as a function of frequency from 100 Hz to 2 MHz. The four-probe measurement technique eliminates any residual inductance or stray capacitance in the test probes and cables by the elimination of external magnetic fields being generated around the conductors. The capacitance and inductance of the cables and probes are balanced out by internal circuitry within the impedance/gain phase analyzer. In our results, we assumed that each capacitor element was an ideal parallel-plate capacitor with a homogeneous dielectric medium to determine dielectric constant and loss.

4. Ferroelectric Films Studied

Two PZT films were used for our study. The first film is a National Institute of Standards and Technology (NIST) excimer-laser-deposited PZT film [2] with a thickness of 0.45 μm. The film was annealed at 600°C for 1 hour. The target composition is 53/47 Zr/Ti + 1 wt% Nb. The other film is an Arizona State University (ASU) sol-gel PZT film [3] with a thickness of 0.60 μm. The film was annealed at 750°C. The composition ratio of the film is 52/48 Zr/Ti; no niobium was added. Both films were configured as arrays of parallel-plate capacitors. Sputter-deposited platinum formed arrays of top electrodes, each 150 × 150 μm. The films were formed on silicon substrates upon which platinum was sputter deposited. The platinum-coated substrate provided the bottom electrode.

5. Premeasurement fatiguing of film: Effect of Elapsed Cycles

Before making useful measurements of switched remanent polarization as a function of frequency, one must determine the effect of elapsed cycles. At a high switching rate, the effects of elapsed cycles or fatigue will generally dominate over the effect of the switching rate itself. For this reason we cycled (i.e., fatigued) the samples first, until the number of elapsed cycles became large compared to the total cycles required for the measurements. The samples were fatigued at a rate of 1 MHz, with a constant applied voltage of 6.63 V zero to peak out to 10^{10} cycles. Results are shown in figure 2. The corresponding 0 to peak applied fields across the ferroelectric capacitors are 147.2 kV/cm for the excimer-laser-deposited film and 110.4 kV/cm for the sol-gel film.

We note that although the switched remanent polarization ($2P_r$) for the sol-gel film was 16.8 μC/cm^2 at 10^8 cycles, it decreased to 6.8 μC/cm^2 after 10^{10} elapsed cycles. The excimer-laser-deposited film showed a switched remanent polarization of 6.28 μC/cm^2 at 10^8 cycles and 4.34 μC/cm^2 at 10^{10} cycles. Interestingly, if the two fatigue curves that are linear with the log of elapsed cycles are extrapolated, the sol-gel film would cross the zero switched remanent polarization axis after about 10^{11} fatigue cycles, whereas the excimer-laser-deposited film would cross the same line at approximately 10^{14} fatigue cycles.

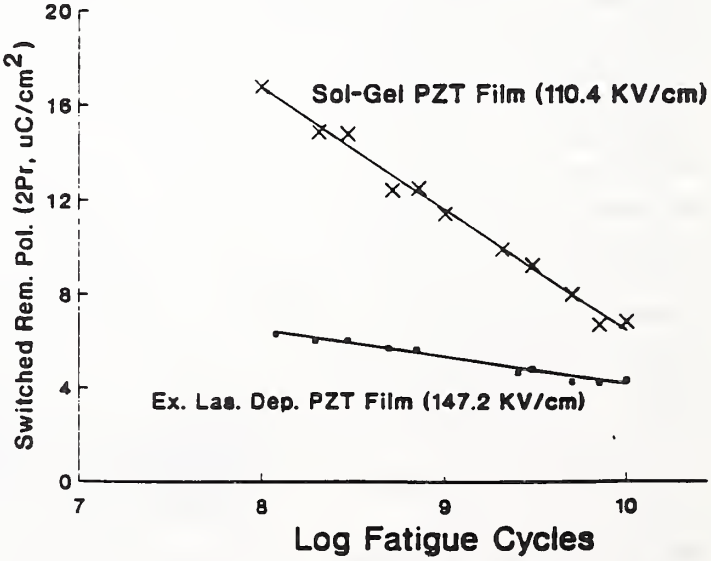

Figure 2. Effect of elapsed cycles (fatiguing) on both PZT films. Voltage (0 to peak) is 6.63 V.

5.1 Switched Remanent Polarization as a Function of Frequency

The switched remanent polarizations were measured after the films were fatigued as described. Results for the excimer-laser-deposited film, for applied voltages (voltage difference across the capacitors) of 4.50, 6.63, and 7.88 V zero to peak for the frequency range from 100 Hz to 2 MHz are shown in figure 3. Results for the sol-gel process film, for the same applied voltages and range of frequencies, are shown in figure 4.

The switched remanent polarization generally decreased sublinearly with increased frequency in both films. There appears to be a low-frequency range for which the switched remanent polarization does not decrease with increasing frequency. This is particularly clear for the sol-gel film, where a rolloff of switched remanent polarization with frequency does not start until a switching frequency of about 10 kHz. This is less clear for the laser-deposited film, where the rolloff appears to start at perhaps a frequency of 100 Hz.

To insure that the measurements were largely unaffected by fatigue effects, the measurements were made both from low to high and from high to low frequency. The results overlapped almost completely, indicating that the effects of elapsed cycles on the measurements were minimal and that the measurements show the effects of switching frequency only.

We made an additional check using the excimer-laser-deposited film to see if the 50-Ω source impedance of the generator was limiting the amount of switched charge and thus introducing an apparent frequency dependence. The check made at 100 kHz and also at 2 MHz

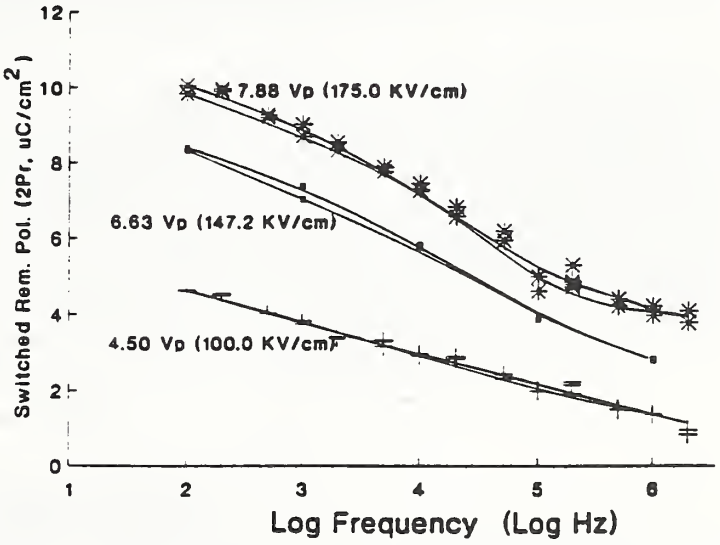

Figure 3. Switched remanent polarization as a function of frequency from 100 Hz to 2 MHz at 3 different voltages across ferroelectric capacitor for excimer-laser-deposited PZT film. Film thickness is 0.45 μm. Elapsed cycles are 1.5×10^{10}.

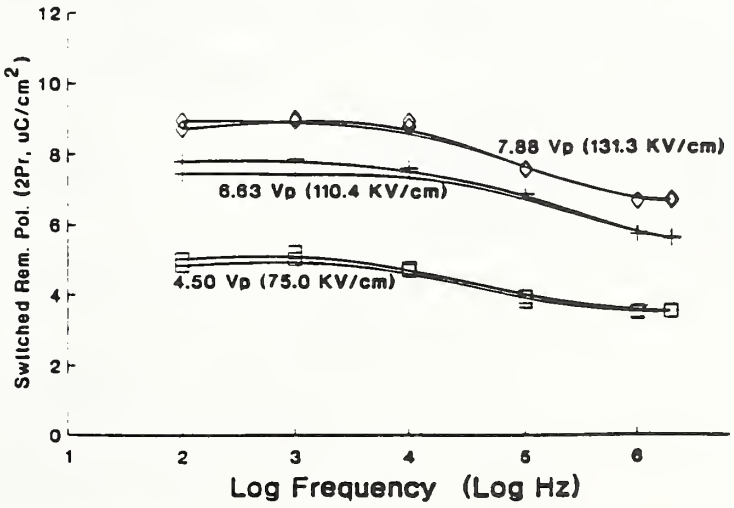

Figure 4. Switched remanent polarization as a function of frequency from 100 Hz to 2 MHz at 3 different voltages across ferroelectric capacitor for sol-gel process PZT film. Film thickness is 0.60 μm. Elapsed cycles are 1.5×10^{10}.

indicated no difference in switched remanent polarization produced by decreasing the source impedance from 50 to 25 Ω (see fig. 1).

Because the two films had different thicknesses, the applied fields at which measurements were made differed (although they do overlap). An examination of the results (fig. 3 and 4) shows a similar switched remanent polarization at low frequencies. At high frequencies (2 MHz), the switched remanent polarization for the sol-gel film is minimally decreased with respect to that of the excimer-laser-deposited film, in which the switched remanent polarization at 2 MHz is less than half that at 100 Hz.

5.2 Dielectric Constant and Dissipation Factor as a Function of Frequency

Using the parallel equivalent circuit option of the HP4194A, capacitance and dissipation factor were measured at signal oscillation levels of 10 mV and 1 V as a function of frequency for the range from 100 Hz to 2 MHz. We calculated the dielectric constant from the capacitance values using the parallel-plate capacitor formula and the film thickness (which is an approximate value), assuming that the dielectric properties of the film are homogeneous throughout the film thickness. The results are shown in figure 5 for the excimer-laser-deposited PZT film and figure 6 for the sol-gel film. The dielectric constant and dissipation factor of both films decreased with increasing frequency at both oscillation levels, but more so at the 1-V level than at the 10-mV level. We believe that the increased dielectric constant at low frequencies and higher fields results from an increase of contributions to the dielectric constant from domain wall motion, which from our preceding results is expected to be higher at lower frequencies and higher fields.

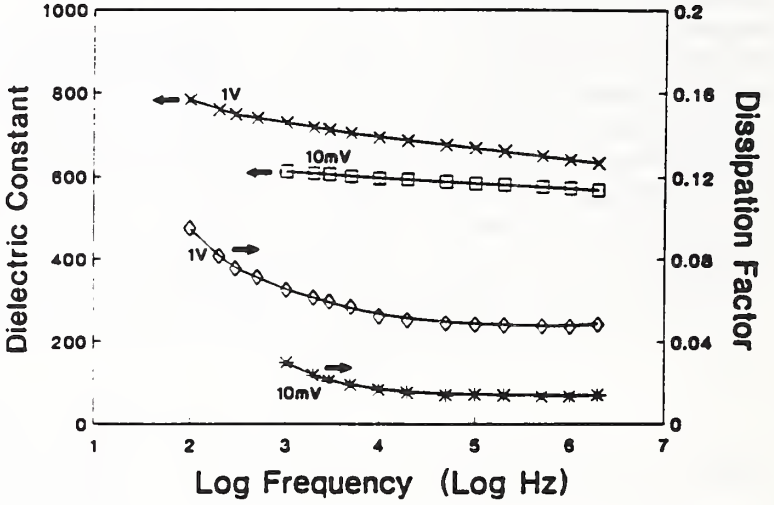

Figure 5. Dielectric constant and dissipation factor as a function of frequency from 100 Hz to 2 MHz at two different oscillation levels for excimer-laser-deposited PZT film. Film thickness is 0.45 μm. Elapsed cycles are 2×10^{10}.

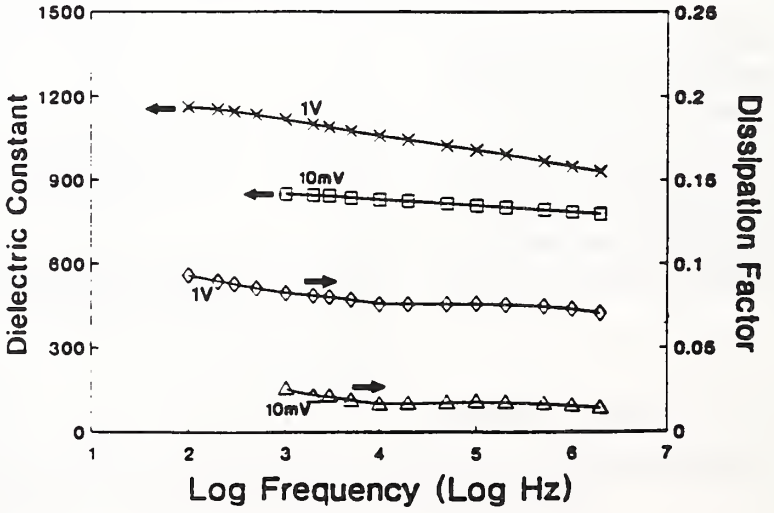

Figure 6. Dielectric constant and dissipation factor as a function of frequency from 100 Hz to 2 MHz at two different oscillation levels for sol-gel process PZT film. Film thickness is 0.60 μm. Elapsed cycles are 2×10^{10}.

6. Discussion

Both films show a sublinear dependence and frequency rolloff of the switched remanent polarization, $2P_r$. We suggest a reason for this behavior in terms of grain size and film quality. Assume that polarization is increased by the lateral motion of a 45° domain wall that is already nucleated [4], moving at a constant velocity for a given applied field, and that the domain wall moves at this velocity the full characteristic lateral dimension (grain width) of a grain and no more (we assume that the film is only one grain thick). At low frequencies, the domain wall moves its maximum possible amount, that is, the grain width. At higher frequencies, the wall moves only a fraction of this amount, and the switched remanent polarization change is reduced. This simple picture suggests a linear decrease with frequency of the switched remanent polarization. We speculate that the sublinear behavior results from a velocity that is modulated by defects within each grain, so that the average velocity for large wall displacements at lower frequencies is much less than that at high frequencies, where fewer defects (or no defects) are encountered within a switching cycle. This discussion is admittedly qualitative and speculative, but it does suggest approaches to a quantitative model and verifying experiments.

The frequency rolloff starts at 100 Hz or less for the laser-deposited material and about 10 kHz for the sol-gel material. This suggests that the grain size of the laser-deposited material is more than an order of magnitude larger than the grain size of the sol-gel material. Again this is a speculation which, however, suggests experiments and observations of microstructure that may improve understanding of the frequency-switching characteristics of the films.

7. Summary and Conclusions

Modifications of the hysteresis loop measurement arrangement, measuring the voltage across the ferroelectric thin film and accounting for the resonant frequency of the Sawyer-Tower circuit, extended the frequency range of electrical characterization ($2P_r$, dielectric constant, and dissipation factor) for continuous sinusoidal switching frequencies up to 2 MHz. Measurements showed that switched remanent polarization and dielectric constant decreased sublinearly with frequency. (The switched remanent polarization decreases sublinearly with increasing frequency, with the rolloff starting at around 10 kHz for the sol-gel film and 100 Hz or less for the excimer-laser-deposited film.) The dependence on frequency is explained as the result of limitations of the finite-domain wall velocities and a defect density modulation of the wall velocities.

References

1. C. B. Sawyer and C. H. Tower, Phys. Rev. 35 (1930), 269.
2. P. S. Brody, B. J. Rod, K. W. Bennett, L. P. Cook, P. K. Schenck, M. D. Vaudin, W. Wong-Ng, and C. K. Chiang, presentation at 3rd International Symposium on Integrated Ferroelectrics, Colorado Springs, CO, 1991 (to be published in proceedings).
3. S. K. Dey and Ranier Zuleeg, Ferroelectrics **108** (1990), 36.
4. Yoshihiro Ishibashi, J. Phys. Soc. Jpn. **99** (1990), 4148.

Photovoltaic Effect in Thin Ferroelectric Films

PHILIP S. BRODY,* B. J. ROD,* L. P. COOK,** AND P. K. SCHENCK**
*Harry Diamond Laboratories, U.S. Army LABCOM, Adelphi, MD 20783
**National Institute of Standards and Technology, Gaithersburg, MD 20899

ABSTRACT

Polarization-dependent photovoltaic currents are observed in continuously illuminated ferroelectric thin films under conditions of polarization reversal. Following reversal, an initial current rapidly decays to an essentially steady current, which then decays slowly with the current decreasing in proportion to the logarithm of elapsed time. These polarization-dependent currents are attributed to the action of internal fields on photocarriers where the fields result from the incomplete screening of the polarization field.

INTRODUCTION

In this paper we describe studies of photovoltaic currents produced in Pb-based perovskite films under conditions of polarization reversal. The studies are a continuation of work described in an earlier paper [1].

Anomalous steady-state photovoltaic currents are well known in bulk ceramic ferroelectrics and are also found in ferroelectric single crystals [2–6]. The photovoltages are considered anomalous because they cannot immediately be ascribed to ordinary photovoltaic mechanisms, such as band bending at metal contacts or the Dember effect. The open-circuit photovoltage (photo-emf) produced by these well-known mechanisms is limited (in volts) to the band-gap energy in electron volts (about 3 eV in the Pb-based perovskites). The photo-emfs found in the ceramics and single crystals can, however, be much larger, exceeding even 1000 V. The phenomenon producing the emfs in single crystals is thought to be a true bulk effect [4,5]. In the ceramics, however, the high-voltage emfs are more likely to result from the series summation of junction emfs originating at grain boundaries [5,7].

Photovoltaic currents are also seen in ferroelectric thin films [1,8,9]. The usual arrangement for producing these currents consists of a film capacitor with a top semitransparent electrode through which the film is illuminated. The current flowing through a circuit connecting the top and bottom electrode in the absence of an applied voltage is the photovoltaic current. The studies described in this paper are primarily observations of the time history of these photovoltaic currents following polarization reversal. We also consider the mechanisms generating the photovoltaic currents.

EXPERIMENT

The films studied were fabricated by the sol-gel process. Substrates were platinum-coated silicon wafers. Film capacitors with top electrodes formed of sputter-deposited semitransparent platinum were fabricated using a micromachined silicon shadow mask. The arrangement for studying the photovoltaic current following polarization reversal consisted of a probe station in which the top electrode and the base electrode were contacted with probes. The capacitor was continuously illuminated by light from a mercury arc lamp. The transparent electrode transmitted between 10 and 30 percent of incident illumination, depending on the sputter deposition time. The illumination could be filtered by a glass absorption filter placed in the optical train, which transmitted wavelengths in a band between 320 and 390 nm. Photocarriers were generated largely by illumination from this wavelength band. When this filter was used the illumination

intensity at the film after the light had passed through the electrode was about 2.4 mW/cm^2. When one took into account the filter attenuation factor, it could be seen that photovoltaic currents were produced almost exclusively from this near ultraviolet band of wavelengths. Removing the filter increased the illumination intensity within this wavelength band to about 7 mW/cm^2.

The arrangement for measurement is shown in Fig. 1. The top electrode was connected to ground through a 50-Ω resistor. Voltage pulses at V_a switched the polarity of polarization domains within the film, reversing or partially reversing the remanent polarization. The lower electrode was connected to ground through a resistance of 10^7 ohms and to the input of an electrometer amplifier at V_m, the output of which went to a chart recorder. The photovoltaic current flowing through the resistance is given by the voltage at the electrode divided by the resistance to ground under conditions of illumination. This current was effectively the short-circuit current, since the resistance to ground was always much less than the internal measured photoresistance of the film element.

Typical results for photovoltaic current versus time during and immediately after switching polarization are shown in Fig. 2 (lead zirconate-titanate film) and in Fig. 3 (lead titanate film). The switching pulses were 100 ms long and either plus or minus 8 V. There is characteristically an initial state photovoltaic current. When a positive switching pulse is applied, the photovoltaic current increases markedly. This peak current then decays rapidly to a new steady value. Switching the polarization again, with a pulse of the opposite polarity, produces a second, oppositely directed peak current. This negative peak current again decays quickly to a second steady-state value.

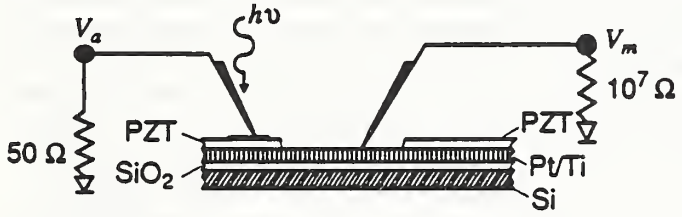

Figure 1. Experimental arrangement for applying voltage pulses and measuring photovoltaic currents. Top semitransparent electrode is a 200-Å-thick platinum layer.

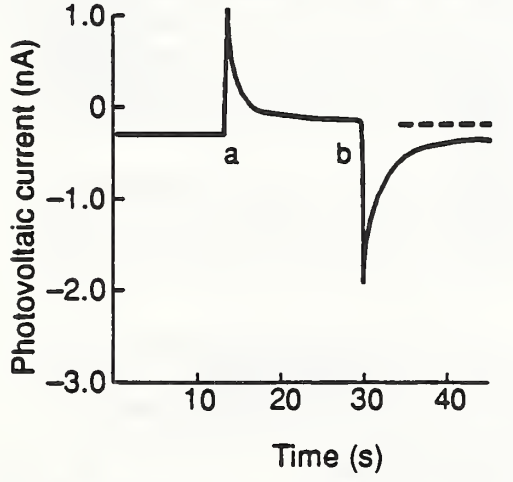

Figure 2. Photovoltaic current as a function of time (linear time scale). Sol-gel process 53/47 Zr/Ti PZT film about 0.2 μm thick: (a) positive pulse applied, (b) negative pulse applied. Photovoltaic current is that with respect to top electrode.

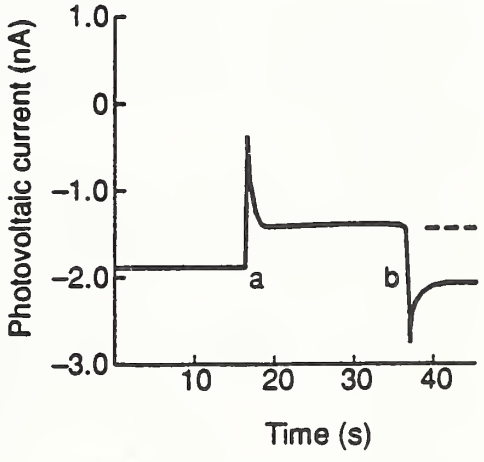

Figure 3. Photovoltaic current as in figure 2. Sol-gel process lead titanate film about 0.35 μm thick.

The steady value after switching is shifted with respect to the steady value before switching. We have shown previously [1] that this shift is linearly proportional to the change in remanent polarization. Note that the photovoltaic current is not switched symmetrically with respect to ground; this a result of an additional photovoltaic current component produced, we believe, by the action of Schottky barriers formed at the electrode/ferroelectric-film contacts [1,9]. The photocarrier-generating illumination is strongly absorbed and creates many more carriers at the top interface than at the substrate electrode interface. There is, thus, a net current flow, which would not occur if the illumination produced a uniform carrier concentration and equal and oppositely directed barrier-generated currents. We also found rectifying effects from these barriers, which affected the response of the films to switching pulses.

The steady-state polarization proportional current which persisted after the initial rapid decay also decayed, but slowly on a logarithmic time scale. The decay was linear with the logarithm of time elapsed after reversing polarization. Figure 4 shows this slow logarithmic decay for a lead titanate film in which the remanent polarization had been switched to saturation positive (curve 1) and negative (curve 2) levels with multiple 100-ms 8-V pulses. The dashed line in Fig. 4 represents the current before any pulse is applied and is the polarization-independent current we ascribe to the illuminated contact. We note that the positive and negative polarization-dependent currents are symmetric with respect to this level.

Mechanism for Polarization-Dependent Current

We now consider the source of the rapidly decaying photovoltaic current transient and the final polarization-dependent (almost) steady current that follows switching. It is our contention that both the rapidly decaying transient and the polarization-dependent steady current are the results of a time-varying potential distribution created as the remanent polarization is screened by mobile charges after polarization reversal.

Internal fields can be expected after polarization reversal. These fields are residuals of the depolarization field $-P/\varepsilon_0\varepsilon$ that would exist in the absence of screening. Only for shorted electrodes with the compensating charges sitting right on top of the polarization discontinuity can such fields be expected to vanish. If there is a displacement between the termination of the remanent polarization and the compensating charges, there will be a potential distribution within the film [7,10]. The fields from such a potential distribution can be expected to generate photovoltaic currents in the way the fields originating in the barrier junction do. The polarity of these photovoltaic currents will, however, depend on the direction of the remanent polarization; their magnitude will depend on the separation of compensating charge and the termination of the polarization.

The experimentally observed polarization-dependent current, we believe, originates in the following way. The initial peak photovoltaic current results from a potential across a surface layer, consisting of an initially charge-free gap between an electrode and the termination of the

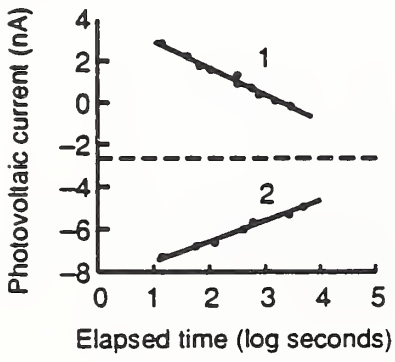

Figure 4. Photovoltaic current versus logarithm of time elapsed after saturation polarization reversals for positive and negative remanent polarization. Sol-gel process lead-titanate film. Fast decay of peak current is not shown.

remanent polarization vectors, when the polarization is screened by charges entirely confined to an electrode. The potential difference is reduced as mobile charges (illumination-generated carriers) are attracted to and populate trap sites within the gap (surface layer). The result is a decay of the field in the surface layer driving the photovoltaic current and a consequent decay in the photovoltaic current. The potential across the surface region then comes to a quasi-equilibrium value, the result of a final almost steady equilibrium potential distribution (the potential distribution screening the polarization in the steady state). Elsewhere [7], Brody and Crowne calculate the potential difference across a surface layer of thickness s for the case of shorted electrodes and compensating charge uniformly distributed within the layer (see Fig. 5). In this case the potential across the surface layer is at one end approximately $-P_0 s/2\varepsilon_0\varepsilon_s$ and at the other $+P_0 s/2\varepsilon_0\varepsilon_s$ where it is assumed that $\varepsilon_b s/\varepsilon_s l << 1$, where $l + 2s$ is the film thickness, P_0 is the remanent polarization, and ε_b and ε_s are the relative dielectric constant of the bulk and surface regions, respectively. These potential differences and thus the fields driving the photovoltaic current are greater initially when the compensating charges (as can be expected) are confined entirely to the conducting electrodes. If this surface layer is charge free and the charges are confined to the electrode, one calculates the potential difference across the surface layer to be twice that obtained for the case in which the compensating charge is uniformly distributed in the gap. The initial photovoltaic current is thus expected to be greater because the potential difference across the surface layer is greater; this is what is observed. We note, however, that the potential across the surface layer cannot exceed the band gap in volts [7,11].

Our calculations are, however, limited in value because they do not take into account the strong dependence of dielectric constant on electric field, which can be expected to be large in the high-field surface regions because of dielectric saturation. A more sophisticated approach is needed that takes this important nonlinearity into account. Even in a more sophisticated calculation, we expect the potential difference across the surface layer to remain proportional to remanent polarization. We conclude that the slow decay in the photovoltaic current that follows the

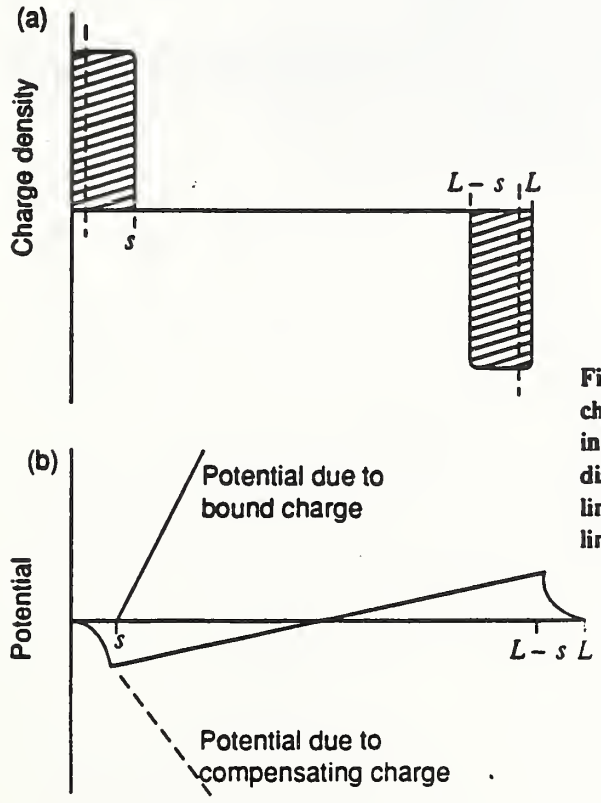

Figure 5. Final equilibrium compensating charge and potential distributions across film, in dark [7]. There is an initial charge distribution where compensating charge is limited to region near or at surfaces (dashed lines).

initial rapid decay is probably therefore the result of a slow decay of the remanent polarization. This decay of remanent polarization may be expected to result from the action of the relatively small but persistent residual depolarization field across the bulk of the film (thickness *l*).

Summary and Conclusion

We have studied polarization-dependent photovoltaic currents in thin ferroelectric film capacitors under conditions of polarization reversal. We have shown that these currents consist of a polarization-dependent current that decays rapidly after reversal, reaching an almost steady state. This steady-state current then decays slowly, in a manner that is linear with the logarithm of elapsed time. We have explained these currents as the result of a potential distribution within the films created by the screening of the remanent polarization. The initial decay results as the potential distribution relaxes from an initial configuration to a final one. The slow logarithmic decay is the result of a slow logarithmic decay of the switched remanent polarization.

Acknowledgements

We thank Dr. S. Bernacki of Raytheon Corporation and Dr. S. W. Dey of Arizona State University for providing films used in this study.

References

1. P. S. Brody and B. J. Rod, presentation at the 3rd International Symposium on Integrated Ferroelectrics, Colorado Springs, CO, 1990, preprint HDL-PP-NW-91-4; available from the authors (to be published in Proceedings).
2. P. S. Brody, Solid State Commun. 12 (1973), 673.
3. P. S. Brody, Solid State Chem. 12 (1975), 193.
4. A. M. Glass, D. von der Linde, and T. J. Negran, Appl. Phys. Lett. 25 (1974), 234.
5. V. M. Fridkin, *Photoferroelectrics*, Springer Verlag, New York (1979), 103.
6. K. Uchino, Y. Miyawaza, and S. Nomura, Jpn. J. Appl. Phys. 2 (1982), 1671.
7. P. S. Brody and F. Crowne, J. Electron. Mater. 4 (1975), 955.
8. V. S. Dharmadhikaru and W. W. Grannemann, J. Appl. Phys. 53 (1982), 1671.
9. S. Thakoor, A. Thakoor, and S. Bernacki, presentation at 3rd International Symposium on Integrated Ferroelectrics, Colorado Springs, CO, 1990 (to be published in Proceedings).
10. P. Wurfel and I. F. Batra, Ferroelectrics 12 (1976), 55.
11. G. M. Guro, I. E. Ivanchik, and N. F. Koutonyuk, JEPT Lett. 5 (1967), 5.

FERROELECTRIC THIN FILM BY PULSED LASER DEPOSITION TECHNIQUE

PROCESSING AND CHARACTERIZATION

LIST OF REFERENCES

1. Ceramic Thin Films by Laser Deposition.
   L. P. Cook, P. K. Schenck, J. Zhao, E. N. Farabaugh, C. K. Chiang and M. Vaudin.
   "Thick and Thin Films", Ceram. Trans., 11, 464, Am. Ceram. Soc. Symp. Proc.,(1990)

2. Lead Zirconate-Titanate Thin Films by the Laser Ablation Technique.
   C. K. Chiang, L. P. Cook, P. K. Schenck, P. S. Brody and J. M. Benedetto.
   "Ferroelectric Thin Films", ed. E. R. Myers and A. I. Kingon, Mat. Res. Soc. Symp. Proc. 200, 133-137, (1990).

3. Laser Vaporization and Deposition of Lead Zirconate Titanate.
   P. K. Schenck, L. P. Cook, J. Zhao, J. W. Hastie, E. N. Farabough, C. K. Chiang, M. D. Vaudin, P. S. Brody.
   "Beam-Solid Interactions: Physical Phenomena", eds. by J. A. Knapp, P. Borgesen, and R. A. Zuhr, Mat. Res. Soc. Symp. Proc., 157, 587-592, (1990).

4. Microstructural Changes During Processing of Laser-Deposited $BaTiO_3$ and PZT Thin Films.
   L.P. Cook, M.D. Vaudin, P.K. Schenck, W. Wong-Ng and C.K. Chiang, P.S. Brody.
   "Evolution of Thin Film and Surface Microstructure", Eds. C. V. Thompson, J. Y. Chao, D. J. Srolovitz, Mat. Res. Soc. Symp. Proc, 202, (1991)

5. Characterization of Lead Zirconate-Titanate Thin Films Prepared by Pulsed Laser Depostion.
   C. K. Chiang, W. Wong-Ng, P. K. Schenck, L. P. Cook, M. D. Vaudin, P.S. Brody, B. J. Rod and K. W. Bennett,
   "Phase Transformation Kinetics in Thin Films", eds. M. Chen, Mat. Res. Soc. Symposium Proc. 230, 321, (1991).

6. PZT Films Prepared by the Pulsed Laser Deposition Technique.
   W. Wong-Ng, T. Huang, L.P. Cook, P.K. Schenck, M.D. Vaudin, C.K. Chiang, P.S. Brody.
   Proc. of Intl. Conf. on Mater. and Process Charac. for VLSI (1991).

7. Thermal Processing of Laser-Deposited $BaTiO_3$.
   L.P. Cook, W. Wong-Ng, T. Huang, P.K. Schenck, M.D. Vaudin, C.K. Chiang, P.S. Brody.
   Proc. of Intl. Conf. on Mater. and Process Charac. for VLSI, (1991).

LIST OF REFERENCES (Continued)

8. Microstructure and Ferroelectric Properties of Lead Zirconate-Titanate Films Produced by Laser Evaporation.
P. S. Brody, J. M. Benedetto, B. J. Rod and K. W. Bennett, L. P. Cook, P. K. Schenck, C. K. Chiang and W. Wong-Ng.
"Intl. Symp. on Applications of Ferroelectrics", 1990 IEEE Proc., 181-184, (1991).

9. Optical Characterization of Thin Film Laser Deposition Processes.
P. K. Schenck, D. W. Bonnell, J. W. Hastie, L. P. Cook and C. K. Chiang
"Microelectronic Processing Integration", SPIE Symp. Proc., 1594, 411-417, (1991).

10. Preparation, Microstructure and Ferroelectric Properties of Laser-Deposited Thin $BaTiO_3$ and Lead Zirconate-Titanate Thin Films.
P. S. Brody, B. J. Rod and K. W. Bennett, L. P. Cook, P. K. Schenck, W. Wong-Ng and C. K. Chiang.
Ferroelectrics, (submitted 1991).

11. Powder X-ray Diffraction Characterization of Laser Deposited Ferroelectric Thin Films.
W. Wong-Ng, T. C. Huang, L. P. Cook, P. K. Schenck, M. D. Vaudin, C. K. Chiang, L. H. Robins, T. C. Huang, and P. S. Brody.
Adv. in X-ray Analysis, (submitted 1991)

12. Post-Processing of Laser Deposited PZT Thin Films. Technique.
C. K. Chiang, W. Wong-Ng, L. P. Cook, P. K. Schenck, H. M. Lee, P.S. Brody, K. W. Bennett, and B. J. Rod,
"Ferroelectric Thin Films II", eds. A. I. Kingon, E. R. Myers and B. Tuttle, Mat. Res. Soc. Symp. Proc, 243, (1992).

13. Crystallographic Aspects of Ferroelectric Thin Films Prepared by Laser Deposition Technique.
W. Wong-Ng, T. C. Huang, L. P. Cook, P. K. Schenck, M. D. Vaudin, and C. K. Chiang and P. S. Brody.
"Ferroelectric Thin Films II", eds. A. I. Kingon, E. R. Myers and B. Tuttle, Mat. Res. Soc. Symp. Proc, 243, (1992).

14. Textureing and Dielectric Properties of laser Deposited $BaTiO_3$ Thin Films Grown on Heated Substrates.
M. D. Vaudin, L. P. Cook, W. Wong-Ng, P. K. Schenck, P. S. Brody, B. J. Rod and K. W. Bennett.
"Ferroelectric Thin Films II", eds. A. I. Kingon, E. R. Myers and B. Tuttle, Mat. Res. Soc. Symp. Proc, 243, (1992).

LIST OF REFERENCES (Continued)

15. Dielectric Constant and Hysteresis Loop Remanent Polarization from 100 Hz to 2 MHz for Thin Ferroelectric Films.
K. W. Bennett, P. S. Brody, B. J. Rod, L. P. Cook, P. K. Schenck, and S. Dey.
"Ferroelectric Thin Films II", eds. A. I. Kingon, E. R. Myers and B. Tuttle, Mat. Res. Soc. Symp. Proc., 243, (1992).

16. Photovoltaic Effect in Thin Ferroelectric Films.
P. S. Brody, B. J. Rod, L. P. Cook, P. K. Schenck.
"Ferroelectric Thin Films II", eds. A. I. Kingon, E. R. Myers and B. Tuttle, Mat. Res. Soc. Symp. Proc., 243, (1992).

NIST-114A
(REV. 3-90)

U.S. DEPARTMENT OF COMMERCE
NATIONAL INSTITUTE OF STANDARDS AND TECHNOLOGY

BIBLIOGRAPHIC DATA SHEET

1. PUBLICATION OR REPORT NUMBER
NISTIR 4844

2. PERFORMING ORGANIZATION REPORT NUMBER

3. PUBLICATION DATE
MAY 1992

4. TITLE AND SUBTITLE

Ferroelectric Thin Films Prepared by Pulsed Laser Deposition Processing and Characterization

5. AUTHOR(S)

L. P. Cook, C. K. Chiang and P. K. Schenck

6. PERFORMING ORGANIZATION (IF JOINT OR OTHER THAN NIST, SEE INSTRUCTIONS)

U.S. DEPARTMENT OF COMMERCE
NATIONAL INSTITUTE OF STANDARDS AND TECHNOLOGY
GAITHERSBURG, MD 20899

7. CONTRACT/GRANT NUMBER

8. TYPE OF REPORT AND PERIOD COVERED

9. SPONSORING ORGANIZATION NAME AND COMPLETE ADDRESS (STREET, CITY, STATE, ZIP)

10. SUPPLEMENTARY NOTES

11. ABSTRACT (A 200-WORD OR LESS FACTUAL SUMMARY OF MOST SIGNIFICANT INFORMATION. IF DOCUMENT INCLUDES A SIGNIFICANT BIBLIOGRAPHY OR LITERATURE SURVEY, MENTION IT HERE.)

This report describes the development of piezoelectric lead zirconate-titanate (PZT) and barium titanate (BT) thin films for application to non-volatile memories for electronic devices such as computers. The work was done in the period from January 1989 to December 1991 in the Ceramics and Metallurgy Divisions at NIST under partial support of the Department of the Army through Harry Diamond Laboratory.

12. KEY WORDS (6 TO 12 ENTRIES; ALPHABETICAL ORDER; CAPITALIZE ONLY PROPER NAMES; AND SEPARATE KEY WORDS BY SEMICOLONS)

characterization; ferroelctricity; laser deposition; processing; thin film

13. AVAILABILITY

[xxx] UNLIMITED

FOR OFFICIAL DISTRIBUTION. DO NOT RELEASE TO NATIONAL TECHNICAL INFORMATION SERVICE (NTIS).

[ ] ORDER FROM SUPERINTENDENT OF DOCUMENTS, U.S. GOVERNMENT PRINTING OFFICE, WASHINGTON, DC 20402.

[xxx] ORDER FROM NATIONAL TECHNICAL INFORMATION SERVICE (NTIS), SPRINGFIELD, VA 22161.

14. NUMBER OF PRINTED PAGES
123

15. PRICE
A06

ELECTRONIC FORM